UNIVERSITY OF CALIFORNIA, SAN DIEGO

Focal Adhesions are Mechanosensitive and Regulate Stem Cell Differentiation

A dissertation submitted in partial satisfaction of the
requirements for the degree Doctor of Philosophy

in

Bioengineering

by

Andrew W. Holle

Committee in charge:

Professor Adam J. Engler, Chair
Professor Juan Lasheras
Professor Robert Ross
Professor Geert Schmid-Schönbein
Professor Shyni Varghese

2013

The dissertation of Andrew W. Holle is approved, and it is acceptable in quality and form for publication on microfilm and electronically:

_____

_____

_____

_____

_____

Chair

University of California, San Diego

2013

DEDICATION

To my parents

EPIGRAPH

“I can see in my heart that the child playing in the creek is me, and that I haven't changed much really in the intervening years. I'm still turning over stones, hoping to find something new.”

- Dr. Craig C. Mello

“For anybody to make their way in the world, there need to be inputs and contributions... and a lot of influences”

- Dr. Andrew Z. Fire

TABLE OF CONTENTS

LIST OF FIGURES AND TABLES

Chapter 1

Chapter 2

Chapter 3

ACKNOWLEDGEMENTS

I would like to thank my doctoral advisor and committee chair, Professor Adam J. Engler, for allowing me to work in his lab, for believing in me, and for all of his invaluable guidance and assistance along the way.

I would also like to acknowledge committee member Dr. Shyni Varghese for her expertise in stem cell biology and polymer science, Dr. Juan Lasheras for his expertise in mechanical engineering, Dr. Geert Schmid-Schönbein for his words of encouragement and advice, and Dr. Robert Ross for all of his vinculin knowledge. These faculty have all contributed to the completion of this work, and I am grateful for their decision to sit on my committee.

I would like to thank all the other UCSD faculty members who have contributed to my research over the past five years, especially Dr. Juan Carlos Del Alamo for all of his help in bringing Traction Force Microscopy to the Engler Lab and Dr. Majid Ghassemian for his expertise and training in Mass Spectroscopy. I would also like to thank Dr. Jamie Kasuboski in the Salk Biophotonics Core for his assistance in High Throughput Imaging.

I would also like to acknowledge the Bioengineering Department at UCSD for giving me the opportunity to participate in the Ph.D. program and for all of their administrative assistance over the years. I would like to especially thank Jan Lenington, Steve Lopez, and Douglas Gurevitch, P.E. I would like thank all of my funding sources for supporting me throughout my degree, namely the National Institutes of Health (1DP02OD006460 and R21HL106529 to A.J.E).

I would like to thank all of my research peers I have interfaced with at UCSD. They have given me advice, knowledge and friendship over the past five years. I would especially like to thank the members of the Engler lab, including Dr. Yu Suk Choi, Dr. Gretchen Meyer, Dr. Alexander Fuhrmann, Dr. Somyot Chirasatitsin, Dr. Jennifer Young, Xinyi Tang, Ludovic Vincent, Gaurav Kaushik, Hermes Taylor-Weiner, Jessica Wen, Matthew Ondeck, Kelsey Thomas, Ayla Sessions, Kyle Kretchmer, Justin Tse, Jacquelyn Schaefer and Andrew Lee. I would also like to acknowledge my undergraduate mentees, Nikhil Joshi, Deepthi Vijayraghavan, Jared Kehe, and Piyumi Wijesekara-Kankanange for all of their hard work. I would also like to thank all of my research peers outside of the Engler lab for their research support and perspective, including Dr. Jeff Gole, Dr. Angelina Altshuler, Jangir Selimkhanov, Brian Sprouse, Athurva Gore, and Tatsuya Arai. In addition, I have tremendous gratitude towards our lab manger Jeremy Tuler for all of his expertise and assistance in procuring almost all of the materials I have worked with.

Chapter 1, in full, is a reformatted version of the published article as it appears in *Current Opinion in Biotechnology*, Volume 22 (2011). The dissertation author was the primary investigator and author of this paper, and thanks co-author Dr. Adam J. Engler for their contributions. This work was supported by an NIH New Innovator Award (1DP02 OD006460 to A.J.E).

Chapter 2, in full, is a reformatted version of the published article as it will appear in *Stem Cells* (volume to be determined). The dissertation author was the primary investigator and author of this paper, and thanks co-authors Xinyi Tang, Deepthi Vijayraghavan, Ludovic Vincent, Dr. Yu Suk Choi, Dr. Alexander Fuhrmann, Dr. Juan

Carlos Del Alamo, and Dr. Adam J. Engler for their contributions. The authors would like to thank Dr. Susan Craig (Johns Hopkins University) for provision of vinculin constructs and Dr. Jeff Gole for assistance with sequencing. This work was supported by an NIH New Innovator Award (1DP02 OD006460 to A.J.E) and an NSF predoctoral fellowship (to L.G.V.)

Chapter 3, in part, is currently being prepared for submission for publication of the material. The dissertation author is the primary investigator and author, and thanks co-authors Ludovic Vincent, Dr. Jamie Kasuboski, and Dr. Adam J. Engler for their contributions to the work. This work was supported by an NIH New Innovator Award (1DP02 OD006460 to A.J.E) and an NSF predoctoral fellowship (to L.G.V.)

VITA

2008	Bachelor of Science in Engineering, Arizona State University; Tempe, AZ
2009-2010	Graduate Teaching Assistant, Department of Bioengineering University of California, San Diego
2013	Doctor of Philosophy, University of California, San Diego; La Jolla, CA

FIELDS OF STUDY

Major Field: Bioengineering

Studies in Drug Delivery and Tissue Engineering
Professor Christine Pauken, Ph.D. (Arizona State University)

Studies in Stem Cell Mechanotransduction and Differentiation
Professor Adam J. Engler, Ph.D. (UC San Diego)

PUBLICATIONS

Holle, A.W. and Engler, A. J. "News and Views: Stressed-out Stem Cells" Nature Materials, Vol. 9, January 2010

Holle, A.W. and Engler, A.J. "More than a Feeling: Discovering, Understanding, and Influencing Mechanosensitive Pathways" Current Opinion in Biotechnology Vol. 22, October 2011.

Choi, Y.S., Holle, A.W., and Engler, A.J. "Engineered ECM Microenvironments and Their Regulation of Stem Cells" Extracellular Matrix in Development, 133-160

Holle, A.W., Tang, X., Vijayraghavan, D., Vincent, L.G., Fuhrmann, A., Choi, Y.S., del Alamo, J.C., and Engler, A.J. "In situ mechanotransduction via vinculin regulates stem cell differentiation" Stem Cells, In Press.

ABSTRACT OF DISSERTATION

Focal Adhesions are Mechanosensitive and Regulate Stem Cell Differentiation

by

Andrew W. Holle

Doctor of Philosophy in Bioengineering

University of California, San Diego, 2013

Professor Adam J. Engler, Chair

Human mesenchymal stem cell (hMSC) proliferation, migration, and differentiation have all been linked to extracellular matrix stiffness, yet the signaling pathway(s) that are necessary for mechanotransduction remain unproven. Vinculin has been implicated as a mechanosensor *in vitro*, but here we demonstrate its ability to also regulate stem cell behavior, including hMSC differentiation. RNA interference-mediated vinculin knockdown significantly decreased stiffness-induced MyoD, a muscle transcription factor, but not Runx2, an osteoblast transcription factor, and impaired stiffness-mediated migration. A kinase binding accessibility screen predicted a cryptic MAPK1 signaling site in vinculin that could regulate these behaviors. Indeed, reintroduction of vinculin domains into knocked-down cells indicated that MAPK1

binding site-containing vinculin constructs were necessary for hMSC expression of MyoD. Vinculin knockdown does not appear to interfere with focal adhesion assembly, significantly alter adhesive properties, or diminish cell traction force generation, indicating that its knockdown only adversely affected MAPK1 signaling. These data provide some of the first evidence that a force-sensitive adhesion protein can regulate stem cell fate.

We build on this research by analyzing 47 different focal adhesion proteins for cryptic MAPK1 binding sites similar to that found in vinculin. Using this parameter we selected 6 candidate focal adhesion proteins for further study in a high content imaging and analysis system in which cells were treated with siRNA, plated onto a 96 well plate containing two dimensional polyacrylamide surfaces, and stained for osteogenic and myogenic differentiation markers. This is the first high throughput system specifically built to analyze stem cell differentiation as a function of substrate stiffness and the first time an siRNA screen has been applied to stem cells for the purpose of studying substrate stiffness mediated mechanotransduction.

Chapter 1

Introduction

Mechanotransduction is the complex process where a cell converts a mechanical stimulus into a biochemical signal. Although all adherent cell types participate in this, the specific mechanical input and the nature of the corresponding output varies widely. As a result, there are two different regimes of mechanotransduction: passive or 'outside-in' sensing, in which the cell responds to a force imparted upon itself, e.g. shear stress [1], extension [2], compression [3], and pressure [4], and active or 'inside-out' sensing, in which the generation of internal forces allows for 'measurement' of the extracellular environment, e.g. cell traction forces feeling changes in stiffness [5], surface topography [6], and ligand density [7] (Figure 1). Despite two decades of serious scientific inquiry, a consensus on the signaling pathways that are necessary and sufficient to undergo mechanosensation and the resulting behaviors that it elicits has yet to be realized. Here, we discuss the context in which mechanotransduction occurs, the categories of known mechanosensitive pathways within the cell, the systems used to perturb these pathways, and provide an opinion on where consensus can be found within the community.

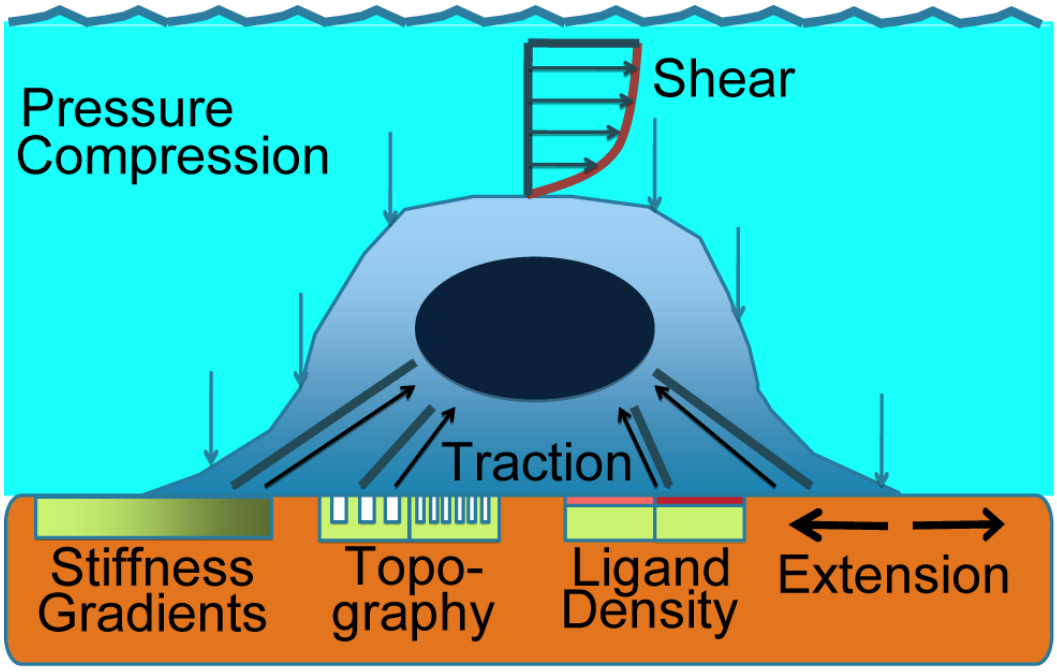

Figure 1: The physiological physical microenvironment of the cell. Outside-in forces are depicted acting on the cell. On the other hand, inside-out transduction of cellular contractility can be affected by changes in stiffness gradients, ECM topography, and ligand density.

1.1 Controlling the Physical Microenvironment of the Cell

To appreciate mechanotransductive mechanisms, it is first necessary to review the systems used that impart "outside-in" forces or modulate "inside-out" cell traction forces by exposing cell populations to a controlled physical microenvironment. Fluid flow assays, which mimic blood or ECM fluid flow, are the historical standard for controlling shear forces and examining "outside-in" mechanosensing [8]. Extracellular pressure variations [4] or pulsatile flow [9] have also been utilized to more specifically recreate a physiological environment. Controlled extension of silicone [10] or hydrogel [11] substrates can mimic ECM stretching in vivo. More targeted methods of physically perturbing cells include the use of optical tweezers [12], atomic force microscopy [13], and magnetic twisting cytometry [14]. Some of these tools have also been used to assess "inside-out" mechanosensing by measuring the force with which a cell pulls on its extracellular environment [15].

To induce "inside-out" changes via adjusting the microenvironment, hydrogels like polyacrylamide [16], pNIPAAM [17], PDMS [18] and PEG [19] have been used to vary substrate stiffness. This change in the physical microenvironment has been shown to influence cell migration [16], cell stiffness [20], and adult stem cell differentiation [21]. These substrates can also be patterned with ligands favorable or unfavorable for cell attachment, effectively controlling cell shape [22], or molded into pillars with different heights, which not only provides a variable topography for cells, but also varies stiffness and provides a method for measuring cell traction forces generated [23]. As previously mentioned, gradients in substrate stiffness, ligand patterning, or topography also serve as

mechanical inputs to cells, with changes in directed cell migration as a common output, i.e. “durotaxis” [24]. While many durotactic studies mimic pathological gradients [25], even those using physiological gradients found at the interfaces of tissue types have detected durotaxis [26, 27]

Regardless of the system used or whether focusing on “inside-out” or “outside-in,” understanding the conversion of physical to chemical signals requires one to focus on where intracellular sensors could exist. Sensors have typically been proposed where clusters of structural and adaptor proteins exist, namely focal adhesions (FA) [28], the complexes that bind the ECM to the cell’s cytoskeleton, and the perinuclear cytoskeleton [29], which binds the cell’s cytoskeleton to the nucleus. Given that cells dramatically change their membrane tension in response to changes in microenvironmental stiffness [21], we will focus our discussion on focal adhesion-based sensing, though a complete picture of overall sensing should likely include both means of signaling.

1.2 The Usual Suspects: Known Mechanosensing Pathways

Cell contractile forces result in varying levels of ECM deformation depending upon its physical characteristics. The force to which FA complex structural proteins are exposed changes as well as they are connected in series between force-generating units within cytoskeleton and the ECM [30]. Here we review the evidence of how 3 separate means of responding to such forces have been proposed (Figure 2).

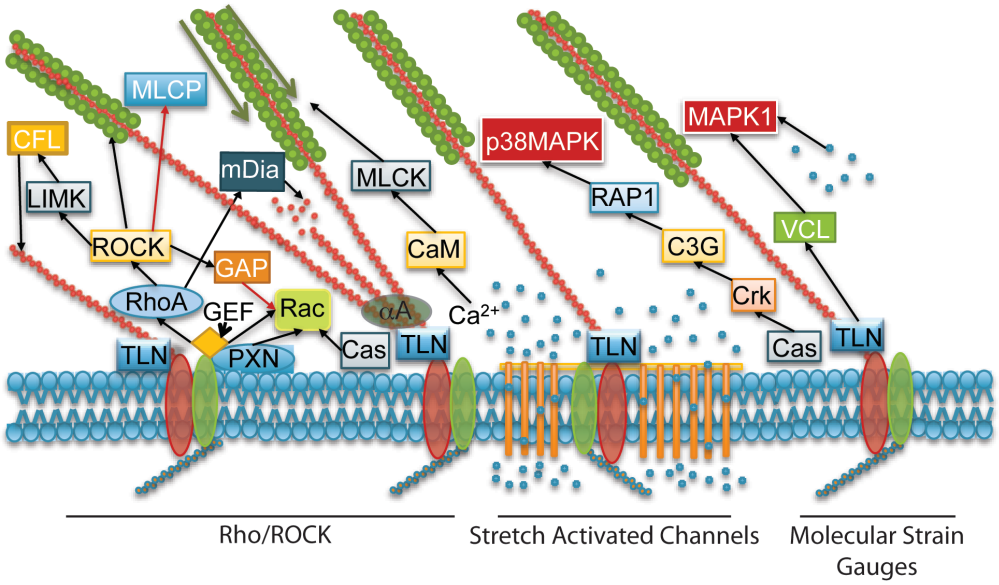

Figure 2: Signaling events of three major candidate mechanosensing pathways. To the left, the **Rho/ROCK** system is summarized, showing the mechanisms for actin nucleation, assembly, and stabilization, as well as myosin contractility. A positive feedback loop results in increasing cellular contractility, visually verified by the robust amount of stress fibers present at focal adhesions of cells on stiff microenvironments. In the center, a network of **mechanosensing ion channels** or "stretch activated channels" (SACs) is responding to membrane stretching, which forces open the channels. An increase in intracellular calcium concentration also provides positive feedback through favorable activation of MLCK, causing further increases in cellular contractility. Finally, **molecular strain gauges**, e.g. p130Cas and talin, are shown responding to increases in cellular contractility by exposing binding sites for Crk and vinculin, respectively. These pathways progress to the activation of two types of MAPK signaling kinases, which may influence changes in cell behavior further downstream. It is of note that the degree of interconnectivity between these paradigms of mechanotransduction, even as briefly overviewed in this figure, is high. Abbreviations: TLN- talin, Cas- p130Cas, VCL- vinculin, CaM-calmodulin, MLCK-myosin light chain kinase, MLCP-myosin light chain phosphatase, CFL-cofilin, LIMK-LIM Kinase, AA-alpha actinin, PXN- paxillin, GEF- guanidine exchange factor.

1.2.1 Rho/Rock Signaling Pathway

Due to its prevalence in cellular processes associated with the cytoskeleton and cellular contractility, the Rho/ROCK signaling pathway has been extensively studied [31]. Upon binding of integrins to the ECM, guanidine exchange factors (GEFs), which associate near FAs, catalyze a number of Rho GTPases, including RhoA and Rac [32, 33]. The amount of contractile force the cell exerts is translated into ROCK phosphorylation via RhoA [34]. Activated ROCK effects several cellular processes, most notably actin organization via LIM kinase and Cofilin activation and cell contractility via phosphorylation of Myosin Light Chain (MLC) [35] and inactivation of MLC Phosphatase [36]. Another RhoA effector protein is mDia, which is responsible for the creation of new actin stress fibers by catalyzing actin nucleation and elongation [37]. Altogether, the Rho/ROCK signaling pathway is the 'muscle' responsible for upregulating and stabilizing the amount of stress fibers the cell displays in response to an increase in 'inside-out' force.

1.2.2 Stretch Activated Channels (SACs)

Mechanosensitive channels that become more permeable to soluble ions in response to contractile force are hypothesized to function through a protein 'gate' which is physically separated under force [38]. Although the specific family of SACs integral to the mechanosensing process has not yet been clearly identified, TRP channels have received the most attention due to their calcium ion permeability [39] and ability to permit transient calcium influx in stretched cells [40]. It has been shown that cells on substrates of differing stiffness exhibit changes in the amplitude of calcium ion

oscillations, proving that SAC permeability is related to active sensing of the physical microenvironment of the cell [41]. Furthermore, cells plated on substrates with a stiffness gradient showed even stronger calcium ion oscillations, indicative of a sensing role for calcium signaling [41]. While changes in calcium ion concentration can affect or effect a number of pathways, one particularly important downstream role is an increased activation of Calmodulin and Myosin Light Chain Kinase (MLCK), which increases cellular contractility by phosphorylating MLC [42]. Other mechanosensitive channels, such as the TREK-1 potassium channel, are currently being investigated both as a model for understanding the protein 'gate' mechanism and as a robust touch sensor [43].

1.2.3 Force-induced Protein Unfolding

The existence of force-inducible protein unfolding, which we refer to as 'molecular strain gauges' (Figure 3), provides a third potential, FA complex-based mechanosensing mechanism. These proteins are capable of unfolding under physiological force, exposing binding domains for other proteins and signaling molecules further down the pathway. Talin, a FA protein that binds to integrins and actin, has been shown to unfold under stretching forces as low as 12 pN and expose up to 11 binding domains for vinculin, another FA protein [44]. Vinculin itself has been shown to have an activation event required for Talin binding [45], which exposes a predicted binding domain for MAPK1 (unpublished), a prominent signaling kinase. Furthermore, the FA protein p130Cas, which binds to FAK and associates with Talin, has been shown to unfold under force to activate the Crk/C3G-Rap1 signaling cascade that results in phosphorylation of a different form of MAPK [46]. Another protein, receptor-like

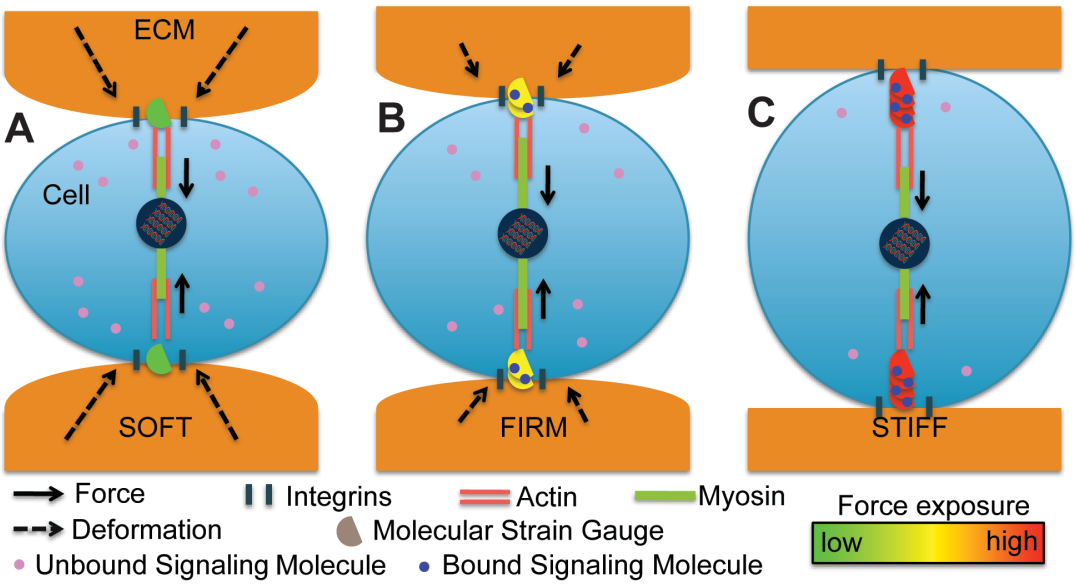

Figure 3: Changes in substrate stiffness result in a spectrum of linker protein force exposure. Because some focal adhesion proteins have been shown to undergo force-responsive unfolding events, it is feasible that changes in ECM stiffness may be a cause of discretized unfolding. Differences in unfolding at focal adhesions may result in modulation of downstream signaling molecules responsible for effecting changes in cell behavior. **A**) On soft substrates (~0-4 kPa), the force generated by cellular contractility is transferred to the ECM through linker proteins, but because of compliance of the ECM, linker proteins are not exposed to a high degree of force. **B**) On firm substrates (~8-15 kPa), compliance of the ECM decreases but does not disappear, resulting in an incremental increase in force exposure at focal adhesions. **C**) On firm substrates (~25 kPa-50 GPa) matrix compliance approaches zero, causing nearly the full force of cellular contractility to be focused on linker proteins in focal adhesions.

tyrosine phosphatase alpha (RPTPα) has been shown to associate with α integrins, catalyzing binding to fibronectin and vitronectin in a force-dependent manner via the Src family kinase cascade [47]. Thus, a connection can be made between force-dependent unfolding of FA proteins and signaling cascades that may ultimately affect gene expression.

While most research focuses on one particular potential regime of mechanosensing, it is becoming more apparent that they interconnected in several respects. If the Rho/ROCK pathway is utilized mainly to strengthen and reinforce adhesions in response to the physical microenvironment, then that increase in contractile force caused by greater MLC activity will likely result in a greater number of SAC's being activated and molecular strain gauges unfolding. The SAC activity can serve to reinforce the activity of the Rho/ROCK cascade, while the molecular strain gauges work more directly in the signaling cascade that ultimately alters gene expression patterns. Furthermore, the MAPK1 signaling cascade associated with vinculin activation has been found to be upregulated in concurrence with an increase in Rho/ROCK activity [19], lending further evidence to a synergistic mechanosensing system utilizing all three paradigms.

1.3 Confounding Factors in Mechanosensitive Pathway Research

One cannot underscore enough the complexity of chemical signaling within FAs, as is illustrated in Figure 4. Many mechanotransduction studies identify a specific mechanism(s) by analyzing the cell's response to perturbations via chemical inhibition to block activation events (e.g. phosphorylation) or by altering the expression of signaling

proteins. Perhaps the most widely used inhibitor towards a mechanosensing pathway element is the molecule Y-27632, which inhibits ROCK by competitively binding to its catalytic site [48]. Reducing or even eliminating mechanosensing proteins by siRNA or knockout systems, and their corresponding 'add back' experiments, can also provide some level of confirmation. However, there is a critical need for developing techniques that monitor real-time changes in the mechanical state of proteins as current methods mentioned here have significant problems associated with their use. For example, Y-27632 is a valid inhibitor for studying ROCK disruption, but it also has potency as an inhibitor of Protein Kinase C-Related Kinase (PRK2) [49]. The cellular effect of PRK2 inhibition is unknown. However, the use of Y-27632 alone potentially opens the door for misleading results caused by unintentional inhibition of other pathways. The same is true for any type of protein knockdown or knockout. In FAK-null cells, cellular adhesion strength has been shown to be over 40% higher than in wild type cells, an effect believed to be due to reduced vinculin recruitment to FAs [50]. Thus, cells that are FAK-null, due to their higher adhesion force, can be expected to transduce force differently than their wild type counterparts, not because FAK is a sole mediator of mechanosensitivity, but because of a disruption in the general structure of the FA. It is important, then, to understand the difference between a heavy-handed FA disruption and the precise, elegant excision of a pathway element that serves one purpose. Whether or not such an elegant element even exists is still an unsettled issue, but the development of more refined inhibitors and the adoption of more specific approaches are both key to moving this question forward.

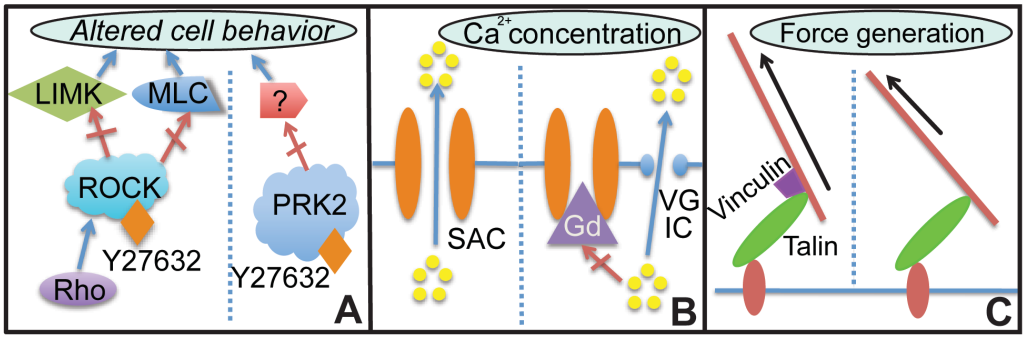

Figure 4 *Confounding factors in manipulating mechanosensitive pathways.* To further understand the mechanosensitive pathways of the cell, interfering with a hypothesized pathway and observing a change in mechanosensing can provide evidence for function. However, for a number of these interferences, confounding factors which may affect cell behavior may exist. **A**) The inhibitor Y27632 is a classic inhibitor of ROCK, and is used to study the role of the Rho/ROCK pathway on mechanosensing. However, Y27632 has also been shown to inhibit PRK2, whose role in mechanosensing is currently unclear. **B**) Intracellular calcium concentration has been shown to be important to substrate stiffness-based mechanosensing, with reduction in calcium ion concentration resulting in a decrease in stiffness-based differentiation. However, blocking stretch activated channels with the potent inhibitor gadolinium did not result in any changes in differentiation (unpublished), suggesting that calcium ions can enter the cell via other routes, including voltage gated ion channels. **C**) siRNA mediated knockdown of vinculin has been shown to reduce stiffness-based differentiation (unpublished), but if perturbing focal adhesions by knocking down constituents has an impact on cellular force generation, any change

1.4 Future Directions for Mechanotransduction

The complexity of FA-based mechanosensing necessitates the drive for more complex tools. At this point, it may not be enough to perturb one pathway, to knock down one protein, or to test one inhibitor. With each new variable, such as knocked down protein, inhibitor and inhibitor concentration, substrate stiffness, and time, comes an exponential increase in the number of cell populations and observations. To fully understand the mechanosensing ability of the cell, and thus more capably influence it, the use of high throughput systems capable of ascertaining the effect of combinatorial treatments of cell populations will be required.

As bioinformatics and proteomics advance, it is easy to foresee the development of a new field of mechanomics, in which the predicted structure of a protein is related to the predicted chemical forces inherent to its structure. Thus far, to learn about the properties of a protein unfolding under physiological force, researchers have had to use a number of costly, time consuming tools, including AFM [51], constitutively active FRET sensors [52], and laser tweezers [53]. With the development of mechanomics, the behavior of proteins and signaling molecules in response to physiological force can be modeled *in silico*, and thus it is reasonable to believe that one day, entire mechanosensing pathways could be modeled instantly and accurately, then verified experimentally.

The ultimate goal of work on discovering and understanding mechanosensing pathways is to be able to effectively influence them for the desired outcomes of a clinical treatment. There are dozens of clinical conditions arising from deficits in

mechanosensing, including muscular dystrophy, cardiomyopathies, developmental disorders, and cancer, as reviewed by Jaalouk [54]. While inhibitory molecules have been suggested to address these deficits, such as Y27632 in the treatment of bronchial asthma [55], successful clinical implementation relies on a fully characterized system. In addition, diseased tissue often exhibits different mechanical properties than healthy tissue, which means that any treatment utilizing cells in such areas necessitates a change in physical microenvironment for the therapeutic cell population. Cellular myoplasty with MSCs on infarcted rat heart has been shown to improve scarred heart muscle compliance but also cause small cardiac calcifications [56], presumably due to the increased stiffness of the physical microenvironment of the infarct. This response illustrates the dangers of cellular misinterpretation of tissue mechanics. By influencing the mechanosensing pathways of these cells to temporally ignore the stiffness of the extracellular environment, and only take cues from the chemical factors present, errant differentiation could be avoided, increasing the clinical relevance of such an approach.

1.5 Summary

The aims of this dissertation are (1) to elucidate the role of vinculin in mechanosensitive stem cell differentiation, (2) use a bioinformatics based approach to better identify cryptic binding sites on vinculin and other focal adhesion proteins, (3) to describe the subsequent pathways propagating from vinculin activation in mechanotransduction, (4) to apply this technique to multiple focal adhesion proteins containing predicted cryptic binding domains, and (5) to detect the role of these focal adhesion proteins in mechanosensitive differentiation along multiple lineages. Chapter 2

of this dissertation describes the investigation of vinculin as a precise mechanosensing element, the analysis of its predicting binding partners and the accessibility of those domains, and the mutation of vinculin in order to test the functionality of these nominal pathways. In chapter 3, this approach to mechanotransduction research is scaled up via a high content imaging platform allowing for the study of multiple focal adhesion proteins and the effect of their knockdown on mechanosensitive stem cell differentiation along multiple lineages.

1.6 References

1. Chen, K.D., Li, Y.S., Kim, M., Li, S., Yuan, S., Chien, S., and Shyy, J.Y. (1999). Mechanotransduction in response to shear stress. Roles of receptor tyrosine kinases, integrins, and Shc. The Journal of biological chemistry *274*, 18393-18400.

2. Ingber, D.E. (1997). Tensegrity: the architectural basis of cellular mechanotransduction. Annu Rev Physiol *59*, 575-599.

3. Szafranski, J.D., Grodzinsky, A.J., Burger, E., Gaschen, V., Hung, H.H., and Hunziker, E.B. (2004). Chondrocyte mechanotransduction: effects of compression on deformation of intracellular organelles and relevance to cellular biosynthesis. Osteoarthritis Cartilage *12*, 937-946.

4. Tschumperlin, D.J., Dai, G.H., Maly, I.V., Kikuchi, T., Laiho, L.H., McVittie, A.K., Haley, K.J., Lilly, C.M., So, P.T.C., Lauffenburger, D.A., et al. (2004). Mechanotransduction through growth-factor shedding into the extracellular space. Nature *429*, 83-86.

5. Pelham, R.J., Jr., and Wang, Y.L. (1998). Cell locomotion and focal adhesions are regulated by the mechanical properties of the substrate. Biol Bull *194*, 348-349; discussion 349-350.

6. Dunn, G.A., and Brown, A.F. (1986). Alignment of fibroblasts on grooved surfaces described by a simple geometric transformation. J Cell Sci *83*, 313-340.

7. Xiao, Y., and Truskey, G.A. (1996). Effect of receptor-ligand affinity on the strength of endothelial cell adhesion. Biophys J *71*, 2869-2884.

8. Gudi, S.R., Clark, C.B., and Frangos, J.A. (1996). Fluid flow rapidly activates G proteins in human endothelial cells. Involvement of G proteins in mechanochemical signal transduction. Circ Res *79*, 834-839.

9. Loth, F., Fischer, P.F., Arslan, N., Bertram, C.D., Lee, S.E., Royston, T.J., Shaalan, W.E., and Bassiouny, H.S. (2003). Transitional flow at the venous anastomosis of an arteriovenous graft: potential activation of the ERK1/2 mechanotransduction pathway. J Biomech Eng *125*, 49-61.

10. Katsumi, A., Naoe, T., Matsushita, T., Kaibuchi, K., and Schwartz, M.A. (2005). Integrin activation and matrix binding mediate cellular responses to mechanical stretch. The Journal of biological chemistry *280*, 16546-16549.

11. Ahmed, W.W., Wolfram, T., Goldyn, A.M., Bruellhoff, K., Rioja, B.A., Moller, M., Spatz, J.P., Saif, T.A., Groll, J., and Kemkemer, R. (2010). Myoblast morphology and organization on biochemically micro-patterned hydrogel coatings under cyclic mechanical strain. Biomaterials *31*, 250-258.

12. Resnick, A. (2010). Use of optical tweezers to probe epithelial mechanosensation. J Biomed Opt *15*, 015005.

13. Lamontagne, C.A., Cuerrier, C.M., and Grandbois, M. (2008). AFM as a tool to probe and manipulate cellular processes. Pflugers Arch *456*, 61-70.

14. Hughes, S., McBain, S., Dobson, J., and El Haj, A.J. (2008). Selective activation of mechanosensitive ion channels using magnetic particles. J R Soc Interface *5*, 855-863.

15. Evans, E., and Kinoshita, K. (2007). Using force to probe single-molecule receptor-cytoskeletal anchoring beneath the surface of a living cell. Methods Cell Biol *83*, 373-396.

16. Pelham, R.J., Jr., and Wang, Y. (1997). Cell locomotion and focal adhesions are regulated by substrate flexibility. Proc Natl Acad Sci U S A *94*, 13661-13665.

17. Yamaki, K., Harada, I., Goto, M., Cho, C.S., and Akaike, T. (2009). Regulation of cellular morphology using temperature-responsive hydrogel for integrin-mediated mechanical force stimulation. Biomaterials *30*, 1421-1427.

18. Gray, D.S., Tien, J., and Chen, C.S. (2003). Repositioning of cells by mechanotaxis on surfaces with micropatterned Young's modulus. J Biomed Mater Res A *66*, 605-614.

19. Khatiwala, C.B., Kim, P.D., Peyton, S.R., and Putnam, A.J. (2009). ECM compliance regulates osteogenesis by influencing MAPK signaling downstream of RhoA and ROCK. J Bone Miner Res *24*, 886-898.

20. Solon, J., Levental, I., Sengupta, K., Georges, P.C., and Janmey, P.A. (2007). Fibroblast adaptation and stiffness matching to soft elastic substrates. Biophys J *93*, 4453-4461.

21. Engler, A.J., Sen, S., Sweeney, H.L., and Discher, D.E. (2006). Matrix elasticity directs stem cell lineage specification. Cell *126*, 677-689.

22. McBeath, R., Pirone, D.M., Nelson, C.M., Bhadriraju, K., and Chen, C.S. (2004). Cell shape, cytoskeletal tension, and RhoA regulate stem cell lineage commitment. Dev Cell *6*, 483-495.

23. Tan, J.L., Tien, J., Pirone, D.M., Gray, D.S., Bhadriraju, K., and Chen, C.S. (2003). Cells lying on a bed of microneedles: an approach to isolate mechanical force. Proc Natl Acad Sci U S A *100*, 1484-1489.

24. Lo, C.M., Wang, H.B., Dembo, M., and Wang, Y.L. (2000). Cell movement is guided by the rigidity of the substrate. Biophysical journal *79*, 144-152.

25. Sant, S., Hancock, M.J., Donnelly, J.P., Iyer, D., and Khademhosseini, A. (2010). Biomimetic Gradient Hydrogels for Tissue Engineering. Can J Chem Eng *88*, 899-911.

26. Tse, J.R., and Engler, A.J. (2011). Stiffness gradients mimicking in vivo tissue variation regulate mesenchymal stem cell fate. PLoS One *6*, e15978.

27. Isenberg, B.C., Dimilla, P.A., Walker, M., Kim, S., and Wong, J.Y. (2009). Vascular smooth muscle cell durotaxis depends on substrate stiffness gradient strength. Biophys J *97*, 1313-1322.

28. Wang, N., Butler, J.P., and Ingber, D.E. (1993). Mechanotransduction across the Cell-Surface and through the Cytoskeleton. Science *260*, 1124-1127.

29. Brosig, M., Ferralli, J., Gelman, L., Chiquet, M., and Chiquet-Ehrismann, R. (2010). Interfering with the connection between the nucleus and the cytoskeleton affects nuclear rotation, mechanotransduction and myogenesis. Int J Biochem Cell B *42*, 1717-1728.

30. Engler, A.J., Carag-Krieger, C., Johnson, C.P., Raab, M., Tang, H.Y., Speicher, D.W., Sanger, J.W., Sanger, J.M., and Discher, D.E. (2008). Embryonic cardiomyocytes beat best on a matrix with heart-like elasticity: scar-like rigidity inhibits beating. J Cell Sci *121*, 3794-3802.

31. Chen, C.S., Tan, J., and Tien, J. (2004). Mechanotransduction at cell-matrix and cell-cell contacts. Annu Rev Biomed Eng *6*, 275-302.

32. Lim, Y., Lim, S.T., Tomar, A., Gardel, M., Bernard-Trifilo, J.A., Chen, X.L., Uryu, S.A., Canete-Soler, R., Zhai, J., Lin, H., et al. (2008). PyK2 and FAK connections to p190Rho guanine nucleotide exchange factor regulate RhoA activity, focal adhesion formation, and cell motility. J Cell Biol *180*, 187-203.

33. Lu, M.J., and Ravichandran, K.S. (2006). Dock180-ELMO cooperation in Rac activation. Method Enzymol *406*, 388-402.

34. VanAelst, L., and DSouzaSchorey, C. (1997). Rho GTPases and signaling networks. Gene Dev *11*, 2295-2322.

35. Amano, M., Ito, M., Kimura, K., Fukata, Y., Chihara, K., Nakano, T., Matsuura, Y., and Kaibuchi, K. (1996). Phosphorylation and activation of myosin by Rho-associated kinase (Rho-kinase). Journal of Biological Chemistry *271*, 20246-20249.

36. Kimura, K., Ito, M., Amano, M., Chihara, K., Fukata, Y., Nakafuku, M., Yamamori, B., Feng, J.H., Nakano, T., Okawa, K., et al. (1996). Regulation of myosin phosphatase by Rho and Rho-Associated kinase (Rho-kinase). Science *273*, 245-248.

37. Palazzo, A.F., Cook, T.A., Alberts, A.S., and Gundersen, G.G. (2001). mDia mediates Rho-regulated formation and orientation of stable microtubules. Nature cell biology *3*, 723-729.

38. Hamill, O.P., and McBride, D.W., Jr. (1996). A supramolecular complex underlying touch sensitivity. Trends Neurosci *19*, 258-261.

39. Clapham, D.E. (2003). TRP channels as cellular sensors. Nature *426*, 517-524.

40. Follonier, L., Schaub, S., Meister, J.J., and Hinz, B. (2008). Myofibroblast communication is controlled by intercellular mechanical coupling. J Cell Sci *121*, 3305-3316.

41. Kobayashi, T., and Sokabe, M. (2010). Sensing substrate rigidity by mechanosensitive ion channels with stress fibers and focal adhesions. Current Opinion in Cell Biology *22*, 669-676.

42. Blumenthal, D.K., and Stull, J.T. (1980). Activation of skeletal muscle myosin light chain kinase by calcium(2+) and calmodulin. Biochemistry *19*, 5608-5614.

43. Dedman, A., Sharif-Naeini, R., Folgering, J.H., Duprat, F., Patel, A., and Honore, E. (2009). The mechano-gated K(2P) channel TREK-1. Eur Biophys J *38*, 293-303.

44. del Rio, A., Perez-Jimenez, R., Liu, R.C., Roca-Cusachs, P., Fernandez, J.M., and Sheetz, M.P. (2009). Stretching Single Talin Rod Molecules Activates Vinculin Binding. Science *323*, 638-641.

45. Golji, J., Lam, J., and Mofrad, M.R. Vinculin activation is necessary for complete talin binding. Biophys J *100*, 332-340.

46. Sawada, Y., Tamada, M., Dubin-Thaler, B.J., Cherniavskaya, O., Sakai, R., Tanaka, S., and Sheetz, M.P. (2006). Force sensing by mechanical extension of the Src family kinase substrate p130Cas. Cell *127*, 1015-1026.

47. von Wichert, G., Jiang, G., Kostic, A., De Vos, K., Sap, J., and Sheetz, M.P. (2003). RPTP-alpha acts as a transducer of mechanical force on alphav/beta3-integrin-cytoskeleton linkages. J Cell Biol *161*, 143-153.

48. Uehata, M., Ishizaki, T., Satoh, H., Ono, T., Kawahara, T., Morishita, T., Tamakawa, H., Yamagami, K., Inui, J., Maekawa, M., et al. (1997). Calcium sensitization of smooth muscle mediated by a Rho-associated protein kinase in hypertension. Nature *389*, 990-994.

49. Darenfed, H., Dayanandan, B., Zhang, T., Hsieh, S.H., Fournier, A.E., and Mandato, C.A. (2007). Molecular characterization of the effects of Y-27632. Cell Motil Cytoskeleton *64*, 97-109.

50. Dumbauld, D.W., Shin, H., Gallant, N.D., Michael, K.E., Radhakrishna, H., and Garcia, A.J. (2010). Contractility Modulates Cell Adhesion Strengthening Through Focal Adhesion Kinase and Assembly of Vinculin-Containing Focal Adhesions. Journal of Cellular Physiology *223*, 746-756.

51. Rief, M., Gautel, M., Oesterhelt, F., Fernandez, J.M., and Gaub, H.E. (1997). Reversible unfolding of individual titin immunoglobulin domains by AFM. Science *276*, 1109-1112.

52. Chen, H., Cohen, D.M., Choudhury, D.M., Kioka, N., and Craig, S.W. (2005). Spatial distribution and functional significance of activated vinculin in living cells. J Cell Biol *169*, 459-470.

53. Kellermayer, M.S., Smith, S.B., Granzier, H.L., and Bustamante, C. (1997). Folding-unfolding transitions in single titin molecules characterized with laser tweezers. Science *276*, 1112-1116.

54. Jaalouk, D.E., and Lammerding, J. (2009). Mechanotransduction gone awry. Nature reviews. Molecular cell biology *10*, 63-73.

55. Aihara, M., Dobashi, K., Iizuka, K., Nakazawa, T., and Mori, M. (2004). Effect of Y-27632 on release of cytokines from peripheral T cells in asthmatic patients and normal subjects. Int Immunopharmacol *4*, 557-561.

56. Berry, M.F., Engler, A.J., Woo, Y.J., Pirolli, T.J., Bish, L.T., Jayasankar, V., Morine, K.J., Gardner, T.J., Discher, D.E., and Sweeney, H.L. (2006). Mesenchymal stem cell injection after myocardial infarction improves myocardial compliance. Am J Physiol Heart Circ Physiol *290*, H2196-2203.

Chapter 2

In Situ Mechanotransduction via Vinculin Regulates Stem Cell Differentiation

Abstract

Human mesenchymal stem cell (hMSC) proliferation, migration, and differentiation have all been linked to extracellular matrix stiffness, yet the signaling pathway(s) that are necessary for mechanotransduction remain unproven. Vinculin has been implicated as a mechanosensor *in vitro*, but here we demonstrate its ability to also regulate stem cell behavior, including hMSC differentiation. RNA interference-mediated vinculin knockdown significantly decreased stiffness-induced MyoD, a muscle transcription factor, but not Runx2, an osteoblast transcription factor, and impaired stiffness-mediated migration. A kinase binding accessibility screen predicted a cryptic MAPK1 signaling site in vinculin that could regulate these behaviors. Indeed, reintroduction of vinculin domains into knocked-down cells indicated that MAPK1 binding site-containing vinculin constructs were necessary for hMSC expression of

MyoD. Vinculin knockdown does not appear to interfere with focal adhesion assembly, significantly alter adhesive properties, or diminish cell traction force generation, indicating that its knockdown only adversely affected MAPK1 signaling. These data provide some of the first evidence that a force-sensitive adhesion protein can regulate stem cell fate.

2.1 Introduction

Multipotent human mesenchymal stem cells (hMSCs) have been shown to differentiate based on a wide variety of cues, including soluble growth factors and insoluble signals from extracellular matrix (ECM) to which cells bind [1], namely stiffness [2, 3], topography [4], and composition [5]. Modulating cell behavior by ECM stiffness has become increasingly relevant since disease-related stiffness increases [6, 7] may give rise to the mixed outcomes of cell-based therapies [8, 9]. hMSCs cultured in serum-containing media have been shown to differentiate as a function of their substrate stiffness, with their fate matching *in vivo* tissue stiffness [2]. Myosin contractility has been implicated in regulating these fate choices via RhoA/ROCK *in situ* [10], and recent evidence has indicated that the transcriptional regulators Yes-associated protein (YAP) and transcriptional coactivator with PDZ-binding motif (TAZ) are required for hMSCs responding to stiffness [11]. While force transmission and nuclear responses are clearly required, the specific upstream signaling cascade(s) from which they initiate remains unclear for stem cells [12, 13].

Ample evidence suggests that cells actively measure the strains they impose on their matrix through myosin contraction [14, 15]; softer matrix deforms more than stiffer

matrix does for a given force. Conversely, intracellular proteins connecting matrix and nucleus stretch more with increasing ECM stiffness under the same force [16]. The conversion of this additional protein stretch into a biochemical cue that could induce RhoA/ROCK activation and lineage specification has been suggested to arise from sensor(s) buried within focal adhesions or the perinuclear cytoskeleton [17, 18]. Since the ECM protein to which stem cells bind can affect whether or not stiffness-induced fate choice occur [3], ligation of a specific integrin pair likely initiates this signal and suggests an initial focus on an adhesion-based sensor capable of regulating hMSC fate. Such a mechanism, i.e. a "molecular strain gauge" [19], would respond to increases in actomyosin force generation by unfolding protein domains to a degree corresponding to the force to which they are subjected; newly exposed internal binding sites would therefore initiate new signaling cascades. *In vitro* data supports this strain gauge hypothesis for focal adhesion proteins, which undergo force-induced conformational changes. For example, forced-unfolding of p130Cas reveals phosphorylation sites responsible for recruiting other proteins necessary for assembly of mature adhesions [20]. Talin exposes up to 11 inaccessible vinculin binding sites under force [21], with vinculin separately binding, unfolding, and functioning differently depending on the amount of force to which it is subjected [22]. Though each adhesion protein may serve as a target for stem cell mechanosensing, a comprehensive list of novel candidates is lacking, and to date, no study has shown this type of sensing mechanism that can regulate stem cell fate. Here we show that one candidate signaling mechanism and potential molecular strain gauge, the talin-vinculin-MAPK1 cascade, may be a regulator of stem cell differentiation into a myogenic-like state.

2.2 Materials and Methods

2.2.1 Cell Culture and Reagents

Human mesenchymal stem cells were obtained from Lonza, Inc. and maintained in growth medium (DMEM, 20% FBS, 100 units/mL penicillin, and 100 μg/mL streptomycin) changed every three days. Only low passage hMSCs were used for experimental studies. For MAPK1 inhibition, the MAPK inhibitors iodotubercidin and pyrazolylpyrrole, dissolved in DMSO, were used at a final concentration of 0.2 μM and 2 nM, respectively, and added to cells immediately post-plating. At 0.2 μM, 5-iodotubercidin is a potent MAPK1 inhibitor, but is not concentrated enough to inhibit PKA, phosphorylase kinase (5 μM), casein kinases I and II (0.4 μM and 11 μM, respectively), Insulin Receptor Kinase (3.5 μM), or PKC (0.4 μM). Adenosine Kinase is inhibited at very low iodotubercidin concentrations (26 nM) [23], but has not been previously implicated in myogenesis. At 2 nM, pyrazolylpyrrole has only been shown to inhibit MAPK1 [24]. As siRNA is diluted in culture over time, all mechanical differences in cell populations were assessed while there was still a large difference in cellular vinculin levels, as biophysical metrics are often a function of the current state of the cell, i.e. day 2 or as otherwise indicated. Conversely, differentiation experiments took place over the course of six days or as otherwise indicated, since differentiation occurs as the integration of cues over time, allowing one to assume that examining the cells over the course of six days still reflects the initial RNAi.

2.2.2 Polyacrylamide Hydrogel Fabrication:

Acrylamide was polymerized on aminosilanized 12 or 25 mm diameter coverslips. A solution containing the crosslinker N, N' methylene-bis-acrylamide, acrylamide, 1/100 volume 10% Ammonium Persulfate and 1/1000 volume of N, N, N', N'-Tetramethylethylenediamine was mixed. Two different combinations of acrylamide and bis-acrylamide were used to make 11 and 34 kPa substrates. Approximately 12 or 50 uL of the mixed solution was placed between the aminosilanized coverslip and a chlorosilanized glass slide. 100 ug/mL collagen I was chemically crosslinked to the substrates using the photoactivating crosslinker Sulfo-SANPAH (Pierce).

2.2.3 siRNA Transfection

siRNA oligonucleotides against human vinculin (ON-TARGETplus SMARTpool; Dharmacon) and a pool of four non-targeting siRNAs control oligonucleotides (ON-TARGETplus siControl; Dharmacon), diluted in DEPC water (OmniPure, EMD) and 5X siRNA buffer (ThermoScientific), were transiently transfected into human hMSCs using Dharmafect (Dharmacon) at a concentration of 50 nM, according to the manufacturers' protocols. Vinculin ON-TARGETplus SMARTpool was a mix consisting of four different siRNAs: Vinculin smart pool duplex 1 (target sequence: CAGCAUUUAUUAAGGUUGA), Vinculin smart pool duplex 2 (target sequence: GCCAAGCAGUGCACAGAUA), Vinculin smart pool duplex 3 (target sequence: GAGCGAAUCCCAACCAUAA), and Vinculin smart pool duplex 4 (target sequence: UGAGAUAAUUCGUGUGUUA). Transfection efficiency was characterized using TYE-563 Transfection Control (IDT). After 24 hours of transfection in antibiotic-free

media (2% FBS), media was replaced with standard hMSC growth media and cells replated onto appropriate substrates.

2.2.4 Plasmid Construct and Transfection

pEGFP-C1 subcloned with vinculin cDNA of head domain (1-851; labeled as H), pEGFP-C3 subcloned with vinculin cDNA of tail domain (884-1066; labeled as T), and pEGFP-C1 subcloned with complete vinculin cDNA, which had been originally excised from p1005 with EcoRI and inserted in EcoRI digested pEGFP-C1 (labeled as FL), were obtained from Dr. Susan Craig [25]. Plasmids were purified using QIAGEN Plasmid Midi Kit (QIAGEN). hMSCs were transfected in antibiotic-free medium with 1 μg of plasmid pre-complexed with 2 μL of Lipofectamine 2000 (Life Technologies) in 100 μL of DMEM. After 24 hours of transfection in antibiotic-free medium with 2% FBS, medium was replaced with standard hMSC growth medium.

2.2.5 Site Directed Mutagenesis

Site-directed mutagenesis was performed on plasmid pEGFP-C1 (full length; FL) by PCR using QuikChange II kits (Agilent) to abolish the predicted MAPK1 binding site from ScanSite analysis. The predicted site (amino acids 762-768) was changed from RILLVAK to HVVILGR by the following base pair substitutions on the leading strand: G3674A, A3676G, C3679G, C3682A, G3685C, C3689G, and A3692G. Mutagenic primers were designed using Agilent Technologies' QuikChange Primer Design software:

CTTCTGAATTTTCAACCTCCCGTCTTCCCAGAATCACGACGTGGTTCGCTCGT

CTAGCAATGCTG and CAGCATTGCTAGACGAGCGAACCACGTCGTGATTC TGGGAAGACGGGAGGTTGAAAATTCAGAAG. Mutagenesis plasmids were sequenced via Sanger Sequencing by GeneWiz (La Jolla, CA).

2.2.6 Western Blots

Cells were plated at a density of 5,000 cells/cm^2 in 24 well plates. Cell lysates were collected by rinsing samples with cold PBS, followed by a five minute lysis in mRIPA buffer (50 mM HEPES pH 7.5, 150 mM NaCl, 1.5 mM $MgCl_2$, 1% Triton, 1% Na-DOC, 0.1% SDS) with 1mM EGTA, 1 mM Na_3VO_4, 10 mM $Na_4P_2O_7$, and 1 mM PMSF. Samples were stored at -80^o C until analysis. Cell lysates were run in 10% SDS-PAGE gels at 150 V until proteins were separated and transferred to PVDF membranes (Bio-Rad) by running at 100 V for 1 hour, 15 minutes in transfer apparatus (Bio-Rad). The membranes were washed in Buffer A (25 mM Tris-HCl, 150 mM NaCl, 0.1% Tween-20) + 5% milk overnight at 4^{o}C. The membranes were then incubated with anti-Vinculin, GAPDH, Actin, ERK2, or p-ERK2 (T202 and Y204) for 1 hour, washed with Buffer A + milk, and incubated in streptavidin horseradish-peroxidase-conjugated anti-mouse antibodies for 30 minutes at room temperature. Immunoblots were visualized using ECL reagent (Adenna). All western blot antibodies were obtained from Abcam.

2.2.7 Immunoprecipitation

1 mM Dithiobis(succinimidyl propionate) (DSP; Pierce), a membrane-permeable amine crosslinker, was used to preserve protein interactions before cell lysis. Protein A-conjugated Magnetic Dynabeads (Invitrogen) (concentration) were bound to rabbit anti-

vinculin antibody for 15 minutes at room temperature, and crosslinked lysates were added for one hour at 4^{o} C. Beads were magnetically captured, lysate decanted, and the beads were then washed with PBS. Protein elution from the beads was performed in 50 mM Glycine, pH 2.8. Supernatants and pellets were prepared for western blot analysis as described above.

2.2.8 Immunofluorescence

hMSC cells were cultured on polyacrylamide gels, fixed with 3.7% formaldehyde, and permeabilized with 1% Triton-X. The cells were then stained with primary antibodies against human Vinculin (ab18058 and ab129002, Abcam), human MyoD (MAB3878, Millipore), human pFAK (16-233, Millipore), human Paxillin (ab32084, Abcam), human pERK2 (ab7948, Abcam), human ERK2 (ab7948, Abcam), human GAPDH (ab8245, Abcam) or human CBFα1 (CBFA11-A, Alpha Diagnostics). Corresponding secondary antibodies were conjugated to Alexa Fluor 488 (FITC) or Alexa Fluor 647 (Cy5) (Invitrogen). Nuclei were counterstained with Hoechst dye (Sigma), and the actin cytoskeleton was stained with Rhodamine-conjugated Phalloidin (Invitrogen). Alternatively for live/dead assays, cells were treated with paraformaldehyde for a positive control. Calcein and EthD-1 were then incubated with cultures to stain live and dead cells, respectively. Cells were imaged with a Nikon Eclipse Ti-S inverted fluorescence microscope equipped with a BD Carv II camera. Images were processed and analyzed with ImageJ software (NIH). Image thresholding for display purposes was consistent for each channel and within a given experiment.

2.2.9 Alkaline Phosphatase (ALP) Staining

Cells in the indicate conditions were fixed in 3.7% formaldehyde, rinse in water, and incubated in a water:Napthol-phosphate:fast red violet solution (1:1:2 ratio) for 30 min according to the manufacturer's instructions (Millipore). Cells were rinsed and imaged in brightfield as with a Nikon Eclipse Ti-S inverted fluorescence microscope equipped with a BD Carv II camera.

2.2.10 Quantitative PCR

mRNA was obtained using a previously published protocol [26]. Briefly, cells were lysed in trizol, separated with chloroform, and precipitated by isopropanol. The samples were centrifuged, the supernatant removed, and the pellet washed with 75% ethanol. After removing the supernatant, samples were resuspended in DEPC water. Reverse transcription polymerase chain reaction was performed at 37^{o} C for 60 minutes, followed by 99^{o} C for 5 minutes, followed by 5^{o} C for 5 minutes. Samples containing 2 μg of cDNA were added to a master mix containing of 10 mM dNTP (Roche), 100 mM DTT (Invitrogen), 5X First Strand Buffer (Invitrogen), 50 mM Random Hexamers (Qiagen), 200U/μL Reverse Transcriptase (Invitrogen), and DEPC H_2O. qPCR was then performed using an 7900HT Fast Real-Time PCR machine (Applied Biosystems). Primers coding for Pax3, Pax7, MyoD, Mrf4, Myf5, GAPDH, and the vinculin constructs H, T and FL are listed in Supplemental Table 2. For differentiation markers, data is shown relative to the undifferentiated cells. Data was analyzed using a previously described method [27].

2.2.11 Traction Force Microscopy

Cells were plated at 10^2 cells/cm^2 onto 2 kPa 25 mm diameter PA hydrogels to ensure that only individual cells spaced far apart were present so that traction fields would not overlap. 0.2 μm diameter fluorescent microspheres (FluoSpheres, Invitrogen) were added to hydrogels in suspension, at a ratio of 30 μL of beads for every 1 mL PA solution. 2 kPa hydrogels were selected due to their optimal deformation levels in response to cellular traction, allowing for an increased resolution of traction force as compared to 11 kPa; tractions scale linearly with stiffness so results from softer matrix should reflect the same trends for stiffer substrates. In order to prevent bead agglomeration, PA/bead suspensions were vortexed, sonicated for 15 minutes in a water bath, then centrifuged for 5 minutes at 12,000 RPM. The aqueous phase of the suspension was then transferred into a fresh eppendorf tube for polymerization initiation. After 2 days, gels were transferred to a 25 mm sealed coverslip dish and placed in a 160 x 110 mm sealed glass chamber insert (ASI Imaging) for imaging. After identifying a candidate cell in brightfield at 60x, the absolute stage position was stored in the computer. A 50 image, 0.4 micron incremented, 20 micron total Z-stack was obtained using the confocal microscope and the automated stage control. After imaging other cells in the same way, warm 2.5% Trypsin was added to the coverslip dish to detach the cells. Using the stored position data, confocal Z-stacks of equal dimensions were taken at each previously imaged location. These stacks were then used to obtain measurements for the total strain energy generated by the cell, broken down into tangential and normal strain, as well as total substrate deformation (Figure 13) [28].

2.2.12 Cell Spinning Assay

Cell spinning assay was performed as described previously [29]. Briefly, knockdown and wild type cells (50,000 cells per gel) were plated onto 25 mm collagen coated coverslips. After 24 hours, coverslips were placed into the spinning apparatus and subjected to 4000 RPM spin for 5 minutes, followed immediately by fixation with 3.7% paraformaldehyde. Cells were then stained with DAPI, and using the ScanSlide function of the automated stage (MetaMorph), the entire coverslip was imaged. Images were then analyzed in MATLAB using unpublished code developed by Alexander Fuhrmann, in which the image is thresholded and the number of nuclei at a given radius 'shell' is plotted against radius (Figure 11).

2.2.13 Statistics

All experiments were performed in triplicate with the number of cells analyzed per condition as indicated. Error bars are shown as standard deviation. Significance was assessed by ANOVA at a significance threshold of $p<0.05$ or lower as indicated. Values between 0.1 and 0.05 are noted as well. For instances where data is not significantly different, N.S. is stated.

2.3 Results

2.3.1 Vinculin Knockdown Adversely Affects hMSC Fate and Behavior

To ascertain vinculin's role in mechanotransduction, hMSC vinculin was transiently knocked down with siRNA up to 80% (Figure 1A), reducing both cytoplasmic

and focal adhesion-localized vinculin (Figure 3A, top). Firm, 11 kPa matrices induce peak expression of early myogenic transcription factors, e.g. MyoD [2], after 4 days in culture with a subsequent decrease in expression consistent sequential activation of myogenic factors in muscle [26, 30]. However, vinculin knockdown hMSCs on the same matrix showed significantly less MyoD (Figure 3A, bottom). Scrambled siRNA showed no effect on MyoD expression (Figure 1B) whereas no MyoD was produced on non-permissive, stiff matrix independent of vinculin (Figure 3B). Quantitative PCR of hMSCs after 4 days in culture, when MyoD expression was strongest, showed that they express significantly more myogenic specification and commitment markers relative to undifferentiated cells; this is consistent with commitment and initial differentiation into a myogenic lineage [31]. Vinculin knockdown cells had significantly reduced expression of the same transcription factors relative to undifferentiated control cells (Figure 3C). Vinculin knockdown was transient (Figure 1A), so we also determined if cells could become myogenic once vinculin expression recovered. Indeed, MyoD expression, which was repressed at 4 days in culture in vinculin knockdown hMSCs relative to wild type cells, was induced in hMSCs after 12 days (Figure 1C). To determine if vinculin also affected osteogenic induction on stiff matrices, hMSCs were plated onto 34 kPa matrix but osteogenic commitment was found to be insensitive to vinculin knockdown as observed by expression of CBFα1 (Figure 2A) and alkaline phosphatase staining (Figure 2B), indicating that vinculin is at least necessary to sense matrix stiffness but only for a specific differentiation program.

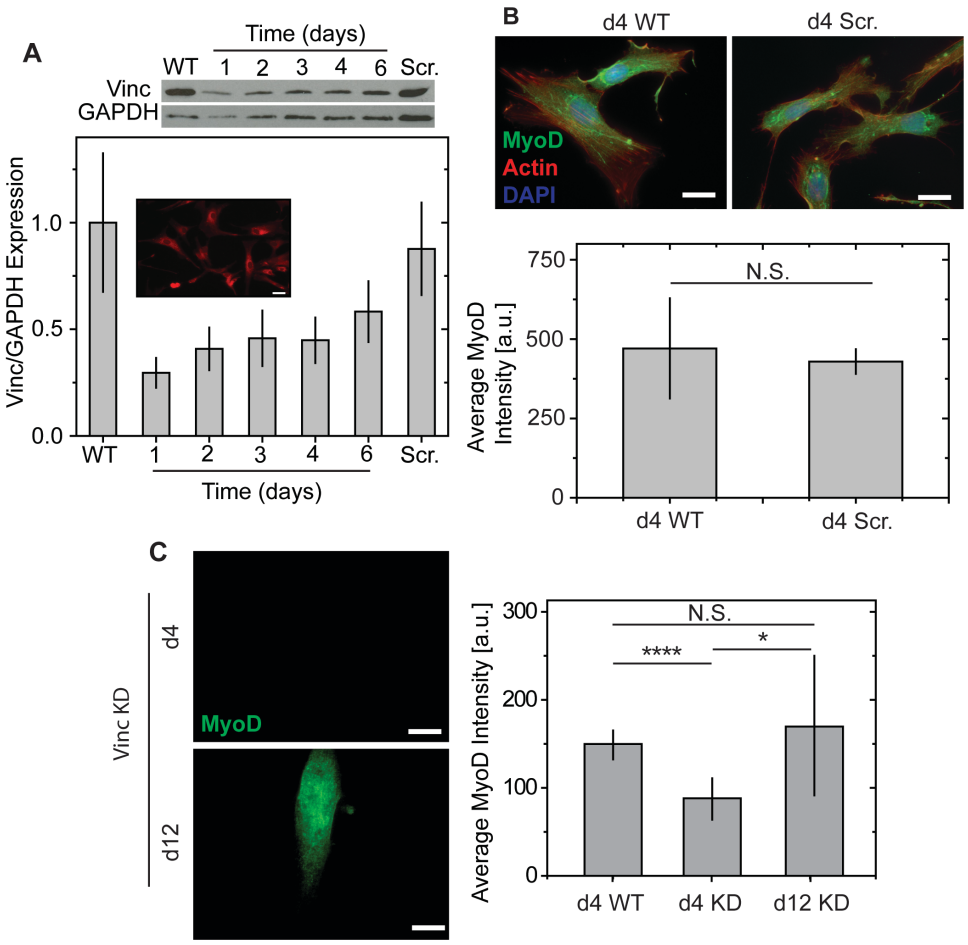

Figure 1: Influence of Vinculin on hMSCs. A) Western blots for vinculin and GAPDH are shown for cells treated with siRNA for vinculin over the indicated time course. The plot quantifies vinculin knock down after 24 hours of approximately 80% when normalized to GAPDH band intensity at each time point or condition. Characteristic recovery was observed over one week. Transfection efficiency was confirmed using a fluorescent siGLO oligomer (inset). B) MyoD stained images of non-targeting control siRNA (scrambled) did not show a significant difference in MyoD expression versus wild type (WT) as quantified by fluorescent intensity. C) MyoD stained images of vinculin knockdown cells cultured for 4 and 12 days recover MyoD expression only after 12 days in culture. *$p < 0.05$, ****$p < 0.0001$, N.S. = not significant. Scale Bars: B, C = 10 μm,

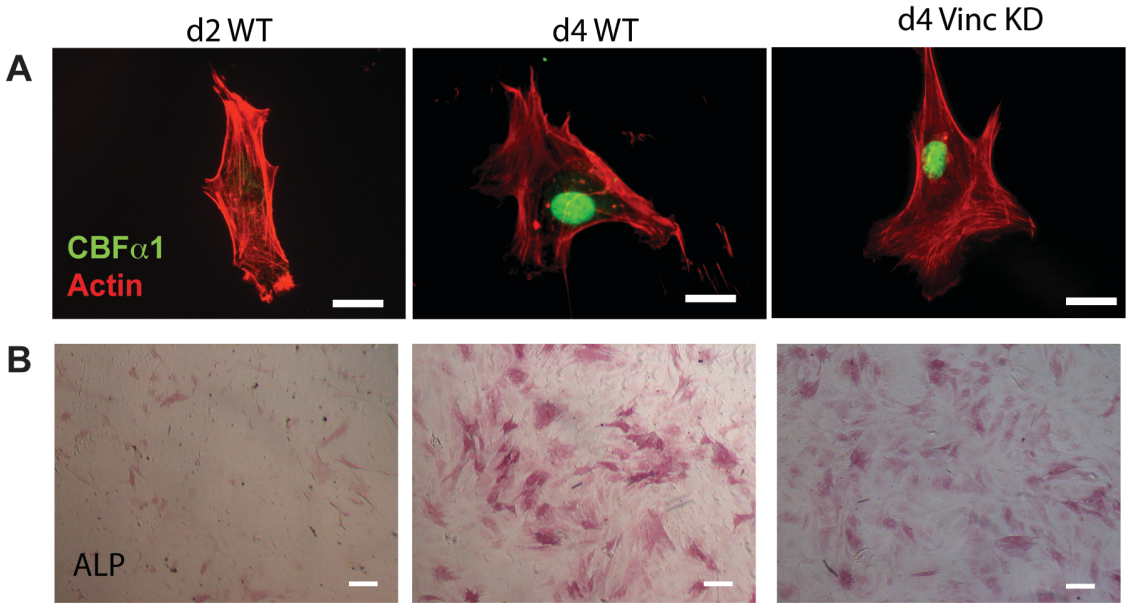

Figure 2: Vinculin Knockdown and Osteogenic Differentiation. hMSCs on 34 kPa matrices acquired expression of CBFA1, an osteogenic marker, between days 2 and 4 in culture. Vinculin knockdown did not affect the expression of A) CBFa1 or B) ALP. Scale Bars: A = 10 μm, B = 50 μm.

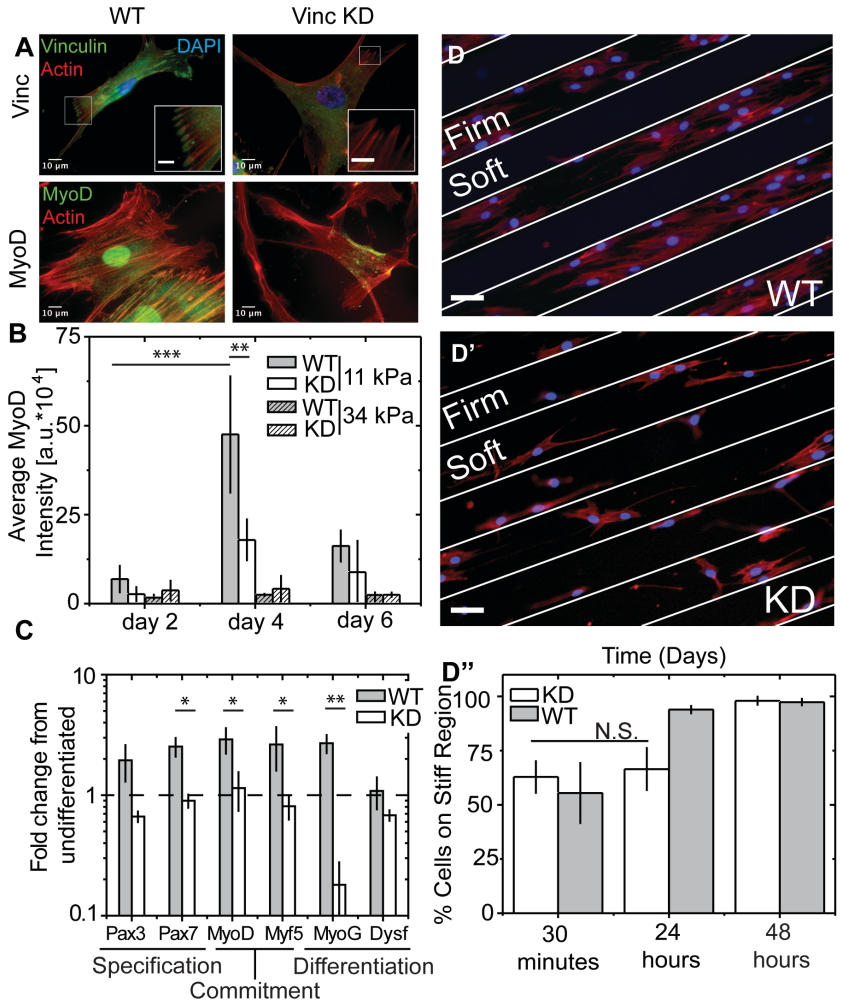

Figure 3: Vinculin Regulates hMSC Fate and Migration. A) Vinculin knockdown in hMSCs two days post-transfection shows a decrease in both cytoplasmic vinculin as well as a reduction in staining for vinculin incorporated into focal adhesions (inset; top). MyoD staining of vinculin knockdown hMSCs on 11 kPa matrices four days post-transfection show a reduction in stiffness-based differentiation. Red Channel: Actin, Blue Channel: DAPI (omitted from MyoD images). B) Average density of MyoD immunofluorescent intensity peaks after four days of plating on 11 kPa matrices, with approximately 60% reduction in signal as a result of vinculin knockdown. Little expression was observed on 34 kPa matrices. $^{**}p < 0.01$, $^{***}p < 0.001$ as determined by ANOVA. C) Quantitative PCR of myogenic markers in wild type hMSCs and vinculin-knockdown cells plated for four days on 11 kPa compared to undifferentiated control hMSCs. $^{*}p < 0.05$ as determined by ANOVA. D, D') hMSCs were plated onto a matrix containing alternating regions of soft (1 kPa) and firm (11 kPa) matrix. Images shown are 24 hours post plating for wild type (top) and vinculin knockdown (bottom). Red Channel: Actin, Blue Channel: DAPI. D") Quantification of the percentage of vinculin knockdown and WT hMSCs on stiff regions at the indicated time. N.S. = not significant as determined by ANOVA. Scale bars: A = 10 μm, A (inset) = 2.5 μm, D = 50 μm

These matrices provide constant stiffness to hMSCs, but rarely does this occur *in vivo*. Spatial stiffness variations can induce migration or 'durotaxis' from non-permissive to permissive matrix. Durotaxis often precedes hMSCs differentiation [32] but may utilize the same sensory machinery. To assess vinculin's involvement in sensing spatial stiffness changes, hMSCs were cultured on matrix containing alternating 'stripes' of soft and firm matrix to create a steep stiffness gradient at their interface (Figure 3D, D'). Vinculin knockdown hMSCs exhibited delayed durotaxis, while within 24 hours, untreated cells preferentially accumulated on myogenic-inducing firm matrix, indicating robust durotaxis (Figure 3D"). Durotactic changes were not the result of cell death [33] or altered cell migration as knockdown and untreated hMSCs on static 1 kPa and 11 kPa substrates had similar migration speed (Figure 4A) and did not display any directionally-biased migration (Figure 4B). Thus, vinculin would appear to be required for sensing stiffness and converting it into an active cell response such as directed migration.

2.3.2 Bioinformatic Analysis of Vinculin's Mechanosensing Potential

A force sensitive unfolding event could change the accessibility of a cryptic kinase site, and thus kinase binding domains and their accessibilities were determined using Scansite [34] for 47 proteins either related to the adhesome or previously implicated in mechanotransduction [35]. This analysis revealed 465 predicted binding sites, which were plotted as a function of their surface accessibility (Figure 5A). Binding sites for MAPK1, also known as ERK2, were found both extremely often (39 times; the most of any binding partner) and were the most inaccessible binding site on average

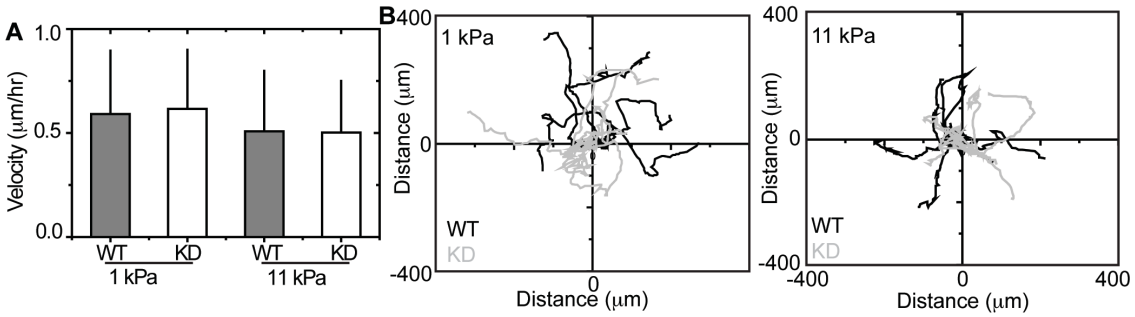

Figure 4: Cell Migration in Knockdown Cells. A) Average hMSC velocity was measured for 24 hours post-plating. Cell velocities were found to be statistically similar regardless of vinculin siRNA treatment. B) Rose plots show no preferential migration patterns of wild type or vinculin knockdown cells on static 1 kPa and 11 kPa hydrogels.

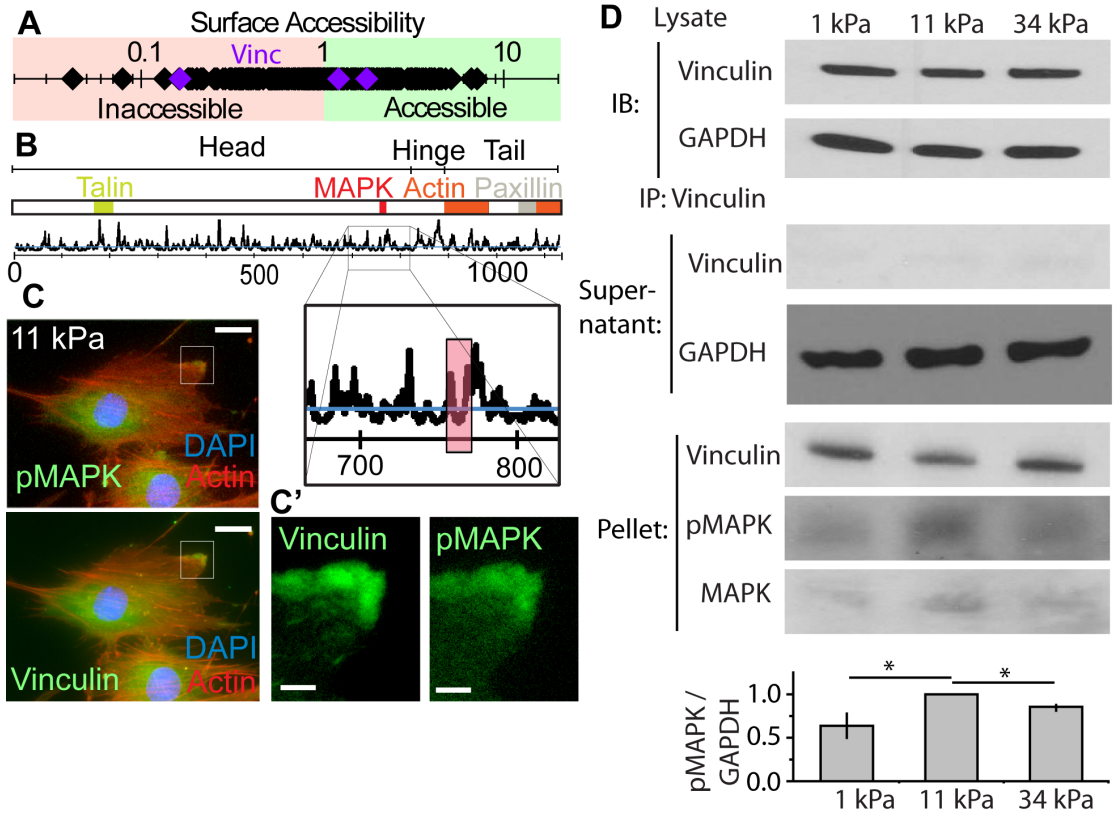

Figure 5: Force-sensitive Cryptic Signaling in Focal Adhesion Proteins. A) Scansite analysis of 47 potential mechanosensing proteins revealed 461 binding motifs at specific accessibility values, each indicated by a black diamond. A value of 1 was used as the threshold for accessibility. Three binding sites were predicted on vinculin indicated by purple diamonds, with one site that is predicated to bind MAPK1 being extremely inaccessible (0.164). B) A domain profile of vinculin, showing binding sites for talin, actin, paxillin, and the predicted inaccessible binding domain for MAPK1, found near the hinge region. The y-axis indicates the amino acid positions along the protein. C) Endogenous expression of vinculin and pMAPK1 in hMSCs cultured on 11 kPa substrates shows co-localization in adhesions. Note that the overall image intensity has been scaled to permit comparison between the two conditions. Scale bars: C = 20 μm, C' = 5 μm. D) Western blots of whole cell lysate from MSCs cultured on the indicated matrices are shown for vinculin and GAPDH (top). Samples were also immunoprecipitated with an antibody for vinculin, and the supernatant and pellet was blotted for vinculin to confirm immunoprecipitation. The pellet was also blotted for MAPK and pMAPK (bottom) as well as GAPDH within the supernatant (center). The graph quantifies band intensity for MAPK normalized to GAPDH for each matrix. *$p < 0.05$ as determined by ANOVA.

(accessibility value of 0.535; Table 1). Vinculin, which has an autoinhibited conformation [36] until it binds to talin and undergoes a force-induced conformational change [21], had three predicted kinase binding sites, one of which is a very inaccessible MAPK1 binding site (Figure 5A, purple; accessibility value of 0.164). This site occurs near vinculin's hinge region and is flanked by structural protein binding sites, implying that a force-induced conformational change in vinculin could occur from relative changes between protein positions; such change may then alter MAPK1 binding site accessibility (Figure 5B). Vinculin and phospho-MAPK1 were also found to co-localize in focal adhesions in hMSC after 48 hours on 11 kPa matrix (Figure 5C). Cell-generated traction force scales with matrix stiffness [16], and thus at an optimal force in hMSCs on 11 kPa matrix, cryptic regions within talin may become accessible via talin unfolding and permit vinculin binding [21] that enhances MAPK1 accessibility. To further substantiate possible vinculin-MAPK1 interaction, vinculin was immunoprecipitated, and MAPK1 and phosphorylated MAPK1 were detected in pulled-down samples (Figure 5D, top). Normalized phosphorylated MAPK also appeared matrix stiffness-dependent (Figure 5D, bottom).

2.3.3 MAPK1-binding Vinculin Domains Rescue Vinculin-Dependent Myogenesis

Despite vinculin's involvement in myogenesis, the specific mechano-signaling pathway(s) regulating stem cell commitment remain unconfirmed. Based on Scansite predictions, constructs expressing GFP and chicken vinculin domains containing or lacking the MAPK1 binding site, i.e. head or tail domains [37], respectively, were

selectively added back to knockdown hMSCs (Figure 6A', Figure 7A). In hMSCs grown on firm matrices for 4 days, wild type cells as well as cells with full length and head domain vinculin added back began to express MyoD at levels similar to wild type (Figure 6A). Tail domain alone was insufficient to completely rescue MyoD expression (Figure 6B), indicating that the head domain of vinculin may be necessary for myogenesis. To assess the necessity of the predicted MAPK1 binding site within the head domain for stiffness-based myogenesis, site directed mutagenesis against the predicted MAPK1 binding domain was performed and confirmed by Sanger Sequencing (Figure 6A', Figure 7B). hMSCs receiving this FL-Mut construct via transfection were unable to express MyoD at wild-type levels after four days (Figure 6C, D). Moreover, Myf5 was detected by immunofluorescence after four days in wild type hMSCs and cells receiving FL constructs, but not FL-Mut constructs (Figure 6E). For all cases, GFP expression, which confirmed vinculin re-expression in knockdown cells, was observed (Figure 6A, C, E, open arrowheads).

Phosphorylated MAPK1 was found to be less abundant on softer matrices as well as in vinculin knockdown cells on stiffer matrices (Figure 8A), indicating that its function may correlate with vinculin expression. MAPK1 is a stage-specific positive regulator of early myogenesis [38-40]. To substantiate that MAPK1 has the same capacity for stiffness-induced hMSC myogenesis, the MAPK1 inhibitor 5-iodotubercidin was selectively added to cells to ablate MAPK1 function and found to down-regulate its expression (Figure 8B). Loss of global MAPK1 function from treatment with 5-iodotubercidin or another highly selective MAPK1 inhibitor, pyrazolylpyrrole, resulted in reduced MyoD expression, similar to the reduction found in vinculin knockdown cells.

Figure 6: Rescue of Myogenesis by Specific Vinculin Domains. A) Wild type hMSCs, vinculin knockdown hMSCs, and vinculin knockdown hMSCs with the addition of GFP and specific chicken vinculin domains containing (head, H; full length, FL) or lacking (tail, T) the MAPK1 binding site predicted by Scansite were plated on 11 kPa matrices. siGLO red positive control confirms transfection in all samples except wild type (closed arrowheads), while GFP is observed in all add back samples (open arrowheads). MyoD staining is observed in wild type, head, and full length samples (arrows). A') Domain charts showing the full length, full length with a mutated MAPK1 binding site to prevent binding, head, and tail constructs. Note that the head domain is orange, the tail domain is yellow, the hinge region is white, and the MAPK1 binding is green unless mutated when it is shown in purple. B) Quantification of average MyoD intensity in the five conditions of panel A. ***$p < 0.001$ as determined by ANOVA. C) Immunofluorescence images of full length and mutated full length rescued cells plated on 11 kPa substrates after 4 days in culture. Images show EGFP (top) and MyoD staining (bottom). GFP and MyoD expression are indicated via open arrowheads and arrows, respectively. D) Quantification of average MyoD intensity in WT, KD, FL, and FL-Mut. *$p<0.05$, ***$p<0.001$, ****$p<0.0001$ as determined by ANOVA. E) Immunofluorescence images of hMSCs at day 0 and 4, with the latter cells being untreated, treated with vinculin siRNA, or treated with vinculin siRNA and a rescue vector as indicated. Wild type cells expressed Myf5 after four days (arrows) while GFP expression (open arrowheads) was used to confirm construct transfection. Scale bars: A, D, and E=20 μm.

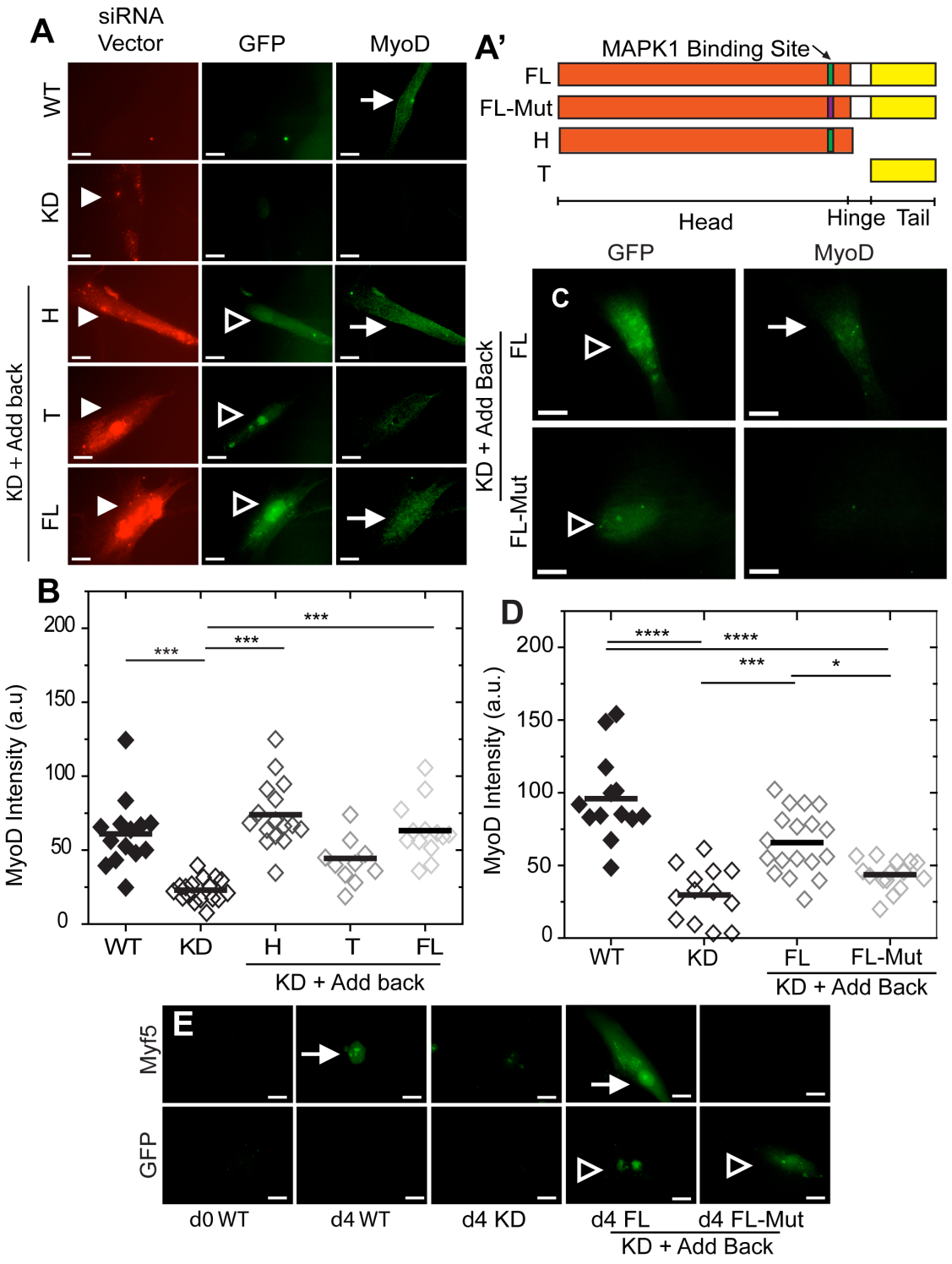
A
siRNA Vector
GFP
MyoD
WT
KD
KD + Add back
H
T
FL
A'
MAPK1 Binding Site
FL
FL-Mut
H
T
Head
Hinge
Tail
GFP
MyoD
C
KD + Add Back
FL
FL-Mut
B
MyoD Intensity (a.u)
200
150
100
50
0
***
***
***
WT
KD
H
T
FL
KD + Add back
D
MyoD Intensity (a.u.)
200
150
100
50
0
****
****
***
*
WT
KD
FL
FL-Mut
KD + Add Back
E
Myf5
GFP
d0 WT
d4 WT
d4 KD
d4 FL
d4 FL-Mut
KD + Add Back

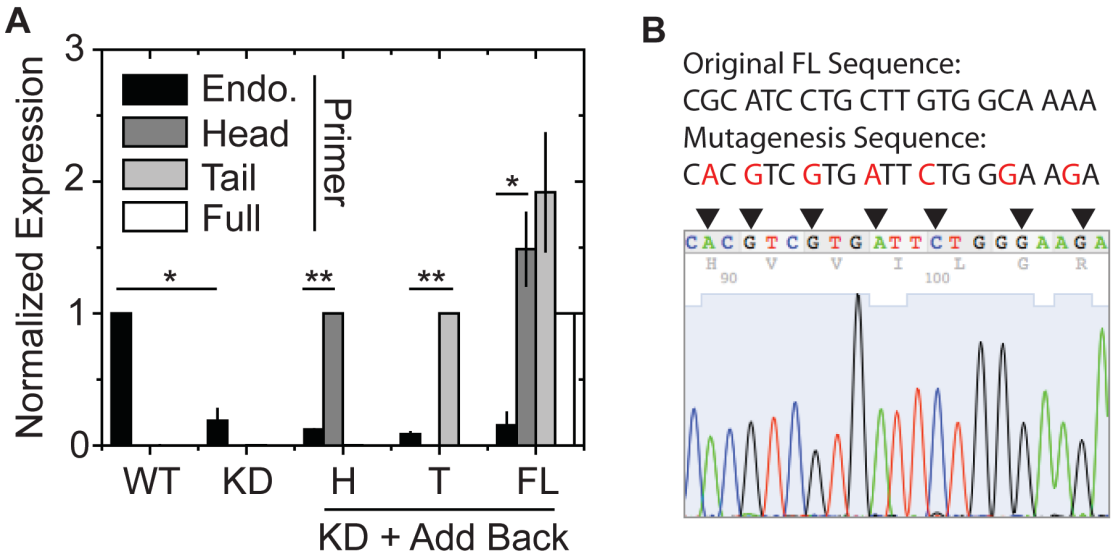

Figure 7: Add-back and Mutagenesis Confirmation. A) qPCR was used to assess uptake and expression of chicken vinculin constructs. For each primer, the corresponding sample was used to normalize its expression, e.g. vinculin tail added cells were used to normalize data using the tail primer. Endogenous mRNA was found in wild type cells and significantly reduced in all knock down samples. The head primer was amplified in the head and full length add back samples, while the tail primer was amplified in the tail and full length add back samples. A full length primer spanning multiple domains was only amplified in the full length add back sample. *$p < 0.05$, **$p < 0.01$ versus WT as indicated by ANOVA. B) Sanger sequencing results confirmed the change in nucleotide sequence (arrowheads) in FL-Mut samples as a result of mutagenesis.

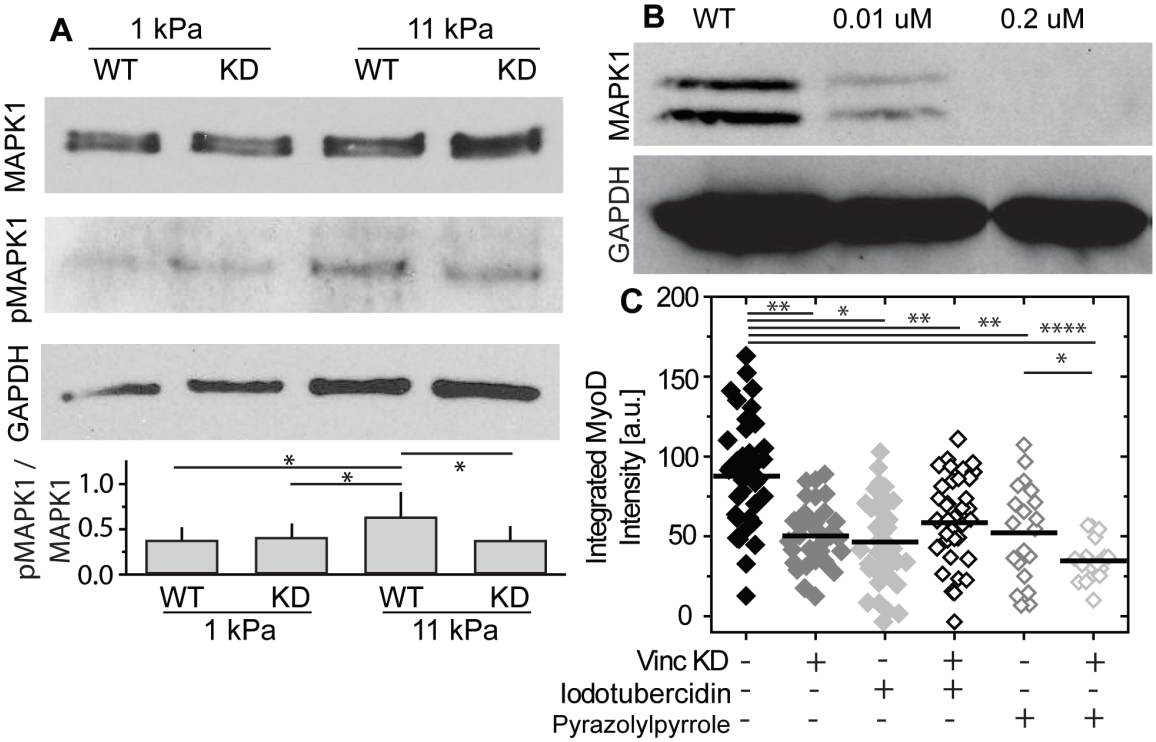

Figure 8: MAPK1 and Mechanosensitive Differentiation. A) Western blot of untreated and knockdown hMSCs at different matrix stiffness for phosphor-MAPK1 and GAPDH. Plot shows the ratio of integrated intensity for pMAPK divided by MAPK bands. * $p < 0.05$ versus other conditions as indicated by ANOVA. B) Western blot for MAPK1 and GAPDH of cells treated with the MAPK1 inhibitor 5-iodotubercidin. C) hMSCs on 11 kPa matrices treated with MAPK1 inhibiters 5-iodotubercidin or pyrazolylpyrrole as indicated showed a significant reduction in average MyoD expression similar to vinculin knockdown alone, regardless of whether knockdown was present in the treated samples. **$p<0.01$, ****$p<0.0001$.

Combining vinculin knockdown with iodotubercidin did not further reduce MyoD expression though the combination of vinculin knockdown and pyrazolylpyrrole did (Figure 8C). Inhibitors did not dramatically alter cell morphology (Figure 9A), perturb vinculin expression (Figure 9B) or assembly (Figure 9C), and they did not alter cell area (Figure 9D), implying that only signaling and not focal adhesions were perturbed. Pyrazolylpyrrole treatment with or without vinculin knockdown also interfered with durotaxis (Figure 9E).

2.3.4 Vinculin Knockdown does not alter Focal Adhesion Structure or Function

To implicate the role of vinculin only as a signaling protein in this context, cell behavior and focal adhesion structure and function as an 'inside-out' force transducer must remain unperturbed; otherwise, changes in cell behavior or focal adhesion super-structure could have induced some of the observations here. Vinculin knockdown was not found to significantly affect cell proliferation, cell area, cell morphology, the number of focal adhesions per cell, or the total focal adhesion area per cell (Figure 10A-D). Vinculin knockdown also did not significantly affect cell viability, as measured by western blots for housekeeper proteins GAPDH and β-actin (Figure 12Ai) and a live/dead assay (Figure 10E). Focal adhesion structure, distribution, and morphology also appeared unchanged, as well as composition as assessed by phospho-Focal Adhesion Kinase (FAK) expression (Figure 12Aii, iii). Focal adhesions must

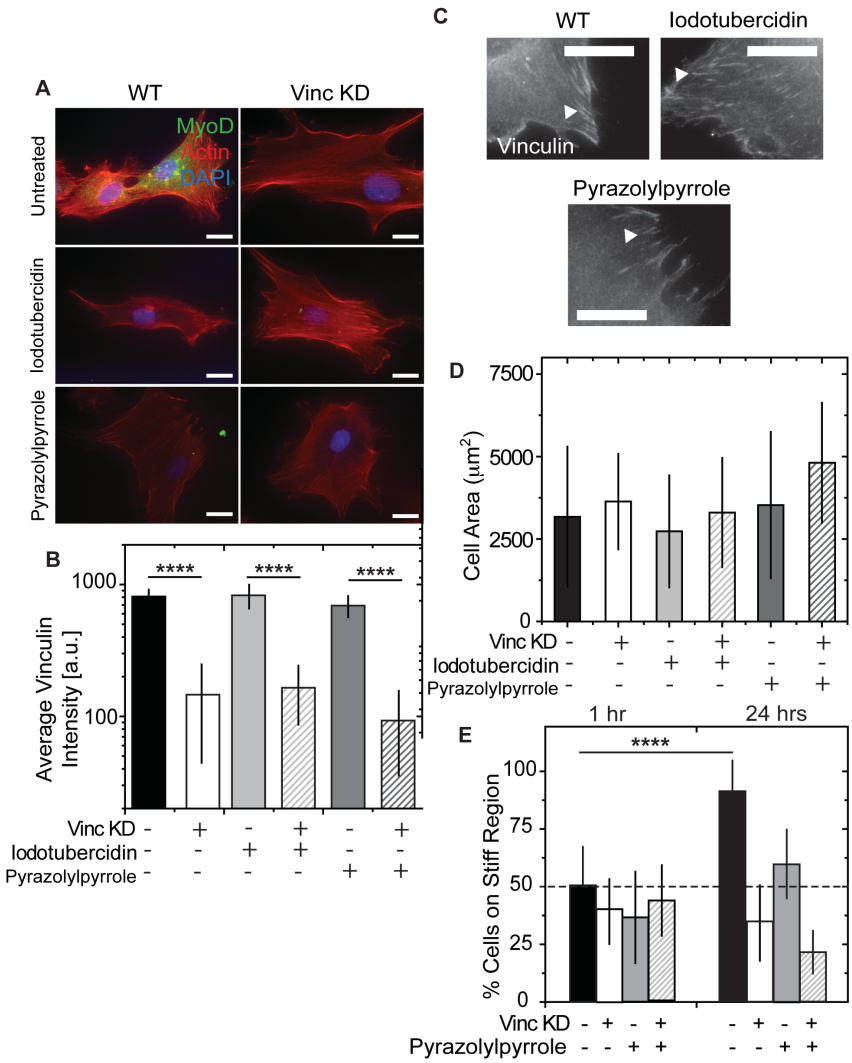

Figure 9: MyoD and MAPK1 inhibition. A) Immunofluorescent images of hMSCs treated with 5-iodotubercidin, pyrazolylpyrrole, and/or vinculin siRNA (Vinc KD) as indicated on 11 kPa matrices and stained for actin, nuclei (DAPI), and MyoD. B) Quantification of vinculin intensity in hMSCs cultured under the indicated conditions. ****$p < 0.0001$ as indicated by ANOVA. C) Immunofluorescent images for vinculin of wild type hMSCs or hMSCs treated with 5-iodotubercidin and pyrazolylpyrrole. Arrowheads indicate focal adhesions. D) Cell area of wild type hMSCs and hMSCs treated with the indicated combinations of 5-iodotubercidin, pyrazolylpyrrole, and vinculin siRNA. No comparisons were statistically significant. E) hMSCs were cultured with or without pyrazolylpyrrole and/or vinculin siRNA, and the percentage of hMSCs on stiff regions of a matrix with alternating stiff and soft stripes was quantified. Data was collected shortly after plating (1 hr) and 24 hrs post-plating. ****$p < 0.0001$ as indicated by ANOVA. Scale Bars: A, C = 20 μm.

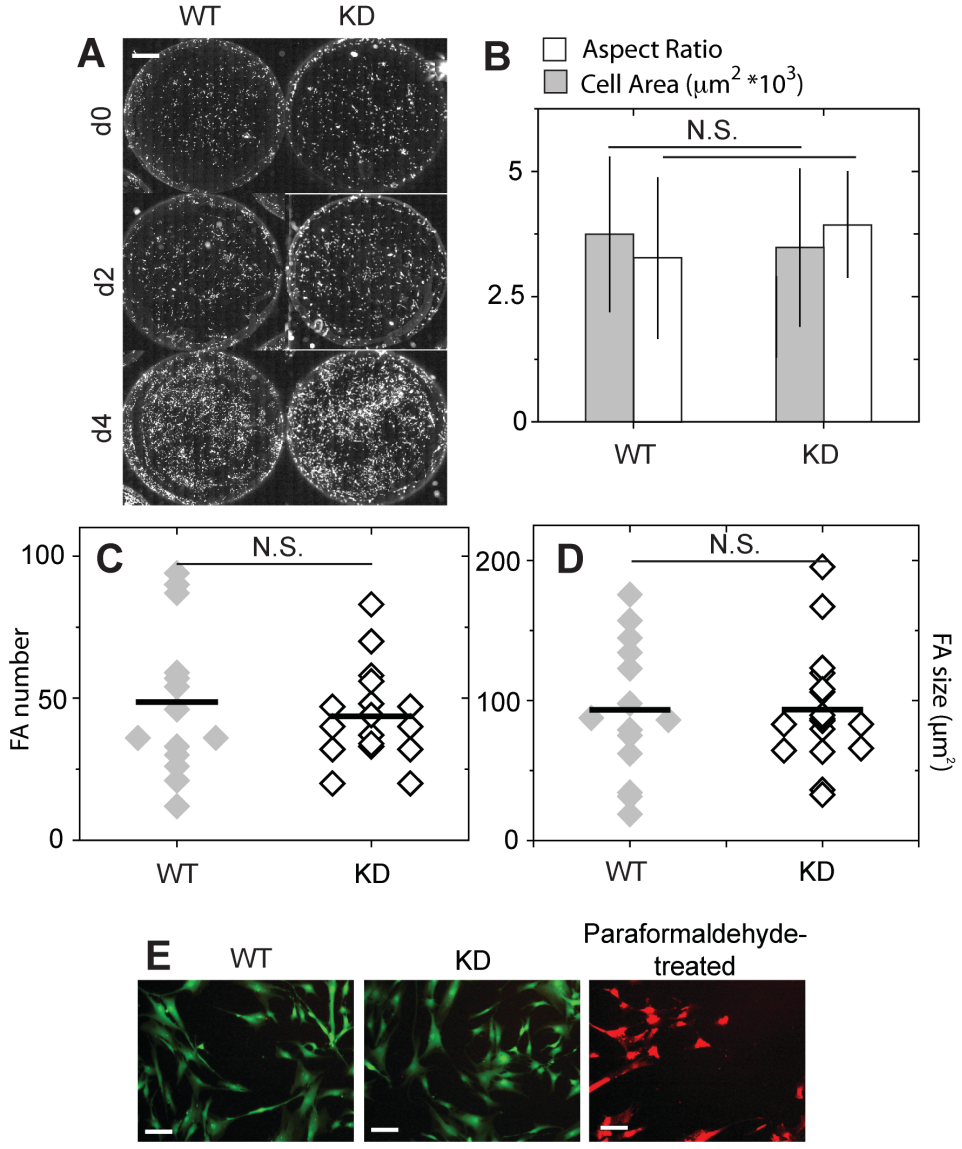

Figure 10: Vinculin knockdown does not affect proliferation or focal adhesion dynamics. A) Low magnification images of wild type (WT) and siRNA-induced vinculin knockdown (KD) hMSCs after 0, 2, and 4 days of culture stained for actin to illustrate cell density over time. Vinculin knockdown's affect on B) cell area (gray) and aspect ratio (the ratio of the major to minor cell axis; white), C) focal adhesion number per cell as measured from Paxillin stained cells, and D) total focal adhesion area as measured from Paxillin stained cells. E) Live (green)/dead (red) assay of cells with the indicated treatments. Scale Bar: A = 2 mm, E = 50 μm. N.S. = not significant.

facilitate cell adhesion and the transmission of actomyosin contractions to the adjacent matrix and cells, and to ensure that their functions were not perturbed, two mechanical assays were employed. First, a spinning disc assay was used to measure adhesion strength by exerting radially dependent shear and monitoring cell adhesion as a function of shear (Figure 11A). The average adhesion strength is defined by the shear required to detach 50% of the cells, i.e. τ_{50}, permitting quantitative comparisons [41] (Figure 11B, C). Vinculin knockdown did not significantly alter τ_{50} relative to untreated cells (Figure 12B), with the shear required to detach cells being well above physiological levels [42]. Focal adhesions are also responsible for transmitting cell-generated traction forces, and traction force microscopy (TFM) can be used to monitor how a cell pulls against its matrix, both normal and tangential to the matrix surface [28, 43]. Matrix deformation (Figure 12C, left) was used to compute the energy required for each deformation (Figure 12C, right). Integration over each cell yields the total strain energy, or work done by the cell to deform the matrix, which can be resolved into normal and tangential contributions (Figure 13A-C). No difference was observed between strain energy contributions (Figure 13D, E) or total strain energy for wild type and vinculin knockdown hMSCs (Figure 12D).

Taken together these data provide the first demonstration that a focal adhesion protein, e.g. vinculin, can act as a regulator of matrix stiffness-induced hMSC differentiation. Moreover, regulation is signaling dependent and not influenced by structural or functional changes in adhesions as a result of the loss of vinculin. The identification of other cryptic signaling sites in focal adhesions may lead to the characterization of new mechano-regulation mechanisms.

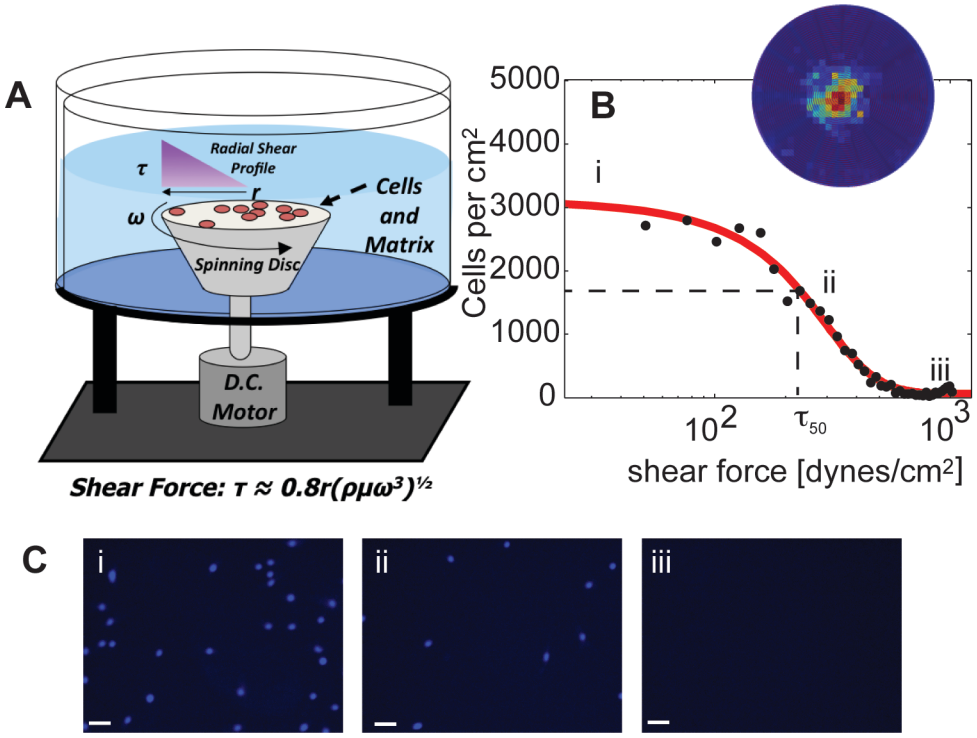

Figure 11: Radial Shear Assay. A) To test adhesion strength of our cells, a spinning disc assay was utilized. Cells were plated onto round coverslips and subjected to circular motion, resulting in a shear force over the cells that is proportional to their distance from the center of the coverslip. B) Binned cell density is plotted against shear force and fitted by a sigmoid function (red line). The average adhesion strength (t_{50}) is defined by the shear required to detach 50% of the cells (dashed lines). C) Representative images for the center (i), middle (ii), and edge (iii) of the cover slips are shown with DAPI stained nuclei. Scale Bar: A = 50 μm.

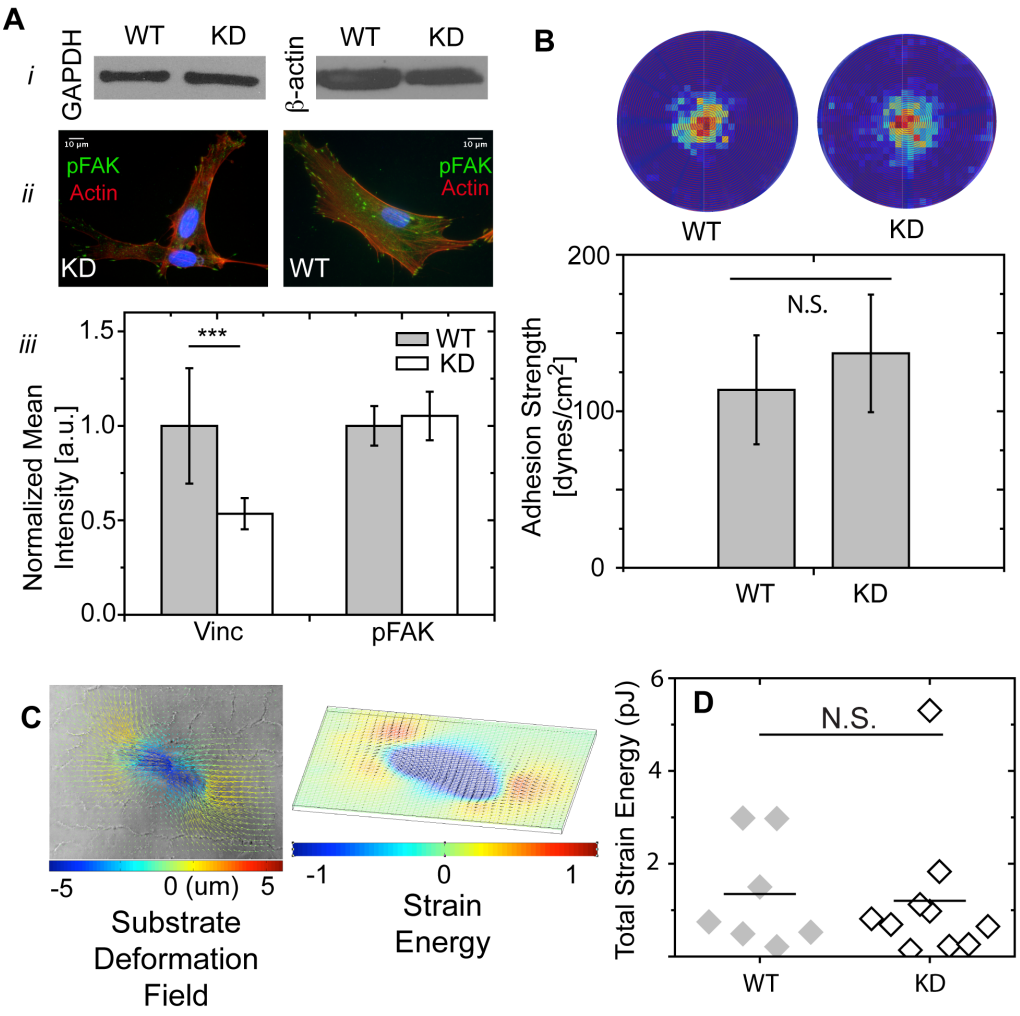

Figure 12: Secondary Effects of Vinculin Knockdown. All samples were analyzed 48 hours post-transfection. Ai) Western blots of GAPDH and actin expression measured indicate that vinculin knockdown does not affect housekeeper protein expression. Aii, iii) Staining for pFAK revealed no reduction in either total or focal adhesion localized pFAK. Vinculin knockdown as quantified by IF integrated density is confirmed. Blue Channel=DAPI. ***$p<0.001$. B) Shear was applied cells to detach them in a radial shear assay. Cell density post-shear is shown as a heat map with little change between wild type and vinculin knockdown hMSCs (top). No significant difference in cellular adhesion strength between wild type and vinculin knockdown populations was observed (bottom). C) Representative images of substrate deformation and strain energy maps obtained by traction force microscopy. D) No significant difference for total strain energy was observed between treated hMSCs and wild type cells as determined by traction force microscopy. N.S. = not significant ($p>0.05$). Scale bars: A=10 μm.

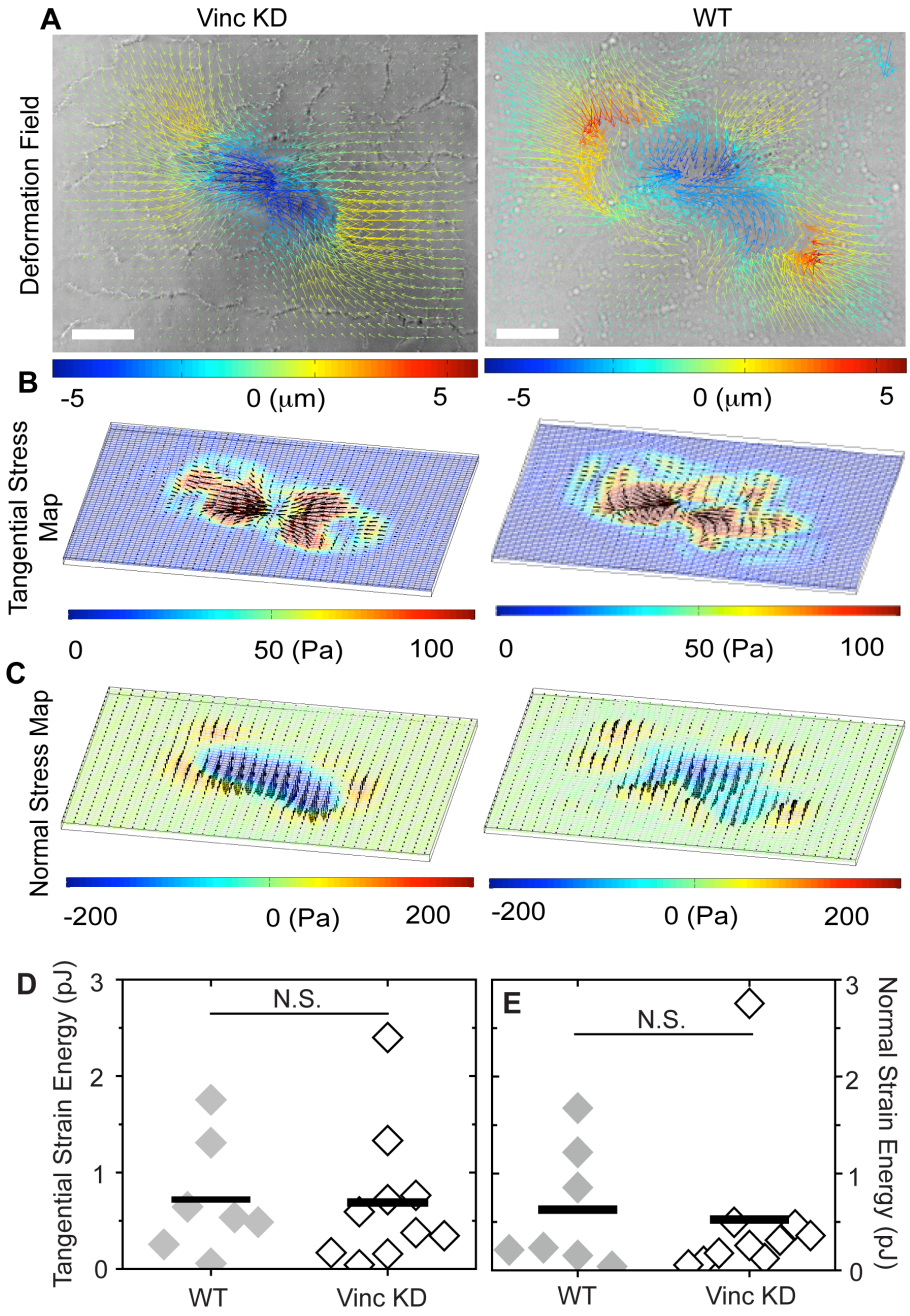

Figure 13: Traction Force Microscopy in hMSCs.
To assess the ability of a cell to generate strain energy against its substrate, Traction Force Microscopy was utilized. Matrix deformation fields (A) can be resolved into tangential (B) and normal (C) stress maps. The tangential and normal strains can then be integrated over each cell to find the work done by the cell to deform the matrix in either direction (D). Scale Bar: A = 20 μm.

2.4 Discussion

Recent discussion has suggested a general link between ECM and the nucleus [17, 18], and even *in vitro* and *in situ* reports identify some potential nuclear targets including YAP and TAZ [11] and a focal adhesion sensor, e.g. vinculin [21, 22], which could lend themselves to this process. While not previously connected in the context of stem cell differentiation, in the present study, we attempted to link the role of an *in situ* change in vinculin with myogenesis observed specifically because of the mechanical environment provided by the surrounding ECM. We document a class of potential focal adhesion-based mechanosensing proteins with internal predicted kinase sites. In the talin-vinculin complex, changes to kinase-binding site accessibility could occur on myogenically favorable substrates. Indeed, when vinculin was knocked down in hMSCs, impaired myogenesis and durotaxis was observed. Rescue experiments identified the distal portion of the head domain, where a cryptic MAPK1 binding site is predicted, to be critical for myogenesis; MAPK1 inhibition produces a similar effect, though the combination with vinculin knockdown was less effective for both myogenesis and durotaxis perhaps via RISC inhibition [44]. Consistent with our hypothesis here, hMSCs appear to exhibit large strains in matrix that induces myogenesis, e.g. 11 kPa [45], which aligns stem cells' cytoskeleton [46] and could stretch vinculin *in situ* and expose cryptic signaling sites.

2.4.1 Elucidation of novel mechanosensors

Recently, there has been a significant effort to expand our understanding of how cells sense matrix stiffness. Nuclear translocation of transcription factors YAP and TAZ [11] has been implicated in regulating shape-dependent endothelial cell survival as

YAP/TAZ expression correlated with stiffness-dependent expression of mammary epithelial genes. An alternative approach has been to screen signaling pathways involved in a behavior, e.g. fibroblast focal adhesion size, cell polarization, and traction force. In this case, protein tyrosine kinase knockdown identified kinases involved in enhancing, suppressing, or not affecting stiffness-sensing [47]. Both approaches produce a wealth of knowledge but do not indicate what or how a biophysical signal like stiffness is converted into a biochemical signal in the cell. FRET-based sensors can accurately measure protein stretching and mechanical activation [22, 48], but have limited throughput for screening. Cells contract and change the conformations of cytoskeletal proteins differently as a function of matrix stiffness [16]; Scansite analysis indicated that the talin-vinculin complex may have this capability *in situ*. This lead to the hypothesis that vinculin may either monotonically or biphasically increase MAPK1 signaling, with stretch leading to differentiation. Interestingly enough, differentiation did not appear to be monotonically increasing with additional stretch, as osteogenic differentiation was not influenced by vinculin knockdown.

2.4.2 The many roles of vinculin in focal adhesions

Our results indicate that there are not significant changes in the structural, adhesive, or mechanical functions of adhesion when vinculin is dramatically reduced but not absent in hMSCs. Reintroduction of vinculin domains containing the MAPK site, e.g. full length and head, also restored MyoD expression to wild type levels whereas constructs specifically lacking it did not, e.g. FL-Mut. Tail only constructs, which lack the MAPK site, partially rescued expression and suggest possible MAPK-independent

alternatives. Yet additional kinase binding sites on vinculin's tail (see Table 1) and its ability to bind paxillin and actin could allow soluble vinculin tail to preferentially induce other signaling pathways or alter focal adhesion composition in such a way as to affect MyoD expression.

Vinculin acting largely as a signaling protein also is in contrast to previous findings with senescent cells, where 3T3 fibroblasts displayed a 20% decrease in adhesion strength as a result of siRNA-induced vinculin knockdown [49]. Tractions and invasion assays are also lower in vinculin-null fibroblasts [50, 51] and vinculin-null carcinoma cells had decreased spreading versus their wild type counterparts [52]. One could argue that there could be a signaling threshold so that null and knockdown cells could have dramatically different signaling capabilities, but differences nonetheless raise the question of what accounts for this discrepancy. First, vinculin's functionality may depend on cell state: in terminally differentiated cells, vinculin may play an increasingly structural role versus only a signaling role in hMSCs. Stem cell adhesions are extremely sensitive to ECM stiffness and composition compared to senescent cells [2, 5, 53, 54], and vinculin may act in a more signaling capacity to compensate. Secondly, serum concentration has been shown to modulate these responses [49]. hMSCs prefer significantly higher serum concentration versus fibroblasts, so differential mechanical effects in fibroblasts but not in hMSCs may be the result of compensatory adhesive mechanisms at high serum concentration. Even if there is some structural contribution in hMSCs that was not detected by the assays here, these data are supportive of a significant role for vinculin in mechanically directed myogenesis as described below.

2.4.3 Mechanosensing myogenic signaling pathways

While regulatory molecules, including many small Rho GTPases, have been implicated in regulating cell behavior [55], the exact pathways between molecules, gene expression, and behavior remain somewhat disconnected. The data here substantiate a link between vinculin and MAPK1 in myogenic regulation, which can be regulated by more or less force generated via changing matrix stiffness or blocked via addition of small molecules such as pyrazolylpyrrole or iodotubercidin. The proposed mechanism is summarized in Figure 14 and likely terminates in the nucleus with transcriptional regulation from MyoD and other myogenic markers measured here. MAPK1's role in this pathway likely involves its nuclear substrates, including the nuclear envelope protein Nesprin-2 [56], which has been shown to play a role in muscle differentiation [57]. Thus MAPK1 could become active upon vinculin binding, act on proteins including Nesprin, and result in MyoD expression. This model of MAPK-regulated MyoD expression has been recently described in satellite cell activation [58] and appears to corroborate our findings where a specific level of strain energy, ~ 1.5 pJ, produces optimal MAPK activation and subsequent induction of myogenic differentiation; too much or too little strain energy may not provide sufficient signaling. MAPK1's modifiers provide further credence for this mechanosensitive model; p38 MAPK and MKK6 function is required not just for MAPK1 activation but also for MyoD expression [59]. Myogenic MAPK1 substrates also include p90 ribosomal S6 kinase [60] and Est1 [61], but their function as substrates may be context specific as PPARϒ, an adipogenic marker, is also a MAPK1 substrate in pre-adipocytes [62]. This begs the question that for hMSCs, which presumably lack such context-dependent function, what downstream signaling cascade is

most appropriate? Jaiswal and co-workers have shown that chemically induced osteogenesis involves MAPK1, suggesting a monotonically increasing signal [63]. However in the context of stiffness-induced differentiation, our data indicates that MAPK1 function is stiffness sensitive and acts via vinculin on myogenic targets including MyoD, not on osteogenic targets such as Runx2. Though induction methods may give rise to these signaling differences, our observations point to the need for additional exploration of how MAPK1 substrates compete for activation in a multi- or pluri-potent cells.

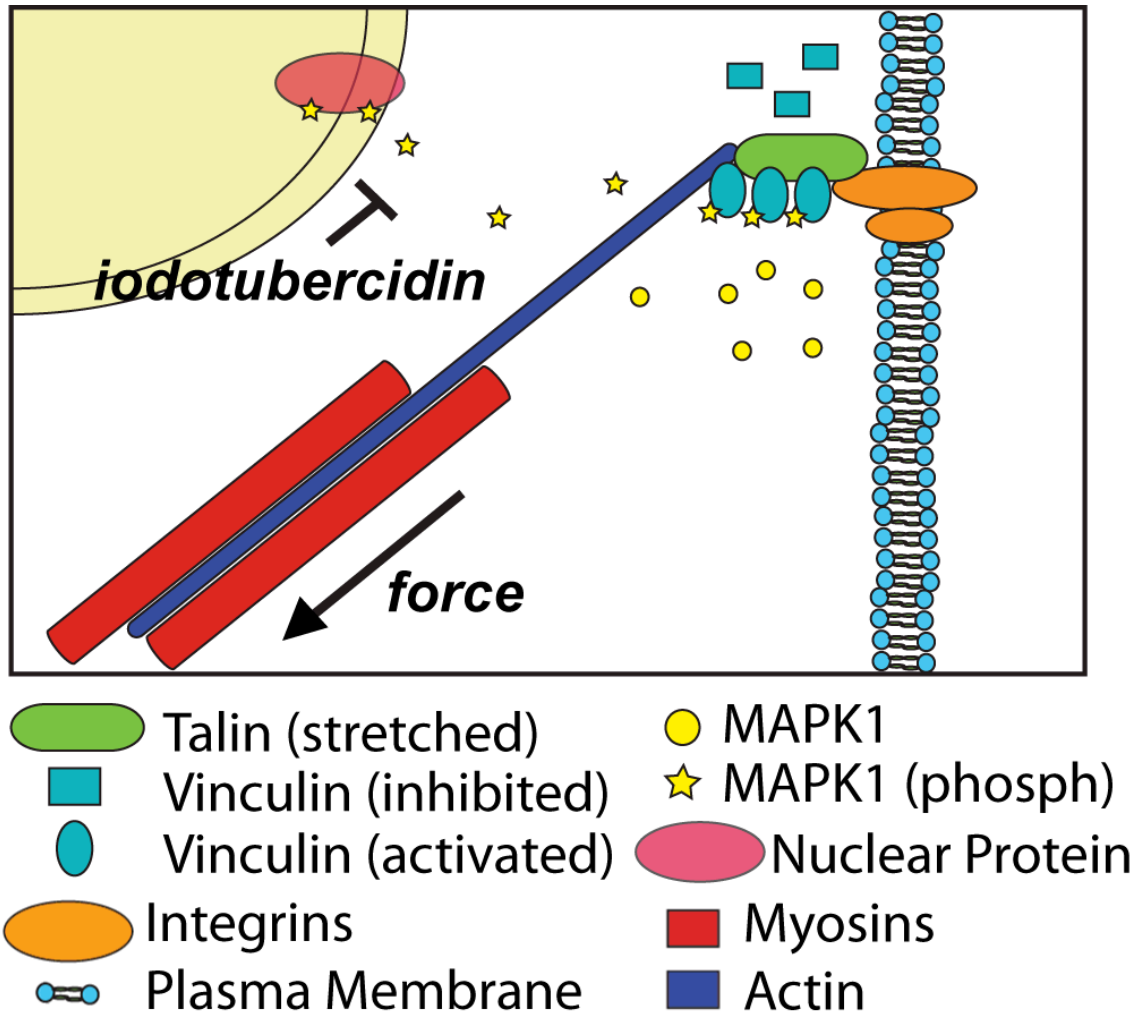

Figure 14: A model of myogenic mechano-sensing.
As increasing force is applied to focal adhesions via actomyosin contraction, talin and vinculin associate and likely undergo a conformational change to activate vinculin. This permits the latter portion of vinculin's head domain, which has predicted MAPK1 binding, to regulate mechanically-induced myogenesis while not altering other structural, adhesive, or mechanical function of the hMSCs. Impaired MAPK1 function blocks this process, and may alter the function of its nuclear targets.

2.5 Acknowledgements

Chapter 2, in full, is a reformatted version of the published article as it appears in *Stem Cells* (In Press). The dissertation author was the primary investigator and author of this paper, and thanks co-authors Xinyi Tang, Deepthi Vijayraghavan, Ludovic Vincent, Dr. Alexander Fuhrmann, Dr. Yu Suk Choi, Dr. Juan Carlos Del Alamo, and Dr. Adam J. Engler for their contributions. The authors would like to thank Dr. Susan Craig (Johns Hopkins University) for providing the full length, head, and tail domain vinculin plasmids and Jeff Gole (UCSD) for assistance with sequencing. This work was funded by an NIH New Innovator Award (1DP02 OD006460 to A.J.E.) and an NSF predoctoral fellowship (to L.G.V.).

2.6 Appendix

Table 1: Surface accessibility values for 49 human focal adhesion proteins. Accessibility was determined by ScanSite analysis [34] where surface accessible and inaccessible kinase binding sites have values above 1 and below 1, respectively. ScanSite provides a single accessibility value based on the amino acid sequence surrounding each point. Kinase abbreviations: c-abl oncogene 1, non-receptor tyrosine kinase, ABL1; RAC-alpha serine/threonine-protein kinase, AKT1; Amphiphysin, AMPH; Ataxia telangiectasia mutated, ATM; calcium/calmodulin-dependent protein kinase II gamma, CAMK2G; Cyclin-dependent kinase 1/Cell division control protein 2, CDC2; Cyclin-dependent kinase 5, CDK5; CDC-like kinase 2, CLK2; p38-CRK sarcoma virus CT10 oncogene homolog, CRK; Casein kinase 1 gamma 2, CSNK1G2; Casein kinase 2 beta polypeptide, CSNK2B; Receptor tyrosine-protein kinase erbB-1, EGFR; p55-FGR, FGR; p59-FYN, FYN; Growth factor receptor-bound protein 2, GRB2; Glycogen synthase kinase 3 alpha, GSK3A; Glycogen synthase kinase 3 beta, GSK3B; Hematopoietic cell-specific Lyn substrate 1, HCLS1; Inositol polyphosphate-5-phosphatase, INPP5D; CD220, INSR; IL2-inducible T-cell kinase, ITK; Intersectin, ITSN; Lymphocyte-specific protein tyrosine kinase, LCK; Mitogen-activated protein kinase 1, MAPK1; Mitogen-activated protein kinase 3, MAPK3; Non-catalytic region of tyrosine kinase 1, NCK1; Platelet-derived growth factor receptor beta, PDGFRB; Phosphoinositide dependent protein kinase-1, PDPK1; Phosphoinositide-3-kinase, regulatory subunit 1, PIK3R1; Phosphoinositide-binding protein, PIP3-E; Phospholipase C gamma 1, PLCG1; Protein kinase, AMP-activated alpha 1, PRKAA1; Protein kinase cAMP-dependent catalytic

Table 1: Surface accessibility values for 49 human focal adhesion proteins (cont.) delta PRKACD; Protein kinase cAMP-dependent catalytic gamma, PRKACG; Protein kinase C alpha, PRKCA; Protein kinase C delta, PRKCD; Protein kinase C epsilon, PRKCE; Protein kinase C mu, PRKCM; Protein kinase C zeta, PRKCZ; Protein kinase, DNA-activated, catalytic polypeptide, PRKDC; Src homology 2 domain containing protein 1, SHC1; Sorbin domain containing 1, SORBS1; c-Src, SRC; 14-3-3 Mode 1, YWHAZ

Protein	Accession #	Kinase Partner	Accessibility
Integrin Alpha 1	P56199	ABL1	0.738
		YWHAZ	0.36
		PRKCD	4.174
		ITK	0.402
		PRKCE	1.819
		CAMK2G	0.847
		PRKACD	0.619
Integrin Alpha 2	P17301	PRKDC	3.115
		PRKCA	0.906
		PRKDC	3.702
Integrin Alpha 3	P26006	ABL1	0.184
		PDPK1	4.361
		ATM	0.633

Table 1: Surface accessibility values for 49 human focal adhesion proteins (cont.)

Protein	Accession #	Kinase Partner	Accessibility
		PIK3R1	0.162
		MAPK1	0.182
		MAPK1	0.202
		MAPK1	0.318
		AMPH	3.219
		CDK5	3.338
		CDC2	3.338
Integrin Alpha 4	P13612	MAPK1	0.221
		MAPK1	0.259
		CAMK2G	0.164
		PRKACG	2.218
Integrin Alpha 5	P08648	SRC	1.129
		PIK3R1	1.129
		MAPK1	0.253
		PIK3R1	0.135
		MAPK1	0.135
		PRKDC	2.326
		MAPK3	0.345
		MAPK1	0.213
Integrin Alpha 6	P23229	PRKCZ	0.332
		CAMK2G	2.112
		PIK3R1	0.31
		PRKDC	2.563
		SRC	0.393
		AKT1	0.841
		YWHAZ	0.841
		CRK	4.011
Integrin Alpha 7	Q13683	MAPK1	0.392
		MAPK1	0.439
Integrin Alpha 8	P53708	PRKDC	3.31
		PRKDC	2.636
		PDPK1	2.705
		MAPK1	0.347
		PRKCE	2.302
		FGR	0.312
		ITK	0.202
Integrin Alpha 9	Q13797	MAPK1	0.079
		PRKCZ	0.507
		MAPK3	0.637
Integrin Alpha V	P06756	ITK	0.192
Integrin Beta 1	P05556	CDK5	1.363
		CDC2	1.363

Table 1: Surface accessibility values for 49 human focal adhesion proteins (cont.)

Protein	Accession #	Kinase Partner	Accessibility
		PDPK1	0.699
Integrin Beta 4	P16144	PIK3R1	0.283
		PRKCZ	2.265
		PRKAA1	0.881
		CAMK2G	0.357
		MAPK1	0.315
		PRKACG	0.817
		MAPK3	0.593
		SORBS1	0.708
		MAPK1	0.562
		AMPH	7.13
		ATM	0.867
Integrin Beta 5	P18084	ABL1	0.204
		PRKAA1	1.035
		PDPK1	0.939
		AKT1	0.953
Integrin Beta 6	P18564	ATM	0.785
		MAPK1	0.181
		SHC1	1.189
Integrin Beta 7	P26010		
Integrin Beta 8	P26012	GRB2	0.253
		PRKCA	1.491
Syndecan-4	P31431		
Urokinase Plasminogen Activator Receptor (uPAR)	P00749	MAPK1	0.182
		PRKCD	0.505
		AKT1	0.505
		MAPK1	0.379
SHP-2 Substrate 1 (SHPS-1)	P78324	MAPK1	1.321
		CSNK1G2	0.831
		INPP5D	0.505
Talin	Q9Y490	PRKCA	1.526
		PRKCM	0.806
		CAMK2G	0.385
		MAPK1	1.355
		YWHAZ	0.435
		PLCG1	0.699
		PRKDC	2.532
		ATM	2.532
Filamin	P21333	PIK3R1	0.903
		ITK	0.903
		PIK3R1	0.885
		ITSN	0.885

Table 1: Surface accessibility values for 49 human focal adhesion proteins (cont.)

Protein	Accession #	Kinase Partner	Accessibility
		PDPK1	0.203
		INSR	1.291
		PRKCD	1.734
		GSK3A	0.394
		INPP5D	0.472
		PRKCD	0.778
		MAPK1	0.213
		AKT1	0.601
		PRKAA1	0.601
		PRKCD	0.601
		PRKACG	0.712
		CAMK2G	0.712
		CDK5	1.258
		CDC2	1.258
		CDC2	2.23
Alpha Actinin	P12814	MAPK1	0.182
		SHC1	2.966
		PRKCE	1.025
		NCK1	3.252
Tensin	Q9HBL0	MAPK1	1.5
		CRK	0.451
		PRKCD	1.139
		CAM2KG	1.432
		CRK	1.222
		SORBS1	0.796
		PIK3R1	0.796
		ITSN	0.796
		GSK3A	0.97
		GSK3A	0.75
		PDPK1	3.891
		AMPH	1.498
		ITSN	1.751
		AKT1	0.897
		GRB2	3.082
		MAPK3	2.353
		GSK3B	1.056
		GSK3A	1.056
		MAPK3	1.056
		YWHAZ	0.562
		CSNK1G2	0.405
		MAPK3	3.871
		YWHAZ	0.576

Table 1: Surface accessibility values for 49 human focal adhesion proteins (cont.)

Protein	Accession #	Kinase Partner	Accessibility
		GSK3A	0.415
		CDK5	1.271
		CDC2	1.271
		YWHAZ	0.934
		GSK3A	0.745
		PRKACG	2.168
		MAPK3	0.863
		GSK3A	0.765
		GSK3A	1.435
		PRKACG	0.73
		YWHAZ	0.654
		PDPK1	2.459
		PRKCM	0.55
Syndesmos	Q9BRJ7	CAMK2G	1.168
Receptor-like tyrosine phosphatase alpha	P18433	CSNK1G2	1.304
		MAPK3	1.864
		PIK3R1	1.12
		PLCG1	1.02
		PLCG1	1.02
		GRB2	0.95
		MAPK1	0.39
		GRB2	1.084
Focal Adhesion Kinase	Q05397	PDPK1	1.615
		PRKCM	1.065
		PRKCZ	1.065
		SRC	0.429
		PIK3R1	0.429
		PDGFRB	1.228
		FGR	1.228
		ABL1	1.911
		ITK	1.911
		CSNK1G2	1.534
		MAPK1	1.653
		CAMK2G	0.366
		CAMK2G	0.605
		AMPH	4.447
		PIK3R1	4.447
		ITSN	4.447
		AMPH	2.23
		CRK	3.423
		PIK3R1	3.423
		ITSN	6.637

Table 1: Surface accessibility values for 49 human focal adhesion proteins (cont.)

Protein	Accession #	Kinase Partner	Accessibility
		PIK3R1	6.637
		HCLS1	1.659
		FGR	1.144
		PDGFRB	1.223
		EGFR	1.223
		INSR	1.223
		PIK3R1	1.223
Paxillin	P49023	LCK	1.483
		FYN	1.483
		FGR	1.483
		SRC	1.483
		HCLS1	1.504
		ITSN	1.504
		PLCG1	1.303
		CRK	0.651
		MAPK3	2.378
		MAPK3	0.511
		ABL1	0.52
		MAPK3	1.305
		CRK	1.112
		HCLS1	1.659
		PLCG1	1.659
		PRKACG	0.353
Integrin-Linked Protein Kinase	Q13418	MAPK1	0.217
		AKT1	1.505
Caveolin	Q03135		
PINCH-1	P48059	PDPK1	1.756
Vasodilator-stimulated phosphoprotein (VASP)	P50552	CRK	1.091
		HCLS1	1.091
		NCK1	1.31
		ABL1	2.005
		NCK1	2.005
		PLCG1	2.005
		ABL1	2.005
		PLCG1	2.005
		NCK1	2.005
		PLCG1	2.005
		PLCG1	2.005
		HCLS1	2.005
		ABL1	2.005
		PLCG1	2.005
		CRK	1.069

Table 1: Surface accessibility values for 49 human focal adhesion proteins (cont.)

Protein	Accession #	Kinase Partner	Accessibility
		CRK	1.091
		GRB2	1.091
		ITSN	1.091
		HCLS1	1.091
		PRKAA1	1.463
		PRKACG	3.912
Parvin	Q9NVD7	CDK5	3.277
		CDC2	3.277
		MAPK3	3.277
		CDK5	3.043
		CDC2	3.043
		MAPK3	0.656
Vinculin	P18206	CAMK2G	1.229
		MAPK1	0.164
		NCK1	1.754
Zyxin	Q15942	ABL1	1.671
		GRB2	1.671
		SRC	1.671
		ABL1	3.132
		NCK1	0.689
		MAPK3	1.52
		GSK3A	0.445
		SORBS1	1.273
		MAPK3	1.004
Palladin	Q8WX93	ATM	1.139
		PRKDC	1.139
		CSNK2B	1.922
		CDK5	3.727
		CDC2	3.727
		MAPK1	0.188
		ABL1	1.774
		NCK1	1.774
		GSK3A	1.52
		MAPK3	1.52
		GRB2	1.52
		GSK3A	0.932
		GSK3B	0.932
		GSK3A	1.155
		GSK3A	0.943
		MAPK3	1.622
		MAPK3	1.767
		MAPK3	2.353

Table 1: Surface accessibility values for 49 human focal adhesion proteins (cont.)

Protein	Accession #	Kinase Partner	Accessibility
		ITK	2.715
		CRK	2.715
		HCLS1	3.132
		ABL1	1.671
		SRC	1.671
		GRB2	1.671
		HCLS1	1.671
		NCK1	1.671
		SRC	1.671
		INPP5D	0.566
		CLK2	4.782
		CLK2	3.533
		GSK3A	0.898
		CAMK2G	3.085
Vinexin	O60504	MAPK1	0.349
		GSK3A	1.623
		GSK3A	1.988
		CDK5	0.92
		CDC2	0.92
		CDC2	4.553
		CDK5	4.553
		MAPK3	1.78
Ponsin	Q9BX66	GSK3A	3.115
		MAPK3	1.318
		ABL1	1.448
		GRB2	0.802
		HCLS1	0.524
		YWHAZ	1.997
		PRKDC	3.099
		PRKCZ	1.776
		ABL1	2.146
		CRK	2.146
		ABL1	1.858
		CRK	1.858
		ABL1	1.858
		MAPK3	1.038
		PRKCE	0.965
		YWHAZ	0.471
		MAPK1	0.737
		SORBS1	1.198
		PDPK1	0.971
		GSK3A	0.75

Table 1: Surface accessibility values for 49 human focal adhesion proteins (cont.)

Protein	Accession #	Kinase Partner	Accessibility
		PLCG1	1.016
		YWHAZ	0.937
		MAPK3	0.543
		GRB2	0.891
		HCLS1	0.891
		GSK3A	1.038
		MAPK1	0.357
		CAMK2G	1.831
		ATM	1.831
ASAP1	Q9ULH1	AKT1	0.528
		NCK1	3.594
		GSK3A	3.043
		CSNK2B	4.137
		CDK5	2.059
		CRK	1.222
		ABL1	1.091
		NCK1	1.091
		ITSN	2.285
		PIK3R1	2.285
		SORBS1	2.285
		ITK	5.132
		ITK	3.968
		SRC	3.132
		ITK	3.132
		PLCG1	2.282
		MAPK3	1.448
		GRB2	0.941
		SRC	0.553
		PIK3R1	0.553
		PIK3R1	1.502
		HCLS1	2.334
		MAPK1	1.493
		HCLS1	2.334
		NCK1	1.383
		MAPK1	1.493
		MAPK1	2.022
		PIK3R1	2.334
		MAPK3	1.572
Syntenin	O00560		
p21-activated kinase (PAK)	Q13153	NCK1	2.647
		ITK	2.647
		SORBS1	1.792

Table 1: Surface accessibility values for 49 human focal adhesion proteins (cont.)

Protein	Accession #	Kinase Partner	Accessibility
		PRKAA1	0.439
		GRB2	1.804
		PDPK1	1.718
		PLCG1	1.316
		SRC	0.748
		MAPK1	0.647
Protein Kinase AKT	P31749	PIP3-E	4.125
		PRKCZ	0.328
		AKT1	0.363
		PRKCE	1.376
		PRKCM	1.122
		INPP5D	0.534
		PDPK1	0.977
Phosphatidyl inositol 3-kinase (PIK3)	P42336	EGFR	0.291
		MAPK1	0.042
		ATM	2.384
		ATM	0.507
Fyn	P06241	PRKCA	1.101
		MAPK3	1.574
		ITK	0.292
Src Kinase	P12931	PRKACG	2.602
		MAPK3	1.187
		ITK	0.292
		CSNK1G2	0.69
p130Cas	P56945	EGFR	0.338
		ABL1	0.338
		PLCG1	0.338
		CRK	0.338
		ABL1	0.582
		CRK	0.582
		ABL1	0.983
		CRK	0.983
		ABL1	0.983
		ITK	0.983
		ABL1	0.835
		CRK	0.835
		ABL1	0.835
		CRK	0.835
		CRK	1.88
		ABL1	0.806
		CRK	0.806
		NCK1	0.806

Table 1: Surface accessibility values for 49 human focal adhesion proteins (cont.)

Protein	Accession #	Kinase Partner	Accessibility
		ABL1	0.806
		ITK	0.806
		NCK1	1.72
		CRK	1.72
		CRK	0.885
		NCK1	0.885
		ABL1	0.885
		ITK	0.885
		CRK	0.516
		NCK1	0.516
		ABL1	0.516
		CRK	1.72
		ABL1	1.72
		NCK1	1.72
		ITK	1.72
		ABL1	0.853
		CRK	0.853
		NCK1	0.853
		ABL1	0.853
		ITK	0.853
		ABL1	0.948
		CRK	0.948
		ABL1	0.948
		NCK1	0.948
		ITK	0.948
		MAPK1	0.524
		ABL1	0.819
		CRK	0.819
		ABL1	0.306
		PLCG1	0.306
		CRK	0.306
		ITK	0.306
		MAPK1	0.315
		YWHAZ	2.951
		SRC	1.448
		PIK3R1	1.448
		PRKCD	1.204
		SORBS1	0.826
Calpain II	P17655	CSNK1G2	0.403
		AKT1	0.75
		MAPK1	0.542
		EGFR	0.264

Table 1: Surface accessibility values for 49 human focal adhesion proteins (cont.)

Protein	Accession #	Kinase Partner	Accessibility
		CSNK2B	1.736
		PRKCZ	0.675
Protein Kinase C (PKC)	P17252	PRKDC	0.961
		PRKCD	0.551
		PRKCZ	0.551
[64]		PDPK1	0.656
		PRKCE	1.756
		PRKACG	0.447
		CAMK2G	0.447
		PDGFRB	1.195
		FGR	1.195
		EGFR	1.195
		GRB2	1.195
		FGR	1.195
		CRK	1.868
		PDPK1	0.511

Table 2: Human qPCR primers. Below is a list of primers used to amplify sample cDNA.

Gene	Unigene ID	Primer
Pax3	NM_181457	Forward: TGTTCAGCTGGGAAATCCGAGACA Reverse: GTCGATGCTGTGTTTGGCCTTCTT
Pax7	NM_002584	Forward: ACTGTGCCCTCAGGTTTAGTGAGT Reverse: GTCGATGCTGTGTTTGGCCTTCTT
MyoD	NM_002478	Forward: TGTAGCAGGTGTAACCGTAACCCA Reverse: ATTCCCTGTAGCACCACACACCAT
Mrf4/Herculin	NM_002469	Forward: AGAAGTGGCAGAAGGCTCTCCTTT Reverse: TCTTGCAAGCCCAGATCAGACACT
Myf5	NM_005593	Forward: TGAGAGAGCAGGTGGAGAACTACT Reverse: AGACAGGACTGTTACATTCGGGCA
GAPDH	NM_002046	Forward: TCGACAGTCAGCCGCATCTTCTTT Reverse: ACCAAATCCGTTGACTCCGACCTT

2.7 References

1. Discher, D.E., Mooney, D.J., and Zandstra, P.W. (2009). Growth factors, matrices, and forces combine and control stem cells. Science *324*, 1673-1677.

2. Engler, A.J., Sen, S., Sweeney, H.L., and Discher, D.E. (2006). Matrix elasticity directs stem cell lineage specification. Cell *126*, 677-689.

3. Rowlands, A.S., George, P.A., and Cooper-White, J.J. (2008). Directing osteogenic and myogenic differentiation of MSCs: interplay of stiffness and adhesive ligand presentation. Am J Physiol Cell Physiol *295*, C1037-1044.

4. Dalby, M.J., Gadegaard, N., Tare, R., Andar, A., Riehle, M.O., Herzyk, P., Wilkinson, C.D., and Oreffo, R.O. (2007). The control of human mesenchymal cell differentiation using nanoscale symmetry and disorder. Nat Mater *6*, 997-1003.

5. Flaim, C.J., Chien, S., and Bhatia, S.N. (2005). An extracellular matrix microarray for probing cellular differentiation. Nat Methods *2*, 119-125.

6. Berry, M.F., Engler, A.J., Woo, Y.J., Pirolli, T.J., Bish, L.T., Jayasankar, V., Morine, K.J., Gardner, T.J., Discher, D.E., and Sweeney, H.L. (2006). Mesenchymal stem cell injection after myocardial infarction improves myocardial compliance. Am J Physiol Heart Circ Physiol *290*, H2196-2203.

7. Stedman, H.H., Sweeney, H.L., Shrager, J.B., Maguire, H.C., Panettieri, R.A., Petrof, B., Narusawa, M., Leferovich, J.M., Sladky, J.T., and Kelly, A.M. (1991). The mdx mouse diaphragm reproduces the degenerative changes of Duchenne muscular dystrophy. Nature *352*, 536-539.

8. Lunde, K., Solheim, S., Aakhus, S., Arnesen, H., Abdelnoor, M., and Forfang, K. (2005). Autologous stem cell transplantation in acute myocardial infarction: The ASTAMI randomized controlled trial. Intracoronary transplantation of autologous mononuclear bone marrow cells, study design and safety aspects. Scand Cardiovasc J *39*, 150-158.

9. Janssens, S., Dubois, C., Bogaert, J., Theunissen, K., Deroose, C., Desmet, W., Kalantzi, M., Herbots, L., Sinnaeve, P., Dens, J., et al. (2006). Autologous bone marrow-derived stem-cell transfer in patients with ST-segment elevation myocardial infarction: double-blind, randomised controlled trial. Lancet *367*, 113-121.

10. McBeath, R., Pirone, D.M., Nelson, C.M., Bhadriraju, K., and Chen, C.S. (2004). Cell Shape, Cytoskeletal Tension, and RhoA Regulate Stem Cell Lineage Commitment. Developmental Cell *6*, 483-495.

11. Dupont, S., Morsut, L., Aragona, M., Enzo, E., Giulitti, S., Cordenonsi, M., Zanconato, F., Le Digabel, J., Forcato, M., Bicciato, S., et al. (2011). Role of YAP/TAZ in mechanotransduction. Nature *474*, 179-183.

12. Guilak, F., Cohen, D.M., Estes, B.T., Gimble, J.M., Liedtke, W., and Chen, C.S. (2009). Control of stem cell fate by physical interactions with the extracellular matrix. Cell Stem Cell *5*, 17-26.

13. Hoffman, B.D., Grashoff, C., and Schwartz, M.A. (2011). Dynamic molecular processes mediate cellular mechanotransduction. Nature *475*, 316-323.

14. Fu, J., Wang, Y.K., Yang, M.T., Desai, R.A., Yu, X., Liu, Z., and Chen, C.S. (2010). Mechanical regulation of cell function with geometrically modulated elastomeric substrates. Nat Methods *7*, 733-736.

15. Saez, A., Buguin, A., Silberzan, P., and Ladoux, B. (2005). Is the mechanical activity of epithelial cells controlled by deformations or forces? Biophysical Journal *89*, L52-L54.

16. Engler, A.J., Carag-Krieger, C., Johnson, C.P., Raab, M., Tang, H.Y., Speicher, D.W., Sanger, J.W., Sanger, J.M., and Discher, D.E. (2008). Embryonic cardiomyocytes beat best on a matrix with heart-like elasticity: scar-like rigidity inhibits beating. J Cell Sci *121*, 3794-3802.

17. Geiger, B., Spatz, J.P., and Bershadsky, A.D. (2009). Environmental sensing through focal adhesions. Nature reviews. Molecular cell biology *10*, 21-33.

18. Jaalouk, D.E., and Lammerding, J. (2009). Mechanotransduction gone awry. Nature reviews. Molecular cell biology *10*, 63-73.

19. Holle, A.W., and Engler, A.J. (2011). More than a feeling: discovering, understanding, and influencing mechanosensing pathways. Curr Opin Biotechnol.

20. Sawada, Y., Tamada, M., Dubin-Thaler, B.J., Cherniavskaya, O., Sakai, R., Tanaka, S., and Sheetz, M.P. (2006). Force sensing by mechanical extension of the Src family kinase substrate p130Cas. Cell *127*, 1015-1026.

21. del Rio, A., Perez-Jimenez, R., Liu, R., Roca-Cusachs, P., Fernandez, J.M., and Sheetz, M.P. (2009). Stretching single talin rod molecules activates vinculin binding. Science *323*, 638-641.

22. Grashoff, C., Hoffman, B.D., Brenner, M.D., Zhou, R., Parsons, M., Yang, M.T., McLean, M.A., Sligar, S.G., Chen, C.S., Ha, T., et al. (2010). Measuring mechanical tension across vinculin reveals regulation of focal adhesion dynamics. Nature *466*, 263-266.

23. Massillon, D., Stalmans, W., van de Werve, G., and Bollen, M. (1994). Identification of the glycogenic compound 5-iodotubercidin as a general protein kinase inhibitor. The Biochemical journal *299 (Pt 1)*, 123-128.

24. Junttila, M.R., Li, S.P., and Westermarck, J. (2008). Phosphatase-mediated crosstalk between MAPK signaling pathways in the regulation of cell survival. FASEB journal : official publication of the Federation of American Societies for Experimental Biology *22*, 954-965.

25. Cohen, D.M., Chen, H., Johnson, R.P., Choudhury, B., and Craig, S.W. (2005). Two distinct head-tail interfaces cooperate to suppress activation of vinculin by talin. The Journal of biological chemistry *280*, 17109-17117.

26. Choi, Y.S., Vincent, L.G., Lee, A.R., Dobke, M.K., and Engler, A.J. (2012). Mechanical derivation of functional myotubes from adipose-derived stem cells. Biomaterials *33*, 2482-2491.

27. Schmittgen, T.D., and Livak, K.J. (2008). Analyzing real-time PCR data by the comparative C(T) method. Nature protocols *3*, 1101-1108.

28. Del Alamo, J.C., Meili, R., Alonso-Latorre, B., Álvarez-González, B., Firtel, R.A., and Lasheras, J.C. (2012). Three-Dimensional Fourier Traction Cytometry. PLoS One *Submitted*.

29. Garcia, A.J., Ducheyne, P., and Boettiger, D. (1997). Quantification of cell adhesion using a spinning disc device and application to surface-reactive materials. Biomaterials *18*, 1091-1098.

30. Lluis, F., Perdiguero, E., Nebreda, A.R., and Munoz-Canoves, P. (2006). Regulation of skeletal muscle gene expression by p38 MAP kinases. Trends in cell biology *16*, 36-44.

31. Bentzinger, C.F., Wang, Y.X., and Rudnicki, M.A. (2012). Building muscle: molecular regulation of myogenesis. Cold Spring Harbor perspectives in biology *4*.

32. Tse, J.R., and Engler, A.J. (2011). Stiffness gradients mimicking in vivo tissue variation regulate mesenchymal stem cell fate. PLoS One *6*, e15978.

33. Choi, Y.S., Vincent, L.G., Lee, A.R., Kretchmer, K.C., Chirasatitsin, S., Dobke, M.K., and Engler, A.J. (2012). The alignment and fusion assembly of adipose-derived stem cells on mechanically patterned matrices. Biomaterials *33*, 6943-6951.

34. Obenauer, J.C., Cantley, L.C., and Yaffe, M.B. (2003). Scansite 2.0: Proteome-wide prediction of cell signaling interactions using short sequence motifs. Nucleic Acids Res *31*, 3635-3641.

35. Bershadsky, A.D., Balaban, N.Q., and Geiger, B. (2003). Adhesion-dependent cell mechanosensitivity. Annu. Rev. Cell Dev. Biol. *19*, 677-695.

36. Bakolitsa, C., Cohen, D.M., Bankston, L.A., Bobkov, A.A., Cadwell, G.W., Jennings, L., Critchley, D.R., Craig, S.W., and Liddington, R.C. (2004). Structural basis for vinculin activation at sites of cell adhesion. Nature *430*, 583-586.

37. Cohen, D.M., Kutscher, B., Chen, H., Murphy, D.B., and Craig, S.W. (2006). A conformational switch in vinculin drives formation and dynamics of a talin-vinculin complex at focal adhesions. The Journal of biological chemistry *281*, 16006-16015.

38. Li, J., and Johnson, S.E. (2006). ERK2 is required for efficient terminal differentiation of skeletal myoblasts. Biochemical and biophysical research communications *345*, 1425-1433.

39. Gredinger, E., Gerber, A.N., Tamir, Y., Tapscott, S.J., and Bengal, E. (1998). Mitogen-activated protein kinase pathway is involved in the differentiation of muscle cells. The Journal of biological chemistry *273*, 10436-10444.

40. Wu, Z., Woodring, P.J., Bhakta, K.S., Tamura, K., Wen, F., Feramisco, J.R., Karin, M., Wang, J.Y., and Puri, P.L. (2000). p38 and extracellular signal-regulated kinases regulate the myogenic program at multiple steps. Molecular and cellular biology *20*, 3951-3964.

41. Boettiger, D. (2007). Quantitative measurements of integrin-mediated adhesion to extracellular matrix. Methods Enzymol. *426*, 1-25.

42. Gurkan, U.A., and Akkus, O. (2008). The mechanical environment of bone marrow: a review. Annals of biomedical engineering *36*, 1978-1991.

43. Del Alamo, J.C., Meili, R., Alonso-Latorre, B., Rodriguez-Rodriguez, J., Aliseda, A., Firtel, R.A., and Lasheras, J.C. (2007). Spatio-temporal analysis of eukaryotic cell motility by improved force cytometry. Proc Natl Acad Sci U S A *104*, 13343-13348.

44. Tan, G.S., Chiu, C.H., Garchow, B.G., Metzler, D., Diamond, S.L., and Kiriakidou, M. (2012). Small molecule inhibition of RISC loading. ACS chemical biology *7*, 403-410.

45. Sen, S., Engler, A.J., and Discher, D.E. (2009). Matrix strains induced by cells: Computing how far cells can feel. Cell Mol Bioeng *2*, 39-48.

46. Zemel, A., Rehfeldt, F., Brown, A.E., Discher, D.E., and Safran, S.A. (2010). Optimal matrix rigidity for stress fiber polarization in stem cells. Nat Phys *6*, 468-473.

47. Prager-Khoutorsky, M., Lichtenstein, A., Krishnan, R., Rajendran, K., Mayo, A., Kam, Z., Geiger, B., and Bershadsky, A.D. (2011). Fibroblast polarization is a matrix-rigidity-dependent process controlled by focal adhesion mechanosensing. Nature cell biology *13*, 1457-1465.

48. Wang, Y., Botvinick, E.L., Zhao, Y., Berns, M.W., Usami, S., Tsien, R.Y., and Chien, S. (2005). Visualizing the mechanical activation of Src. Nature *434*, 1040-1045.

49. Gallant, N.D., Michael, K.E., and Garcia, A.J. (2005). Cell adhesion strengthening: contributions of adhesive area, integrin binding, and focal adhesion assembly. Molecular Biology of the Cell *16*, 4329-4340.

50. Diez, G., Auernheimer, V., Fabry, B., and Goldmann, W.H. (2011). Head/tail interaction of vinculin influences cell mechanical behavior. Biochemical and biophysical research communications *406*, 85-88.

51. Mierke, C.T., Kollmannsberger, P., Zitterbart, D.P., Diez, G., Koch, T.M., Marg, S., Ziegler, W.H., Goldmann, W.H., and Fabry, B. (2010). Vinculin facilitates cell invasion into three-dimensional collagen matrices. The Journal of biological chemistry *285*, 13121-13130.

52. Mierke, C.T., Kollmannsberger, P., Zitterbart, D.P., Smith, J., Fabry, B., and Goldmann, W.H. (2008). Mechano-coupling and regulation of contractility by the vinculin tail domain. Biophys J *94*, 661-670.

53. Flaim, C.J., Teng, D., Chien, S., and Bhatia, S.N. (2008). Combinatorial signaling microenvironments for studying stem cell fate. Stem Cells Dev *17*, 29-39.

54. Evans, N.D., Minelli, C., Gentleman, E., LaPointe, V., Patankar, S.N., Kallivretaki, M., Chen, X., Roberts, C.J., and Stevens, M.M. (2009). Substrate stiffness affects early differentiation events in embryonic stem cells. Eur Cell Mater *18*, 1-13; discussion 13-14.

55. Discher, D.E., Janmey, P., and Wang, Y.L. (2005). Tissue cells feel and respond to the stiffness of their substrate. Science *310*, 1139-1143.

56. Warren, D.T., Tajsic, T., Mellad, J.A., Searles, R., Zhang, Q., and Shanahan, C.M. (2010). Novel nuclear nesprin-2 variants tether active extracellular signal-regulated MAPK1 and MAPK2 at promyelocytic leukemia protein nuclear bodies and act to regulate smooth muscle cell proliferation. The Journal of biological chemistry *285*, 1311-1320.

57. Zhang, Q., Ragnauth, C.D., Skepper, J.N., Worth, N.F., Warren, D.T., Roberts, R.G., Weissberg, P.L., Ellis, J.A., and Shanahan, C.M. (2005). Nesprin-2 is a multi-isomeric protein that binds lamin and emerin at the nuclear envelope and forms a subcellular network in skeletal muscle. J Cell Sci *118*, 673-687.

58. Troy, A., Cadwallader, A.B., Fedorov, Y., Tyner, K., Tanaka, K.K., and Olwin, B.B. (2012). Coordination of Satellite Cell Activation and Self-Renewal by Par-Complex-Dependent Asymmetric Activation of p38±/≤ MAPK. Cell Stem Cell *11*, 541-553.

59. Zetser, A., Gredinger, E., and Bengal, E. (1999). p38 mitogen-activated protein kinase pathway promotes skeletal muscle differentiation. Participation of the Mef2c transcription factor. The Journal of biological chemistry *274*, 5193-5200.

60. Osman, A.A., Hancock, J., Hunt, D.G., Ivy, J.L., and Mandarino, L.J. (2001). Exercise training increases ERK2 activity in skeletal muscle of obese Zucker rats. J Appl Physiol *90*, 454-460.

61. Rottinger, E., Besnardeau, L., and Lepage, T. (2004). A Raf/MEK/ERK signaling pathway is required for development of the sea urchin embryo micromere lineage through phosphorylation of the transcription factor Ets. Development *131*, 1075-1087.

62. Prusty, D., Park, B.H., Davis, K.E., and Farmer, S.R. (2002). Activation of MEK/ERK signaling promotes adipogenesis by enhancing peroxisome proliferator-activated receptor gamma (PPARgamma) and C/EBPalpha gene expression during the differentiation of 3T3-L1 preadipocytes. The Journal of biological chemistry *277*, 46226-46232.

63. Jaiswal, R.K., Jaiswal, N., Bruder, S.P., Mbalaviele, G., Marshak, D.R., and Pittenger, M.F. (2000). Adult human mesenchymal stem cell differentiation to the osteogenic or adipogenic lineage is regulated by mitogen-activated protein kinase. The Journal of biological chemistry *275*, 9645-9652.

64. Flores, G.V., Duan, H., Yan, H., Nagaraj, R., Fu, W., Zou, Y., Noll, M., and Banerjee, U. (2000). Combinatorial signaling in the specification of unique cell fates. Cell *103*, 75-85.

Chapter 3

High Content Imaging and Analysis are Useful Tools for Understanding the Roles of Focal Adhesion Proteins in Mechanotransduction

Abstract

Human mesenchymal stem cells (hMSCs) have been shown to differentiate based on the stiffness of their extracellular matrix (ECM), but there is little consensus on the specific pathways needed for this process to occur. The role of some focal adhesion proteins in stem cell mechanotransduction has been demonstrated, as siRNA-induced vinculin knockdown has been shown to inhibit hMSC myogenesis on myogenically favorable substrates. Here we build on this research by analyzing 47 different focal adhesion proteins for cryptic MAPK1 binding sites similar to that found in vinculin.

Using this parameter we selected 6 candidate focal adhesion proteins for further study in a high content imaging and analysis system in which cells were treated with siRNA, plated onto a 96 well plate containing two dimensional polyacrylamide surfaces, and stained for osteogenic and myogenic differentiation markers. This is the first high throughput system specifically built to analyze stem cell differentiation as a function of substrate stiffness and the first time an siRNA screen has been applied to stem cells for the purpose of studying substrate stiffness mediated mechanotransduction.

3.1 Introduction

The emergence of high throughput screening and high content imaging as techniques has enabled the collection and analysis of data at increasing rates. While the techniques are related, important differences must be highlighted. While formal definitions are nebulous, high throughput screening, or HTS, generally refers to the process of screening a large number of compounds, or library, against one or more functional markers[1]. High throughput screening and ultra high throughput screening have been described as those capable of between 10,000 and 100,000 or over 100,000 compounds tested per day, respectively[2]. HTS systems often take advantage of combinatorial chemistry to provide the library of compounds with which to screen, especially in the pursuit of drug discovery[3]. Characteristics of these systems include low fluid volume, mechanized fluid handling, and the miniaturization of cell-containing wells[4]. While HTS platforms are usually based in microplates containing 96, 384, or 1536 wells (advanced platforms can utilize 6144 or 24,576 well plates [5]), a number of alternative high throughput systems have been reported, including high throughput

fluorescence activated cell sorting (FACS) [6], mass spectroscopy [7], and droplet microfluidics[8].

High Content Screening (HCS), to contrast, is centered around analyzing the multiple cells based on a number of parameters, most often phenotypic characteristics [9]. These quantitative parameters can include simple measurements like cell area, aspect ratio, absolute position, or perimeter, as well as more complex features such as granularity, intensity distributions, texture features, and edge features[10]. There are numerous studies utilizing high content screening with applications as far ranging as cancer biology[11], drug discovery[12], stem cell biology[13], and neurobiology[14]. High throughput, high content siRNA screens have been performed using multi-channel immunofluorescence by plating cells on pre-fabricated siRNA arrays in which the siRNA has been immobilized onto the surface of the plate [14].

While the role of substrate mechanics in stem cell mechanotransduction has seen advances in recent years[15-17], high throughput and high content systems have yet to play as significant of a role as they have in cancer biology or drug discovery. This is mainly due to technical limitations inherent to working with physiologically relevant substrates, including fabrication hurdles and imaging limits.

In order to study stem cell mechanotransduction on a higher throughput scale, one challenge is the fabrication of physiological substrates that can be adapted to a high content system. Creating numerous substrates with which to study stem cell behavior in a low throughput system has been performed with great success. The effect of different combinations of cell shape, substrate elasticity, and ECM protein composition has been explored[18]. Combinatorial control over matrix characteristics by the addition of side

chains of varying lengths to polymer networks has been used to elucidate optimal substrate conditions for stem cell behaviors[19].

The most advanced combination of a high throughput, high content system with a biological analysis of substrate mechanics was performed by Wei et al., who seeded cells onto a diverse polymer array consisting of 496 monomer combinations[20]. By using high content imaging to analyze human embryonic stem cells (hESCs) plated on these arrays, an optimal substrate profile for the maintenance of hESC pluripotency was identified.

Despite these advances, there has yet to be any high throughput research on the mechanically sensitive differentiation of stem cells as a function of substrate stiffness. Here, we aim to fill this void with an emphasis on the elucidation of focal adhesion proteins that are necessary for this substrate mediated differentiation by combining a pilot focal adhesion siRNA screen with a 96 well array of tunable substrate stiffnesses [21]. We report the identification of several hits with proteins that may play a role in substrate-stiffness dependent differentiation.

3.2 Materials and Methods

3.2.1 Cell Culture and Reagents

Human mesenchymal stem cells were obtained from Lonza, Inc. and maintained in growth medium (DMEM, 10% FBS, 100 units/mL penicillin, and 100 μg/mL streptomycin) changed every four days (except those in 96 well plates). Only low passage hMSCs were used for experimental studies, typically between passage 5 and

passage 9. Latex lab gloves were used at all times (Adenna, Ontario, CA). For MAPK1 inhibition, the MAPK inhibitor pyrazolylpyrrole, dissolved in DMSO, was used at a final concentration of 2 nM and added to cells immediately post-plating. At 2 nM, pyrazolylpyrrole has only been shown to inhibit MAPK1[22]. Non-differentiation based experiments, including MAPK1 immunofluorescence and western blots and durotaxis assays were performed after 24 hours while siRNA-induced protein knockdown was at a maximum. Conversely, differentiation experiments took place over the course of six, since differentiation occurs as the integration of cues over time, allowing one to assume that examining the cells over the course of six days still reflects the initial RNAi.

3.2.2 Polyacrylamide Hydrogel Fabrication

Acrylamide was polymerized on aminosilanized 12 or 25 mm diameter coverslips. A solution containing the crosslinker N, N' methylene-bis-acrylamide, acrylamide, 1/100 volume 10% Ammonium Persulfate and 1/1000 volume of N, N, N', N'-Tetramethylethylenediamine was mixed. Two different combinations of acrylamide and bis-acrylamide were used to make 11 and 34 kPa substrates. Approximately 12 or 50 uL of the mixed solution was placed between the aminosilanized coverslip and a chlorosilanized glass slide. 100 ug/mL collagen I was chemically crosslinked to the substrates using the photoactivating crosslinker Sulfo-SANPAH (Pierce).

3.2.3 96-Well Polyacrylamide Hydrogel System

Custom 96 well plates containing polyacrylamide hydrogels (Softwell 96) crosslinked to glass bottom surfaces and surface coated with collagen type I were obtained from Matrigen (Brea, CA). Plates contained 48 12 kPa wells and 48 50 kPa wells for inducing myogenesis and osteogenesis, respectively. Stiffness values were verified by AFM (Figure 1B) (Asylum, Santa Barbara, CA). PA gel thickness was also verified via confocal microscopy (Figure 1C,D) (Nikon, Tokyo, Japan).

3.2.4 siRNA Transfection

siRNA oligonucleotides against human vinculin, p130Cas, SORBS1, SORBS3, Palladin, Paxillin, and Filamin (ON-TARGETplus SMARTpool; Thermo Fisher Scientific, Waltham, MA) and a pool of four non-targeting siRNAs control oligonucleotides (Supplemental Figure 1B) (ON-TARGETplus siControl; Dharmacon), diluted in DEPC water (OmniPure, EMD) and 5X siRNA buffer (Thermo Fisher Scientific, Waltham, MA), were transiently transfected into human hMSCs using Dharmafect 1 (Thermo Fisher Scientific, Waltham, MA) at an optimized concentration of 50 nM in low serum antibiotic free growth media, according to the manufacturers' protocols. Specific siRNA sequences can be found in Table 1. Protein knockdown was characterized by western blot and immunofluorescence. After 24 hours of transfection in antibiotic-free media (2% FBS), media was replaced with standard hMSC growth media and cells replated onto appropriate substrates.

3.2.5 Immunofluorescence

hMSC cells were cultured on polyacrylamide gels or 96 well plates, fixed with 3.7% formaldehyde, and permeabilized with 1% Triton-X. The cells were then stained with primary antibodies against human MyoD (sc-32758, Santa Cruz, Dallas, TX), Myf5 (sc-302, Santa Cruz, Dallas, TX), Osterix (ab22552, Abcam, Cambridge, England), CBFA1 (sc-101145, Santa Cruz, Dallas, TX), pMAPK1 (ab76165, Abcam, Cambridge, England), MAPK1 (ab124362, Abcam, Cambridge, England), Vinculin (ab129002, Abcam, Cambridge, England), p130Cas (ab108320, Abcam, Cambridge, England), SORBS1 (ab4551, Abcam, Cambridge, England), SORBS3 (GTX-115362, Genetex, Irvine, CA), Filamin (ab51217, Abcam, Cambridge, England), or Paxillin (ab32084, Abcam, Cambridge, England). Corresponding secondary antibodies were conjugated to Alexa Fluor 488 (FITC) or Alexa Fluor 647 (Cy5) (Invitrogen, Carlsbad, CA). Nuclei were counterstained with Hoechst dye (Sigma, St. Louis, MO), and the actin cytoskeleton was stained with Rhodamine-conjugated Phalloidin (Invitrogen, Carlsbad, CA). Cells not plated in 96 well plates were imaged with a Nikon Eclipse Ti-S inverted fluorescence microscope equipped with a BD Carv II camera.

3.2.6 High Content Imaging

96 well plates were imaged on a CV1000 Cell Voyager (Yokogawa Electric Co., Tokyo, Japan). Briefly, 20 confocal images were taken 25 different points in each well (forming a 5x5 map) with three different wavelengths (FITC, TXRD, and DAPI). Maximum Intensity Projections (MIPs) were constructed from the 20 confocal images, resulting in a single map for each well.

3.2.7 Automated Image Analysis

A semi-automated custom image analysis pipeline using CellProfiler[23] was utilized on all MIP maps. Outlines of nuclei were obtained as primary objects with automatic Otsu Global thresholding, and cell outlines were obtained using the rhodamine phalloidin channel as secondary objects using a Watershed Gradient algorithm. The pipeline calculated morphological attributes (such as cell area, aspect ratio, and eccentricity) for each cell, as well as the mean and integrated density of the green channel signal in nuclei, cell outlines, and cytoplasm outlines. Data analysis was performed with Microsoft Excel, GraphPad Prism and CellAnalyst[24].

3.2.8 Western Blots

Cell lysates were collected by rinsing samples with cold PBS, followed by a five minute lysis in mRIPA buffer (50 mM HEPES pH 7.5, 150 mM NaCl, 1.5 mM $MgCl_2$, 1% Triton, 1% Na-DOC, 0.1% SDS) with 1mM EGTA, 1 mM Na_3VO_4, 10 mM $Na_4P_2O_7$, and 1 mM PMSF. Samples were stored at -80^o C until analysis. Cell lysates were run in 10% SDS-PAGE gels at 150 V until proteins were separated and transferred to PVDF membranes (Bio-Rad, Hercules, CA) by running at 100 V for 1 hour, 15 minutes in a transfer apparatus (Bio-Rad, Hercules, CA). The membranes were washed in Buffer A (25 mM Tris-HCl, 150 mM NaCl, 0.1% Tween-20) + 4% SeaBlock (Thermo Fisher Scientific, Waltham, MA) overnight at 4^{o}C. The membranes were then incubated with anti-Vinculin, GAPDH, Actin, ERK2, p-ERK2 (T202 and Y204), p130Cas, SORBS1, SORBS3, Filamin, or Paxillin for 1 hour, washed with Buffer A + SeaBlock, and incubated in streptavidin horseradish-peroxidase-conjugated secondary antibodies (Bio-

Rad, Hercules, CA) for 30 minutes at room temperature. Immunoblots were visualized using ECL reagent (Pierce, Rockford, IL). All western blot antibodies were obtained from Abcam (Cambridge, ENG).

3.2.9 Durotaxis Assay

A two-step polymerization process described by Choi et al. [25] was used to fabricate substrates for the durotaxis assays. Briefly, glass coverslips (Thermo Fisher Scientific, Waltham, MA) were functionalized with 20 mM 3-(Trimethoxysilyl)propyl methacrylate and dried. A polyacrylamide solution consisting of 4% acrylamide, 0.4% bis-acrylamide, 1/100 volume 10% ammonium persulfate (APS) and 1/1000 volume of N, N, N', N'-tetramethylethylenediamine (TEMED) was pipetted in 20 μL volumes onto silicon wafers patterned with 25 mm long by 100 μm wide by 20 μm high rectangular ridges and allowed to polymerize for 15 minutes. After separating the wafer from the hydrogel, the hydrogel was placed onto a 20 uL drop of a second polyacrylamide solution consisting of 3.2% acrylamide and 0.4% bis-acrylamide and allowed to polymerize for 15 minutes. The final gel was soaked in phosphate buffered saline (PBS) before functionalization and cell plating.

3.2.10 Statistics

All experiments were performed in triplicate with the number of cells analyzed per condition as indicated. Error bars are shown as standard deviation. Significance was assessed by ANOVA at a significance threshold of $p<0.05$ or lower as indicated. Values

between 0.1 and 0.05 are noted as well. For instances where data is not significantly different, N.S. is stated.

3.3 Results

3.3.1 Characterization of 96 Well Plate System

96 well plates were ordered from Matrigen in a custom stiffness pattern, with the left 48 wells coated with 12 kPa myogenic polyacrylamide (PA) substrates and the right 48 wells coated with 50 kPa osteogenic PA substrates (Figure 1A). AFM analysis of these substrates revealed that the 12 kPa substrates were actually 38.0 kPa, making them osteogenic (Figure 1B). The advertised 50 kPa gels were actually 79.0 kPa, making them non permissive to osteogenesis or myogenesis. To analyze myogenesis, 12 mm coverslips were fabricated with 11 kPa substrates as per previously described methods[16]. These myogenic substrates had a measured stiffness of 15.8 kPa (Figure 1B).

To ensure that the thickness of the gels in the 96 well plate was high enough to avoid bilayer effects from the glass layer, a 4 kilodalton fluorescein labeled dextran bead solution was added to the gels and allowed to diffuse throughout the gels. Following this, a gel impermeable 0.1 μm phalloidin bead solution was added to delineate the surface of the gel from the solution (Figure 1C). By measuring the distance from the start of the green signal to the red signal, an average thickness of 254.7 μm was obtained (Figure 1D).

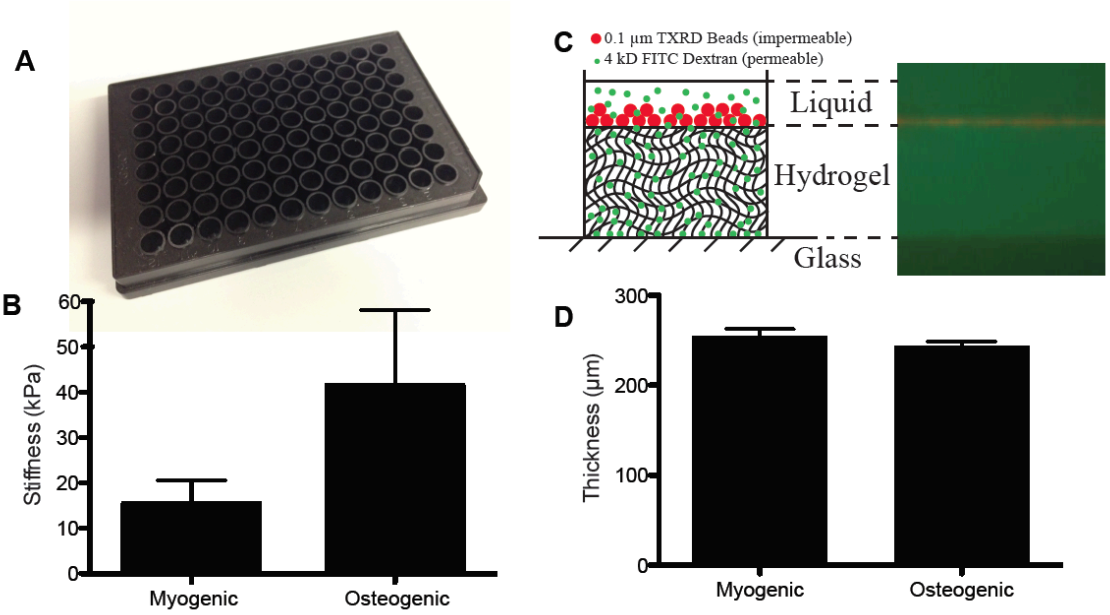

Figure 1: Characterization of Matrigen 96 Well Plates and Polyacrylamide Gels. A) The 96 well plate. B) AFM measurements of myogenic and osteogenic hydrogels. C) Schematic illustrating the diffusion based technique used to determine gel thickness. D) Gel thickness of myogenic and osteogenic hydrogels.

3.3.2 Focal Adhesion Protein Selection and Knockdown Verification

47 focal adhesion protein candidates were analyzed to determine the number of cryptic binding sites contained within their structure using the web tool ScanSite. Five proteins, Vinculin, p130Cas, Filamin, SORBS1 (Ponsin), SORBS3 (Vinexin) (Figure 2A), were selected for siRNA knockdown and analysis due to their predicted cryptic MAPK1 binding sites (Figure 2B). A sixth protein, Paxillin, was selected as a non-cryptic binding site containing control protein.

siRNAs coding for these six proteins (Table 1) were used to transiently knock down candidate protein levels. Knockdown was verified by western blot (Figure 3A) and immunofluorescence (Figure 3B,C).

3.3.3 The Role of Focal Adhesion Proteins in Myogenesis and Osteogenesis

To analyze images collected using the high content imaging system, a CellProfiler pipeline was built to do the following tasks: 1) Input images containing the DAPI signal, the rhodamine phalloidin signal, and the differentiation marker signal. 2) Calculate an Otsu-Global threshold for the DAPI image to find all nuclei (Figure 4A). 3) Using the identified nuclei as a seed region, move outward to identify corresponding outlines of the cell using the rhodamine phalloidin stain (Figure 4B). 4) Using the identified cell outlines and nuclei outlines, calculate the signal intensity of the differentiation marker channel on a per-object basis (Figure 4B). Using this pipeline, it is possible to distinguish cells with nuclear expression only, cytoplasm expression only, uniform positive expression, and uniform negative expression (Figure 4C).

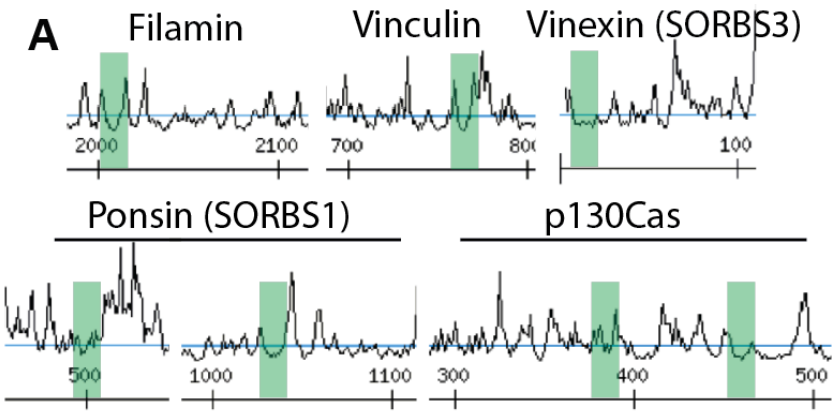

B

Protein	*Site*	*Sequence*	*Accessibility*
Vinculin	L765	RRANRILLVAKREVE	0.164
p130Cas	L386	RRPGPGTLYDVPRER	0.524
	V458	REPLELEVAVEALAR	0.315
Filamin	V2007	KRLRNGHVGISFVPK	0.213
Paxillin	N/A	N/A	N/A
Ponsin	L500	KRSATLPLPARSSSL	0.737
	L1033	RASPSLSLSLPHLSW	0.357
Vinexin	L12	PRSLRAGLSLDDFIP	0.349

Figure 2: ScanSite Analysis of 6 Candidate Mechanosensors. A) Plots of surface accessibility reveal regions corresponding to predicted MAPK1 domains. B) Actual sites and surface accessibility values for given predicted MAPK1 binding domains.

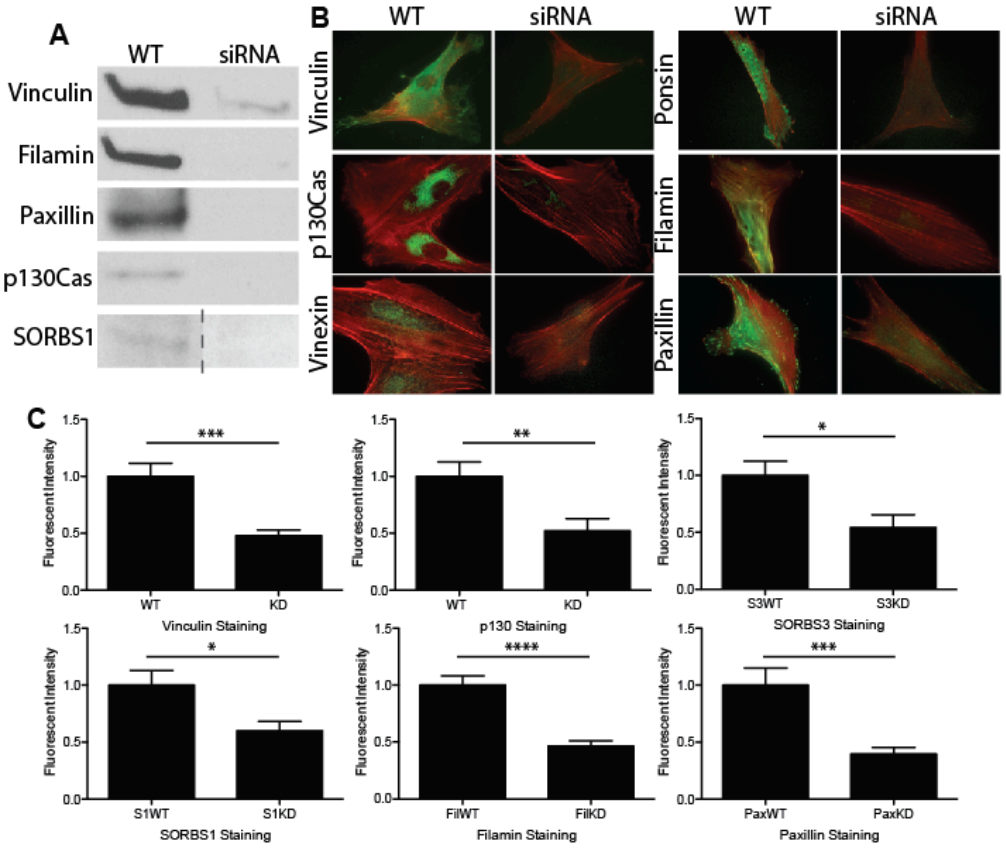

Figure 3: Confirmation of siRNA-induced Knockdown. A) Western blots of lysates collected 2 days post-treatment. B) Immunofluorescence images of proteins being knocked down. C) Quantification of mean immunofluorescence intensity from knockdown cells.

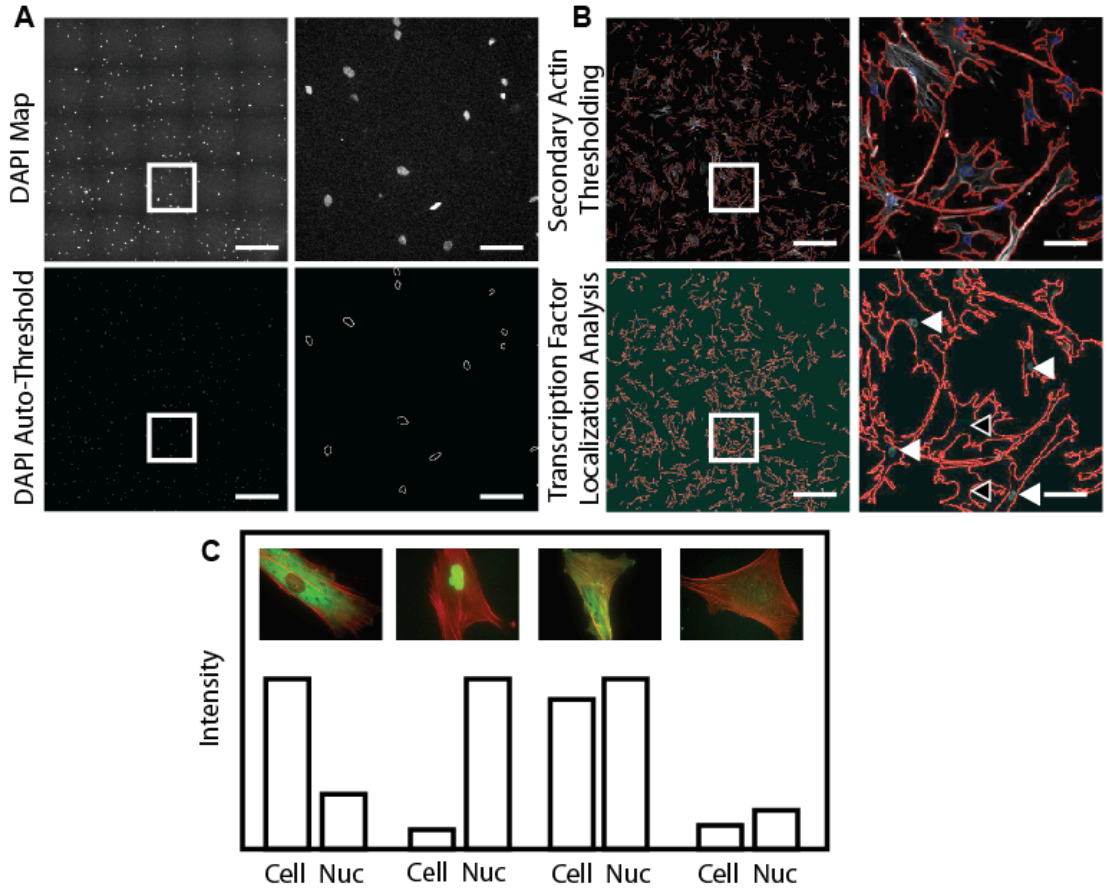

Figure 4: CellProfiler Pipeline. A) Nuclei are identified first from the DAPI channel. B) Using the nuclei as seed regions, cell outlines are identified for each nucleus. C) By analyzing the cells and the nuclei separately, important marker distribution information can be obtained.

Applying this pipeline to images collected from wells stained for osteogenic markers revealed that p130Cas, filamin, paxillin, and SORBS3 (Vinexin) knockdown did not affect osteogenic differentiation signals after four days. However, the knockdown of SORBS1, or ponsin, was shown to reduce osteogenic signal by over 50% (Figure 5A-E). This reduction was found in both CBFA1 and Osterix expression. SORBS1 has been shown to interact with vinculin[26] and play a role in insulin signaling [27].

Interestingly, vinculin knockdown, which was shown to not affect CBFA1 expression in previous works[16], was responsible for a significant (Bonferroni post-test on ANOVA) 25% reduction in CBFA1 signal. This significance was not found in Osterix staining (Figure 5).

Cells plated on myogenic substrates exhibited elevated levels of the myogenic markers MyoD and Myf5 (Figure 6). siRNA knockdown of vinculin resulted in a loss of both MyoD and Myf5, confirming previous results[16]. Furthermore, the knockdown of a number of other cryptic-MAPK1-binding domain containing proteins significantly reduced the expression of both MyoD and Myf5, including p130Cas and SORBS3. Filamin, SORBS1, and Paxillin were found to significantly reduce the expression of one of the two myogenic markers (Figure 6). Paxillin does not contain a cryptic MAPK1 binding site, yet still significantly reduced the expression of Myf5 after four days. This could be due to the fact that Paxillin does have a cryptic binding domain for MAPK3.

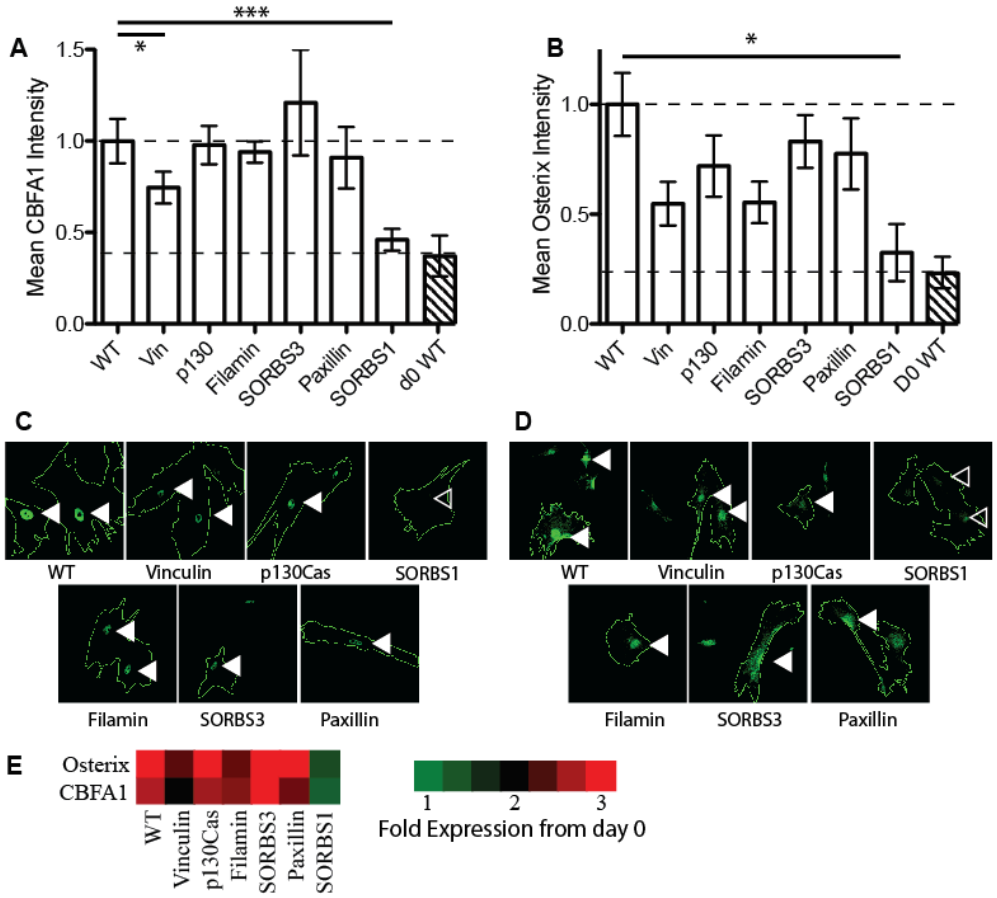

Figure 5: Osteogenic Differentiation and Focal Adhesion Protein Knockdown. Normalized mean intensity levels of A) CBFA1 and B) Osterix immunofluorescence staining after four days of culture of osteogenically favorable 34 kPa substrates. Representative images showing cell outlines along with C) CBFA1 and D) Osterix expression. E) Heat map indicating fold-change in expression of the osteogenic markers from day 0 wild type cells.

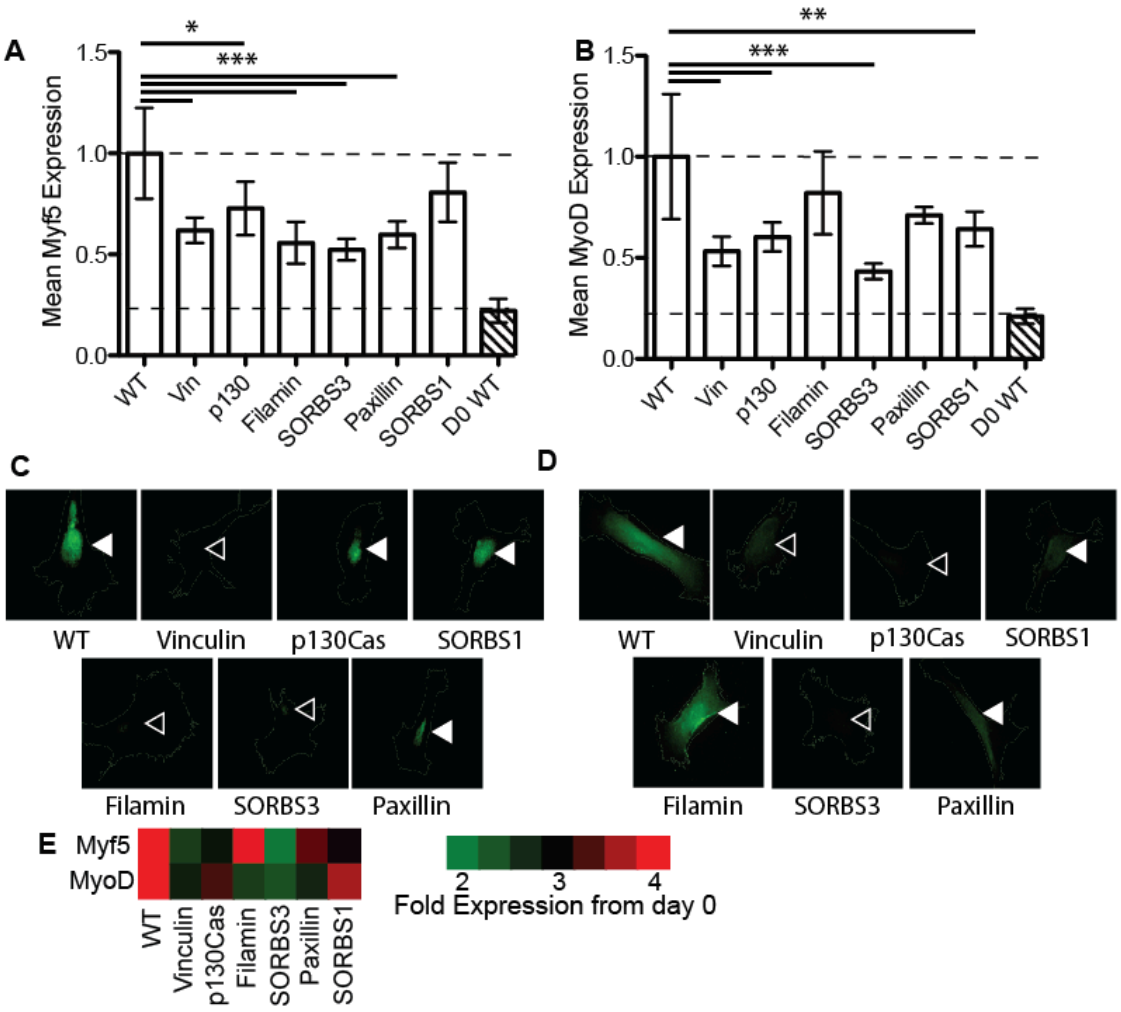

Figure 6: Myogenic Differentiation and Focal Adhesion Protein Knockdown. Normalized mean intensity levels of A) Myf5 and B) MyoD immunofluorescence staining after four days of culture of myogenically favorable 11 kPa substrates. Representative images showing cell outlines along with C) Myf5 and D) MyoD expression. E) Heat map indicating fold-change in expression of the myogenic markers from day 0 wild type cells.

To analyze the effects of multiple siRNA induced knockdowns on stiffness-mediated hMSC differentiation, vinculin knockdown was used in tandem with SORBS1 knockdown or p130Cas knockdown. When these knockdown combinations were applied to cells plated on myogenically favorable 11 kPa substrates, a statistically insignificant reduction in both MyoD expression and Myf5 expression was observed (Figure 7A). Conversely, on osteogenically favorable 34 kPa substrates, the combination of vinculin knockdown with either SORBS1 or p130Cas knockdown resulted in osteogenic marker expression equivalent to wild type levels, indicating that complex compensatory mechanisms may play a role in restoring osteogenesis (Figure 7B).

3.3.4 MAPK1 Inhibition in Mechanosensing hMSCs

To analyze the effect of MAPK1 inhibition on substrate stiffness directed hMSC differentiation, the potent MAPK1 inhibitor pyrazolylpyrrole was applied to cells at the beginning of the time course. While this was previously done on myogenically favorable 11 kPa substrates[16], the effect of MAPK1 inhibition on osteogenesis is unknown. After four days on osteogenically favorable substrates, cells treated with the MAPK1 inhibitor showed a loss in osteogenic signal equivalent to SORBS1 knockdown (Figure 8B). This may be due to the fact that a global MAPK1 inhibitor can affect many different pathways, as MAPK1 is a well-known integrator protein. Loss of myogenic differentiation marker expression was confirmed (Figure 8A).

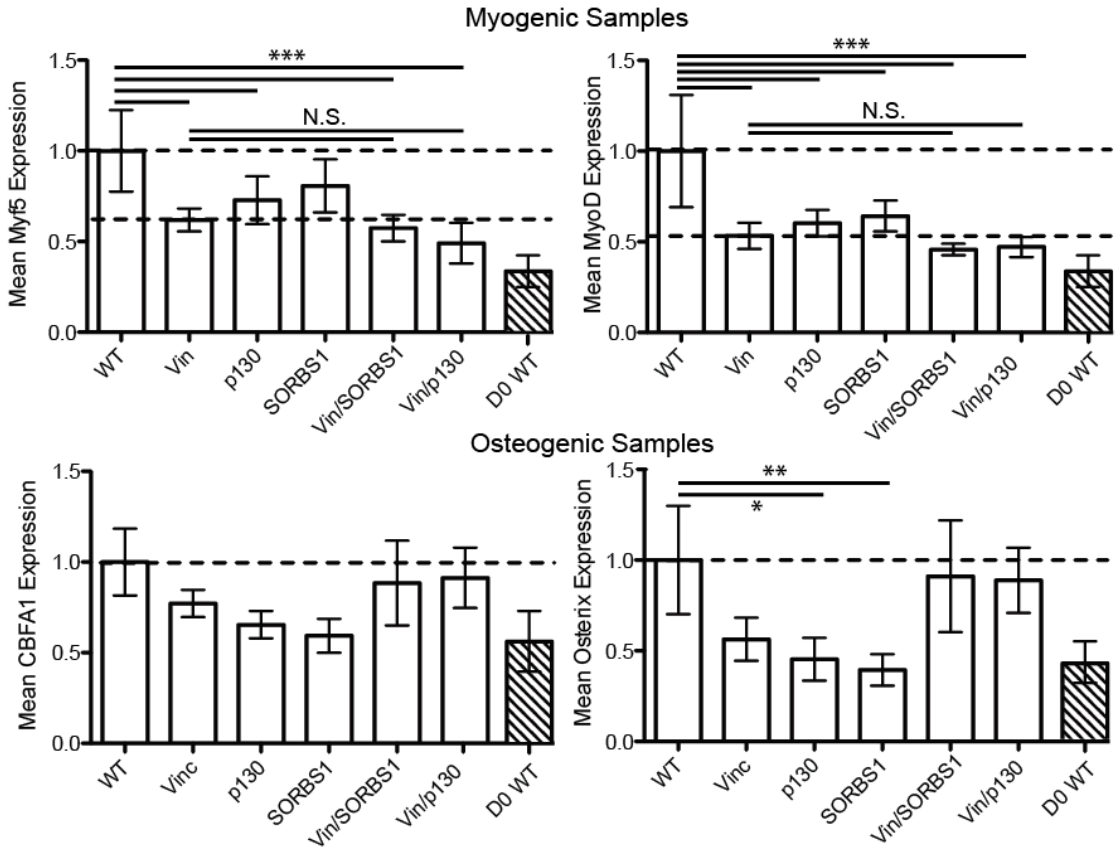

Figure 7: Combinatorial Knockdown of Focal Adhesion Proteins. Vinculin knockdown was used in tandem with SORBS1 knockdown or p130Cas knockdown on both A-B) myogenically favorable substrates and C-D) osteogenically favorable substrates. Respectively, cells were stained for A) Myf5 or B) MyoD and C) CBFA1 or D) Osterix.

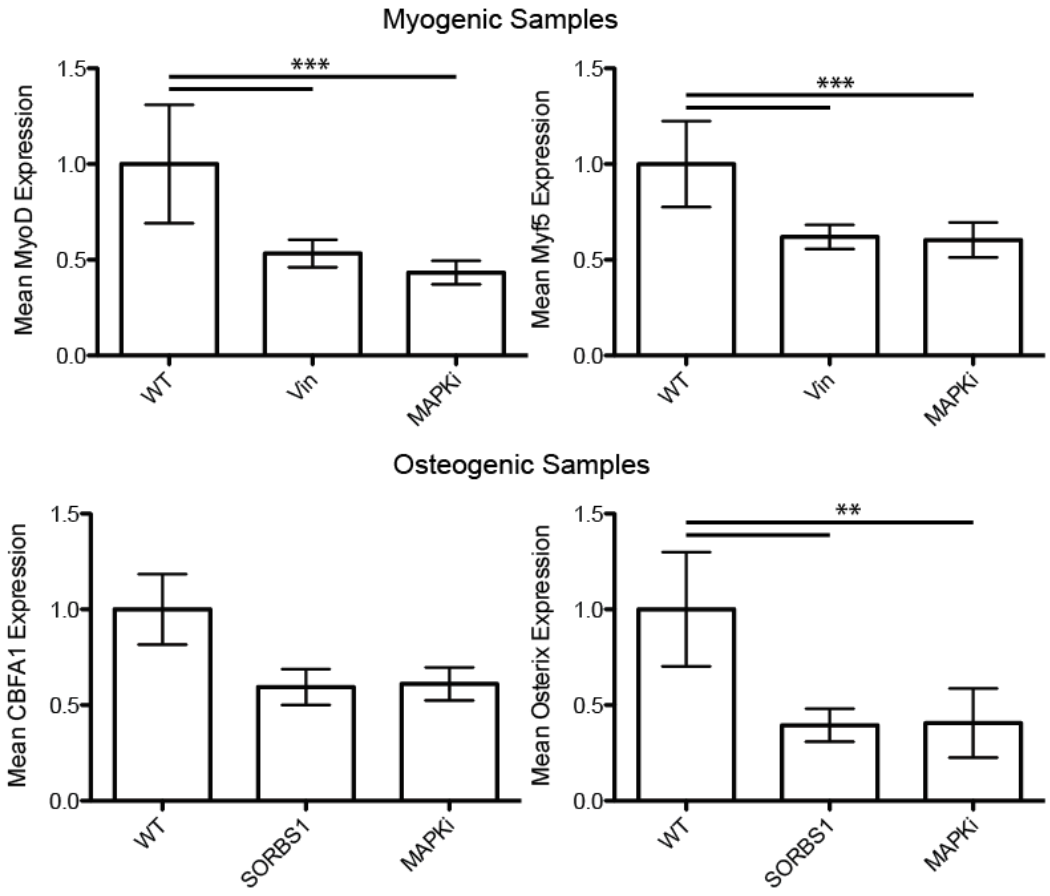

Figure 8: MAPK1 inhibition and Myogenic and Osteogenic Differentiation. The potent MAPK1 inhibitor pyrazolylpyrrole was applied to cells at the beginning of the four day time course on both A-B) myogenic and C-D) osteogenic substrates and stained for A) MyoD, B) Myf5, C) CBFA1, or D) Osterix.

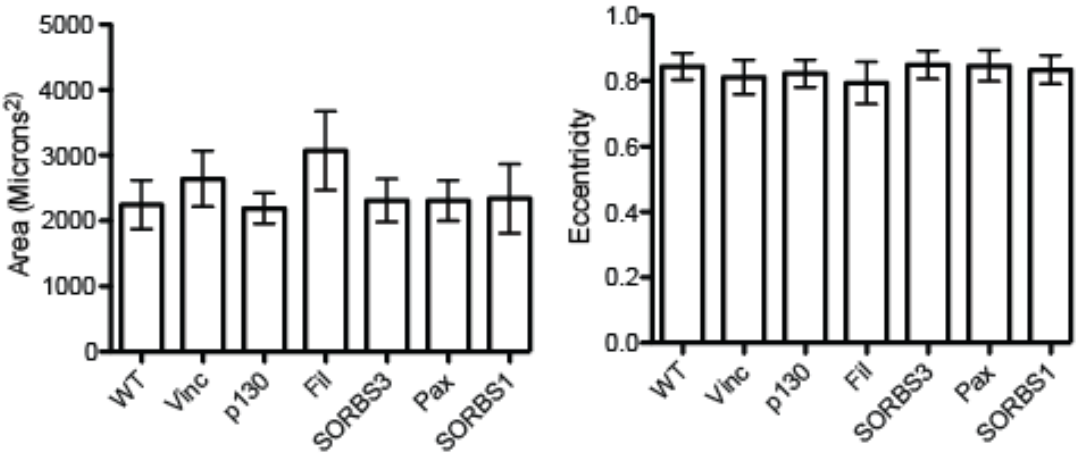

Figure 9: Secondary Metrics from High Content Image Analysis. A) Average cell area and B) Average cell eccentricity were used as metrics to assess cell morphology. Eccentricity is calculated as the ratio between the distance between the two foci of a fitted ellipse and the major axis length of the cell.

3.3.5 Secondary Metrics of Focal Adhesion Protein Knockdown

To ensure that the knockdown of the candidate focal adhesion proteins was not disrupting normal cell behavior, two metrics were chosen for initial analysis in the high throughput system. As the CellProfiler software is able to gather these metrics automatically, they lend themselves to simple and effective high content analysis. The addition siRNA against each focal adhesion protein did not significantly affect cell area (Figure 9A) or cell eccentricity (Figure 9B), which is a metric for the spindle factor of cells, calculated by finding the ratio of the distance between the foci of a fitted ellipse to the major axis length.

3.4 Conclusions

We used Scansite to select five candidate proteins that could potentially play a role in MAPK1-based mechanosensitive differentiation. We then built a high throughput, high content analysis based system capable of finding hits much more quickly and efficiently. Finally, we used this system to identify SORBS1 as a potential effector of osteogenesis in hMSCs, confirmed vinculin's role in myogenesis, and identified p130Cas and SORBS3 as potential effectors of myogenesis. This method can be applied to a number of applications in cell biology in which an immunofluorescently labeled marker is differentially upregulated or downregulated in response to substrate stiffness changes.

3.5 Acknowledgements

Chapter 3, in part, is currently being prepared for submission for publication of the material. The dissertation author is the primary investigator and author, and thanks co-authors Ludovic Vincent, Dr. Jamie Kasuboski, and Dr. Adam J. Engler for their contributions to the work. This work was supported by an NIH New Innovator Award (1DP02 OD006460 to A.J.E) and an NSF predoctoral fellowship (to L.G.V.)

3.6 Appendix

Table 1: siRNA sequences.

Gene	Accession Number	Sequences
Vinculin	P18206	CAGCAUUUAUUAAGGUUGA, GCCAAGCAGUGCACAGAUA, GAGCGAAUCCCAACCAUAA, UGAGAUAAUUCGUGUGUUA
p130Cas	P56945	GGUCGACAGUGGUGUGUAU, GGCCACAGGACAUCUAUGA, GCAAUGCUGCCCACACAUC, CCAGAUGGGCAGUACGAGA
Paxillin	P49023	GAGCUAACAUCCAUAUUUA, GUGCAACUGUCUUUAAUAU, CCAGUAACUUUCACAUGUA, GAGUUUAUCUGGAGUGUAG
Filamin	P21333	GCAGGAGGCUGGCGAGUAU, GCACCCAGACCGUCAAUUA, GCACAUGUUCCGUGUCCUA, GAAUGGCGUUUACCUGAUU
SORBS1	Q9BX66	CAAGAGCAUUUACGAAUAU, GAGAUGAGCUACAUUGAUG, UAUACCAGCUGAUUACUUG, GAAGAGCACUCAGGACUUA
SORBS3	O60504	GAGAGGCUGUGGCCCAGUA, CAUCUUCCCUGCUAAUUAU, CCAAGGAGCUGACUCUGCA, CCUAACACCUCUCAGAUAC

3.7 References

1. Zhang, J., and Chung, T. (1999). Validation of High Throughput Screening Assays. … of biomolecular screening.

2. Mayr, L. M., and Bojanic, D. (2009). Novel trends in high-throughput screening. Current opinion in pharmacology.

3. Gordon, E. M., Barrett, R. W., Dower, W. J., Fodor, S. P. A., and Gallop, M. A. (2002). Applications of Combinatorial Technologies to Drug Discovery. 2. Combinatorial Organic Synthesis, Library Screening Strategies, and Future Directions. Journal of medicinal … *37*, 1385–1401.

4. Oldenburg, K. R., Zhang, J.-H., Chen, T., Maffia, A., III, Blom, K. F., Combs, A. P., and Chung, T. D. Y. (1998). Assay Miniaturization for Ultra-High Throughput Screening of Combinatorial and Discrete Compound Libraries: A 9600-Well (0.2 Microliter) Assay System. J Biomol Screen *3*, 55–62.

5. Stockwell, B. R., Haggarty, S. J., and Schreiber, S. L. (1999). High-throughput screening of small molecules in miniaturized mammalian cell-based assays involving post-translational modifications. Chemistry & biology.

6. Olsen, M. J., Gam, J., Iverson, B. L., and Georgiou, G. (2003). High-Throughput FACS Method for Directed Evolution of Substrate Specificity. Directed Enzyme Evolution *230*, 329–342.

7. Liu, H., Felten, C., Xue, Q., and Zhang, B. (2000). Development of multichannel devices with an array of electrospray tips for high-throughput mass spectrometry. Analytical ….

8. Droplet microfluidic technology for single-cell high-throughput screening. (2009). Droplet microfluidic technology for single-cell high-throughput screening. PNAS *106*, 14195–14200.

9. Gasparri, F. (2009). An overview of cell phenotypes in HCS: limitations and advantages. Expert Opin Drug Discov *4*, 643–657.

10. Automatic identification of subcellular phenotypes on human cell arrays. (2004). Automatic identification of subcellular phenotypes on human cell arrays. Genome Res. *14*, 1130–1136.

11. Giuliano, K. A., DeBiasio, R. L., Dunlay, R. T., Gough, A., Volosky, J. M., Zock, J., Pavlakis, G. N., and Taylor, D. L. (1997). High-Content Screening: A New Approach to Easing Key Bottlenecks in the Drug Discovery Process. J Biomol Screen *2*, 249–259.

12. Kapur, R., Giuliano, K. A., Campana, M., Adams, T., Olson, K., Jung, D., Mrksich, M., Vasudevan, C., and Taylor, D. L. (1999). Streamlining the Drug Discovery Process by Integrating Miniaturization, High Throughput Screening, High Content Screening, and Automation on the CellChip™ System. Biomedical Microdevices *2*, 99–109.

13. Desbordes, S. C., Placantonakis, D. G., Ciro, A., and Socci, N. D. (2008). High-throughput screening assay for the identification of compounds regulating self-renewal and differentiation in human embryonic stem cells. Cell Stem Cell.

14. Erfle, H., Neumann, B., Liebel, U., Rogers, P., and Held, M. (2007). Reverse transfection on cell arrays for high content screening microscopy. Nature protocols.

15. Engler, A. J., Sen, S., Sweeney, H. L., and Discher, D. E. (2006). Matrix elasticity directs stem cell lineage specification. Cell *126*, 677–689.

16. Holle, A. W., Tang, X., Vijayraghavan, D., Vincent, L. G., Fuhrmann, A., Choi, Y. S., del Álamo, J. C., and Engler, A. J. (2013). In situ mechanotransduction via vinculin regulates stem cell differentiation. STEM CELLS, n/a–n/a.

17. Lakins, J. N., Chin, A. R., and Weaver, V. M. (2012). Exploring the Link Between Human Embryonic Stem Cell Organization and Fate Using Tension-Calibrated Extracellular Matrix Functionalized Polyacrylamide Gels. *916*, 317–350.

18. Lee, J., Abdeen, A. A., Zhang, D., and Kilian, K. A. (2013). Directing stem cell fate on hydrogel substrates by controlling cell geometry, matrix mechanics and adhesion ligand composition. Biomaterials.

19. Ayala, R., Zhang, C., Yang, D., Hwang, Y., and Aung, A. (2011). Engineering the cell–material interface for controlling stem cell adhesion, migration, and differentiation. Biomaterials.

20. Mei, Y., Saha, K., Bogatyrev, S. R., Yang, J., and Hook, A. L. (2010). Combinatorial development of biomaterials for clonal growth of human pluripotent stem cells. Nature Materials.

21. Mih, J. D., Sharif, A. S., Liu, F., Marinkovic, A., Symer, M. M., and Tschumperlin, D. J. (2011). A Multiwell Platform for Studying Stiffness-Dependent Cell Biology. PLoS ONE *6*, e19929.

22. Aronov, A. M., Baker, C., Bemis, G. W., and Cao, J. (2007). Flipped out: structure-guided design of selective pyrazolylpyrrole ERK inhibitors. Journal of medicinal ….

23. Carpenter, A. E., Jones, T. R., Lamprecht, M. R., Clarke, C., Kang, I. H., Friman, O., Guertin, D. A., Chang, J. H., Lindquist, R. A., Moffat, J., et al. (2006).

CellProfiler: image analysis software for identifying and quantifying cell phenotypes. Genome Biology *7*, R100.

24. Jones, T. R., Kang, I. H., Wheeler, D. B., Lindquist, R. A., Papallo, A., Sabatini, D. M., Golland, P., and Carpenter, A. E. (2008). CellProfiler Analyst: data exploration and analysis software for complex image-based screens. BMC Bioinformatics *9*, 482.

25. Choi, Y. S., Vincent, L. G., Lee, A. R., and Kretchmer, K. C. (2012). The alignment and fusion assembly of adipose-derived stem cells on mechanically patterned matrices. Biomaterials.

26. Ponsin/SH3P12: an l-afadin- and vinculin-binding protein localized at cell-cell and cell-matrix adherens junctions. (1999). Ponsin/SH3P12: an l-afadin- and vinculin-binding protein localized at cell-cell and cell-matrix adherens junctions. J Cell Biol *144*, 1001–1017.

27. Lin, W. H., Huang, C. J., Liu, M. W., Chang, H. M., and Chen, Y. J. (2001). … of the human sorbin and SH3 domain containing 1 (SORBS1) gene: a protein associated with c-Abl during insulin signaling in the hepatoma cell line Hep3B. Genomics.

Chapter 4

Conclusion

Human mesenchymal stem cell (hMSC) proliferation, migration, and differentiation have all been linked to extracellular matrix stiffness, yet the signaling pathway(s) that are necessary for mechanotransduction remain unproven. Vinculin has been implicated as a mechanosensor *in vitro*, but here we demonstrate its ability to also regulate stem cell behavior, including hMSC differentiation. RNA interference-mediated vinculin knockdown significantly decreased stiffness-induced MyoD, a muscle transcription factor, but not Runx2, an osteoblast transcription factor, and impaired stiffness-mediated migration. A kinase binding accessibility screen predicted a cryptic MAPK1 signaling site in vinculin that could regulate these behaviors. Indeed, reintroduction of vinculin domains into knocked-down cells indicated that MAPK1 binding site-containing vinculin constructs were necessary for hMSC expression of MyoD. Vinculin knockdown does not appear to interfere with focal adhesion assembly, significantly alter adhesive properties, or diminish cell traction force generation, indicating that its knockdown only adversely affected MAPK1 signaling. These data

provide some of the first evidence that a force-sensitive adhesion protein can regulate stem cell fate.

We build on this research by analyzing 47 different focal adhesion proteins for cryptic MAPK1 binding sites similar to that found in vinculin. We used Scansite to select five candidate proteins that could potentially play a role in MAPK1-based mechanosensitive differentiation. We then built a high throughput, high content analysis based system capable of finding hits much more quickly and efficiently. Finally, we used this system to identify SORBS1 as a potential effector of osteogenesis in hMSCs, confirmed vinculin's role in myogenesis, and identified p130Cas and SORBS3 as potential effectors of myogenesis. In addition, the high throughput system was also used to analyze combinatorial application of siRNA and global chemical inhibitors for MAPK1. This method can be applied to a number of applications in cell biology in which an immunofluorescently labeled marker is differentially upregulated or downregulated in response to substrate stiffness changes.